4.0 Results and Discussion:

Unsteady IGV Surface and Wake Measurements

This section is divided between the Phase I unsteady on-vane pressure measurements and the Phase II unsteady total pressure measurements between the IGV and fan. The data acquisition techniques, results and discussion for the on-vane and total pressure measurements are presented in section 4.1 and 4.2, respectively. The unsteady total pressure measurements are divided between the cases of subsonic and transonic relative fan blade velocity.

4.1 High-Frequency On-Vane Pressure Measurements

The primary purpose of the on-vane measurements is to detect the unsteady pressure fluctuations at the IGV trailing edge caused by the downstream fan, for the IGV placed at a distance upstream of the fan that corresponds to typical component spacing. This first phase of the unsteady experiments is used to determine whether upstream propagating potential flow fields (PFF) and/or shock waves from the fan blades are present at the IGV trailing edge. As discussed in section 1.2, hot-wire measurements taken upstream of the F109 at the Air Force Academy found strong velocity fluctuations propagating directly upstream of the fan, which were reported to be caused by the fan potential flow field (Falk, et. al, 1998). The same study reported that these fluctuations decayed

exponentially as the probe was moved upstream from the fan. At the axial location of the IGV trailing edge relative to the fan leading edge in the current study (0.43 C_F), Falk measured the unsteady velocity fluctuations to have a Peak-to-Peak amplitude of 7% and 15% the axial velocity in the axial and circumferential directions respectively. These values correspond to maximum unsteady pressure fluctuations between 0.04% and 0.17% of the inlet total pressure, respectively. If these results are accurate, the fan PFF would have a minimal effect on the IGV wake development. However, calculations of the relative fan velocity in the current study, discussed in section 4.1.2, show that the fan is transonic for the higher speeds tested. A recent study by Sanders and Fleeter, 1999, found that a transonic rotor produced strong unsteady pressure fluctuations on an upstream IGV, at the same spacing as the current study, which produced unsteady pressure fluctuations as high as 35% of the inlet total pressure, as discussed in section 1.2. Therefore, the amplitude of the unsteady pressure fluctuations at the IGV trailing edge in the current study is unknown. If the IGV trailing edge transducer detects a weak or absent unsteady pressure field, as the Falk study suggests, any unsteadiness measured in the wake (in the next phase of the study) would be caused by interaction with the fan PFF after the boundary layer separation (wake) leaves the vane. Conversely, if the IGV trailing edge transducer detects a strong unsteady pressure field, as the Johnson and Fleeter study suggests for a transonic rotor, the pressure field may alter the strength and the shape of the wake by impinging on the IGV surface. Moreover, if the unsteady pressure field at the IGV trailing edge is strong, it may interfere with the effectiveness of

the trailing edge jets. Therefore, the pressure fluctuations at the IGV trailing edge must be determined before the second phase of the experiments begins.

The secondary purpose of the on-blade measurements is to determine if the stator row downstream of the fan, the outlet guide vanes (OGV), cause any disturbances that are detected at the IGV trailing edge, as discussed in section 2.3.3. In the next phase of the unsteady experiments, the total pressure probe is fixed to the engine casing. The IGV ring is indexed circumferentially in order to map the wakes in the pitchwise direction. This results in the IGV trailing edge position varying in the circumferential direction relative to the OGV. If the OGV PFF is detectable at the IGV trailing edge, then the indexing of the IGV may compromise the wake measurements. Therefore, unsteady on-blade pressure measurements are taken for the IGV directly upstream and between the downstream OGV.

4.1.1 Data Reduction

The voltage signals from the on-blade Kulite transducer are divided into the DC and AC components, as discussed in section 2.3.1. The DC component is used to determine the time averaged absolute pressure from the transducer. The filtered AC component is used to determine the unsteady gage pressure fluctuations and is acquired with the high speed LeCroy Waveform DAQ system. The signal from the one-per-revolution fiber-optic trigger is acquired simultaneously with the AC signal. The data are acquired at a sampling frequency of 500 kHz, over a period of 0.262 seconds, which corresponds to

approximately 50 fan revolutions per acquisition. For each measuring location and fan speed tested, four data sets were acquired for a total of 200 fan revolutions.

The fiber-optic trigger (FOT) initiates a square wave voltage signal when the reflective tape on the spinner is detected. An example output from the FOT is shown in Fig. 4.1 for three fan revolutions. This figure shows an instantaneous step response when the reflective tape is detected. These step signals are used to phase lock the pressure signals with each fan revolution. This phase locking is used for the ensemble averaging of the pressure signals with each fan revolution, discussed below. In order to accurately ensemble average the data so that a direct comparison can be made at different measuring locations for a given fan speed, the same number of sampling points is required for each revolution. If the fan speed drifts during the testing, each acquisition will contain a different number of sampling points per revolution. Therefore, the engine speed was monitored with the monopole speed sensor, discussed in section 2.1, and with an oscilloscope connected to the FOT signal to insure that the fan speed did not drift from run to run.

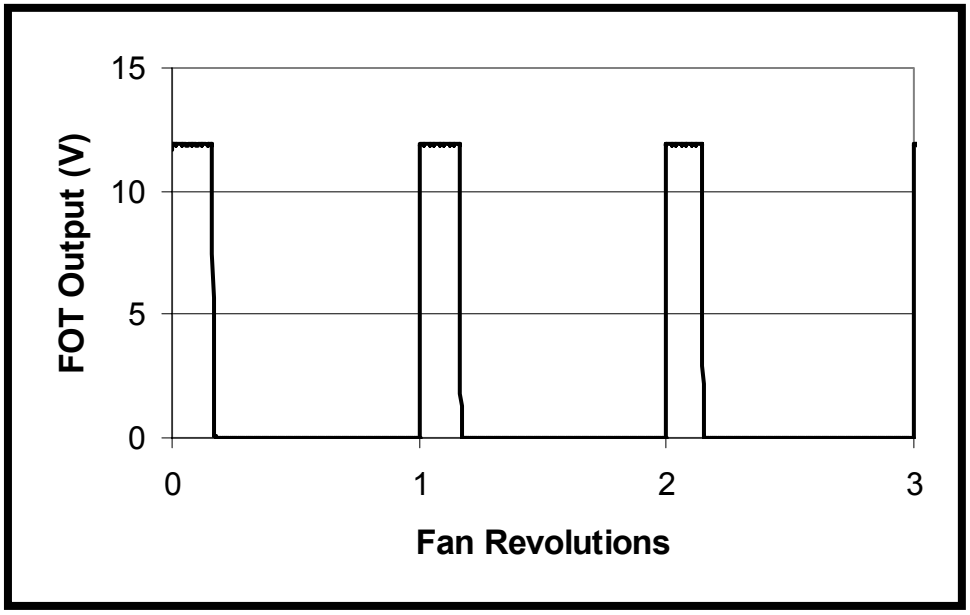

Figure 4.1 Square Wave output from one-per-rev fiber-optic trigger

The flows in and around fans and axial compressors are inherently unsteady. Wakes, potential flow fields, and shock interactions between blade rows generate the majority of this unsteadiness, as discussed in section 1.2. However, local flow instabilities exist from blade pass to blade pass, and revolution to revolution, which are both random and unpredictable (Johnston and Fleeter, 1998). In order to accurately compare flow results from different measuring locations and fan speeds, these random instabilities have to be removed from the data. The most common and accepted method for removing these random instabilities is the ensemble averaging of the data over one revolution. This method was employed by each of the previous investigations of unsteady stator-rotor interactions discussed in section 1.2. In the current study, the unsteady pressure signals are separated into one fan revolution in the time domain using the signals from the FOT

to phase lock the data to each fan revolution. Each specific point in time is averaged with that specific point in the other signals. This is done for each sampling point location in time over the fan revolution. The ensemble average for the pressure at a given point in time is:

$$\overline{P}_{time} = \left[\frac{\sum_{i=0}^{N} P_N}{N} \right]_{time} \qquad \textbf{(4.1)}$$

Where, N is the number of fan revolutions, or ensembles, averaged. An example of the ensemble averaging technique for four different phase locked signals is shown in Figure 4.2. Note that the signals are offset on the voltage scale for the example. A program was written in Matlab to ensemble average the pressure data. The ensemble averaging of the pressure signals will be discussed further in the next section.

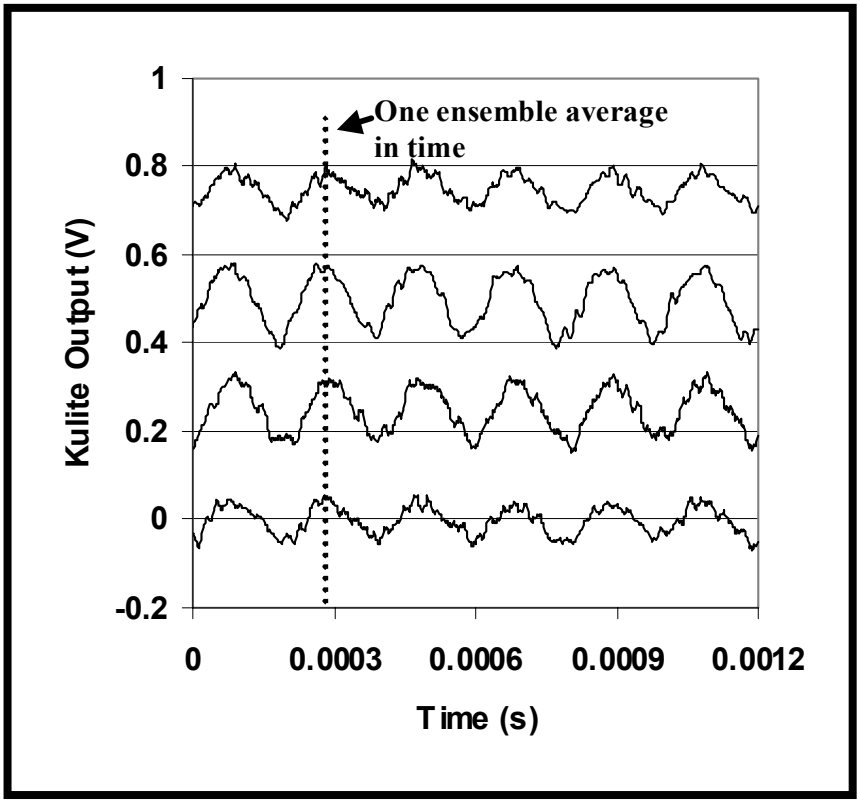

Figure 4.2 Example of ensemble averaging

A spectral analysis is performed on the unsteady pressure data to determine the frequency content of the signal so that a comparison can be made with the previous studies. The frequency domain is obtained from the raw pressure signals, i.e. not ensemble averaged. A Matlab program was written to perform a Fast Fourier Transform (FFT) on the unsteady pressure data. The resolution of the frequency bandwidth for a given time series is:

$$f_{BW} = \frac{f_s}{N} \qquad \textbf{(4.2)}$$

Where f_s is the sampling frequency, 500 kHz, and N is the total number of sampling points, 131070. Therefore, the bandwidth resolution in the current study is 3.8 Hz.

4.1.2 Results and Discussion

High frequency pressure measurements were performed with a Kulite pressure transducer facing downstream toward the fan and mounted flush at the IGV centerline in a TEB hole at 1.1 in immersion from the engine cowling. The IGV trailing edge was placed 0.43 fan chords upstream of the fan, which is in the range of typical IGV-fan spacings in modern military engines. The fan leading edge is at an axial distance of 0.4 IGV chords downstream of the IGV. The IGV was initially placed between two of the downstream OGV. The rear-facing pressure transducer is used to detect the upstream propagating unsteady pressure fluctuations generated by the rotor. For subsonic relative fan velocities, the fan generates an upstream propagating potential flow field, also called potential waves, as discussed in section 1.2. For transonic relative fan velocities, bow shocks form on the fan blade leading edge and propagate upstream, as discussed in section 1.2. Both of these conditions generate unsteady pressure fields upstream of the fan at the fan blade passing frequency (BPF) and harmonics there of.

The first step in the on-blade measurements was determining the testing speeds for the unsteady experiments. Measurements were performed between 7k and 14k rpm, in 0.5k rpm increments. The converted DC component of the pressure signal was found to correspond to the inlet static pressure at a given fan speed. The amplitudes of the signal

AC component, the unsteady pressure fluctuations, were observed on an oscilloscope in real time. These results showed small pressure fluctuations at the blade passing frequency (BPF) between 7k and 11k rpm fan speeds with amplitudes ranging from 0.05 to 0.3 psi peak to peak (P-P). At approximately 11.5k rpm, the pressure fluctuation waveform changed and the amplitude dramatically increased to over 1 psi P-P at the BPF. Furthermore, the noise emitted from the engine grew much louder and took on a 'buzzsaw' type tone, indicative of a transonic fan. The P-P pressure amplitudes continued to increase with fan speed, reaching a maximum of 4.7 psi at 14k rpm, which corresponds to 35% of the inlet total pressure. Since the objective of this study is to examine the effectiveness of IGV TEB for both subsonic and transonic fan speeds, measurements were taken for fan speeds of 10, 11, 12, 13 and 14k, corresponding to 70, 77, 85, 90 and 100% maximum fan speed. The calculated relative fan blade velocities and Mach numbers for these fan speeds are shown in Table 4.1 for the blade tip and 1.1 in immersion from the engine inlet, the location of the transducer on the IGV. These calculations show that transonic relative blade speeds are likely between 12k and 14k rpm at 1.1 in immersion.

Fan Speed (rpm)	Fan Tip Velocity (m/s)	Fan Tip Mach #	1.1 in immersion Velocity (m/s)	1.1 in immersion Mach #
10000	260	0.812	232	0.715
11000	286	0.906	255	0.795
12000	312	1.004	279	0.900
13000	339	1.111	303	0.970
14000	366	1.225	327	1.063

Table 4.1 Calculated relative fan blade velocity and Mach number

In order to determine if the fan in the F109 is at a transonic condition at the higher fan speeds, the pressure waveforms are compared to previous investigations. The AC component of the pressure signals was routed through signal filters and into a LeCroy Waveform Recorder, as discussed in section 2.3.1. These raw signals of the pressure fluctuations show different waveforms for 10 and 11k rpm, compared to 12-14k rpm fan speeds, as shown in Fig. 4.3 for 10 and 13k over 25% of one fan rotation. Note that the pressure scales are different for each plot. The waveform of the lower fan speed consists of a sinusoidal type wave, where the waveform at the higher speed consists of a step followed by a roll-off of the signal for each blade pass. The step in the signal at the higher fan speeds is indicative of a shock wave passing over the transducer. The ensemble averaged waveforms measured by Sanders and Fleeter (1999) near the trailing edge of an IGV for both subsonic and transonic rotor speeds is shown in Fig. 4.4, note that the pressure scales are different on each plot. The larger amplitude transonic waveform agrees with the waveform at 13k rpm in the current study in that a step is

observed followed by a roll-off in the signal at each blade pass. The smaller amplitude subsonic waveform is similar to the 10k rpm waveform. Furthermore, the differences in P-P pressure amplitude between 10k and 13k is of the same order as the difference between the subsonic and transonic pressure amplitudes in the Fleeter study. Therefore, it is concluded that subsonic relative fan blade velocities exist at fan speeds of 10k and 11k rpm, where the fan generates an upstream propagating potential flow field. Moreover, transonic relative fan blade velocities exist at fan speeds of 12, 13 and 14k rpm, where the fan leading edge shocks propagate upstream.

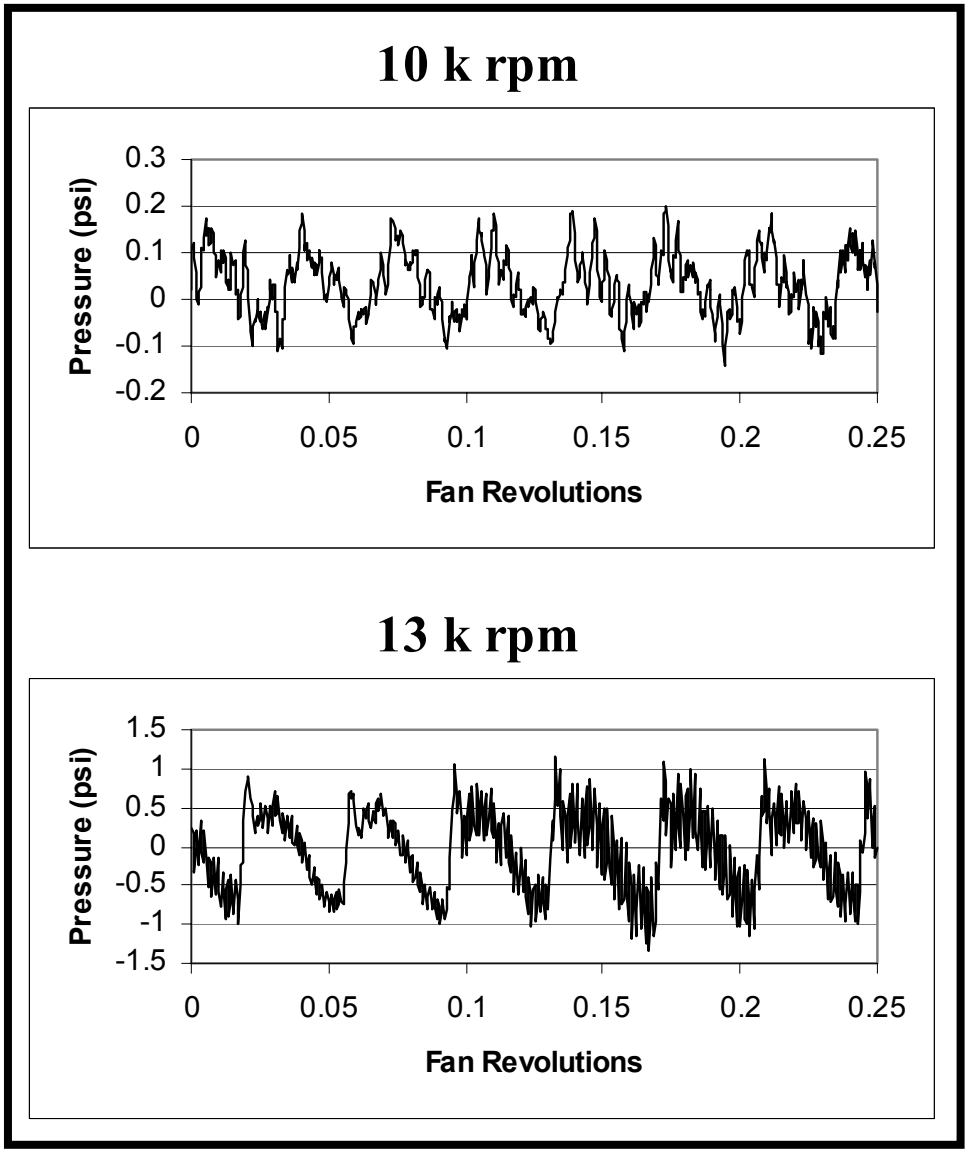

Figure 4.3 Waveform comparison between subsonic and transonic fan

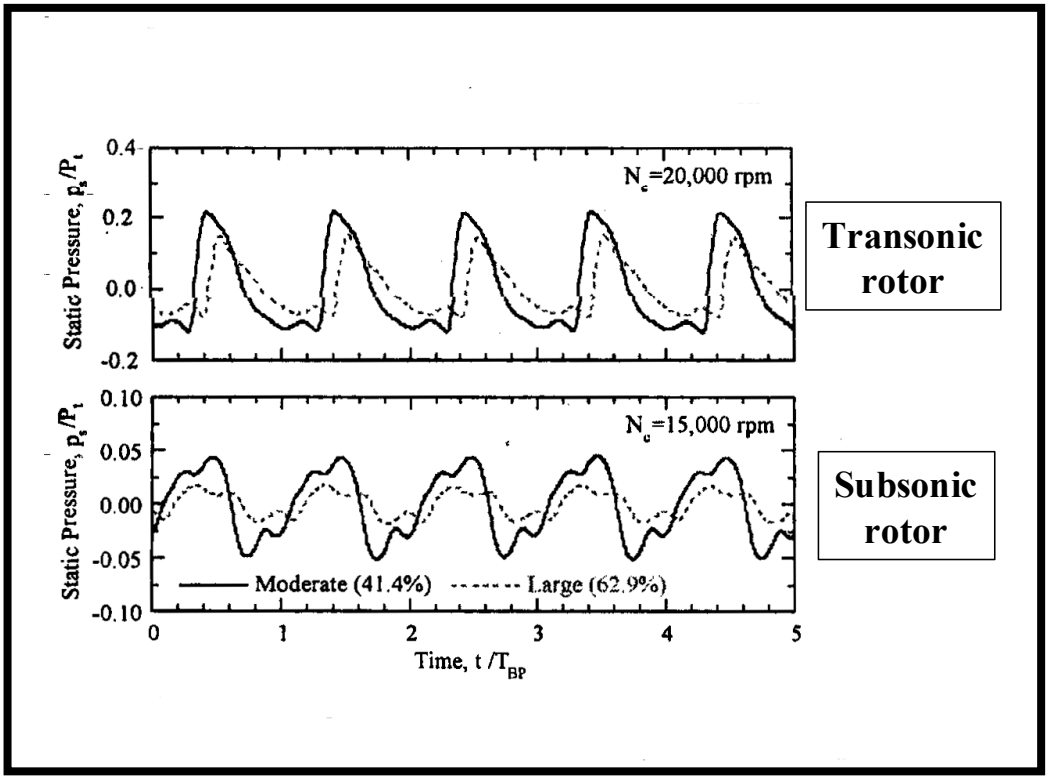

Figure 4.4 IGV on-blade pressure waveforms (Sanders and Fleeter, 1999)

It should be noted that the waveform from the 10k rpm subsonic fan speed, Fig. 4.3, agree with the waveforms of the upstream propagating potential waves measured with hot-wire probes in an F109 engine by Falk and Jumper, 1998. However, that study was performed for fan speeds between 12k and 14k rpm, as discussed in section 1.2, which are transonic in the current study. In recent discussions with Falk and Jumper, 2000, they believe that the fan blades of the F109 used in their study do not reach a transonic velocity due to the higher altitude at the Air Force Academy. Therefore, the measurements made in that study were performed for subsonic relative blade velocities only.

The average peak to peak (P-P) pressure amplitudes of the raw on-blade measurements are shown in Figure 4.5 for each fan speed tested, the ensemble average results are addressed later. These average P-P amplitudes correspond to 1.9, 2.7, 5.9, 9.9, and 18.2% of the inlet total pressure for the fan speeds tested. Maximum P-P amplitudes of 4.7 psi, 35% of the inlet P_T, were observed at 14k rpm. These results show a significant increase in P-P unsteady pressure amplitudes between the subsonic and transonic fan speeds, with the average amplitude at 14k being 9.6 times greater than that at 10k. Furthermore, the amplitudes for the transonic fan cases increase exponentially with increasing fan speed.

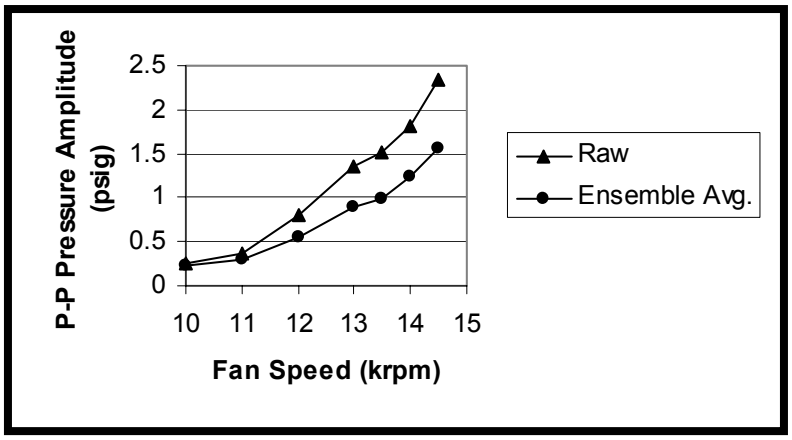

Figure 4.5 Peak to Peak amplitude of unsteady pressure fluctuations at IGV TE

As discussed in section 1.2, Sanders and Fleeter (1999) found higher average IGV surface unsteady pressure amplitudes of 10% and 35% of the inlet total pressure for the

subsonic and transonic rotor conditions, respectively. The IGV-rotor spacing was 0.414 C_r, compared to 0.43 in the current study. Inlet flow conditions and relative rotor speeds were not reported. However, in personal communications with Fleeter (2000), the inlet velocity and relative fan speeds were similar to those in the current study. Therefore, the higher pressure amplitudes in that study were due to the thicker leading edge of the NACA65 rotor blades compared to the relatively thin fan blades of the F109. Previous studies have shown that thicker leading edge rotor blades generate stronger bow shocks under the same flow conditions (Breugelmans, 1978).

The high amplitude pressure fluctuations at the IGV trailing edge, in the current study, demonstrate the significance of the upstream propagating forcing function generated by the fan's PFF and passing shocks on the IGV surface. Until recently, the interaction of the rotor PFF and passing shocks on an upstream stator have been considered second order compared to the forcing function generated by the IGV wakes on the downstream rotor. However, recent IGV failures and premature maintenance replacements have been attributed to HCF. The results of the current study agree with the previous studies by demonstrating a first order forcing function at the IGV trailing edge, which generates a periodic loading and lift on the vane. Furthermore, these results demonstrate the likelihood of the fan unsteady pressure fields altering the strength and the shape of the IGV wakes. For transonic fan speeds, the strong passing shock waves may induce a flow separation on the IGV surface further upstream on the vane chord, thereby creating a larger wake compared the baseline results presented in Chapter 3.0. Finally, these results

present a concern for the TEB investigation in the Phase II experiments. Since P-P pressure fluctuations as high as 4.7 psi, maximum, and 2.5 psi, average, were detected at the TEB holes, the effectiveness of wake filling may be reduced by periodic blocking, or resistance, at the exit of the TEB jet holes. These results will be discussed further in Chapter 5.0.

The power spectral density (PSD) of the unsteady pressure signals is shown in Fig. 4.6 for each fan speed tested. Note that the magnitude of the PSD differs on each plot so that the harmonics can be viewed at each fan speed. These results show that the fundamental frequency for each signal is the blade passing frequency for a given fan speed, with much smaller higher order harmonics of the BPF. In previous studies of IGV on-blade unsteady pressure measurements upstream of a transonic rotor, the magnitude of higher harmonic content was significant to the sixth harmonic of the BPF (Sanders and Fleeter, 1999; Probasco, et. al, 1998). Sanders speculated that shock reflections off of adjacent vanes generated this higher harmonic content, as discussed in section 1.2. The results of the current study, using only one IGV, validate this assumption. Therefore, using an isolated IGV in the current study is advantageous by eliminating PFF and shock reflections encountered in previous studies which used multiple IGV. This becomes significant in the resolution of the IGV wake profiles in the unsteady total pressure investigation in the next section.

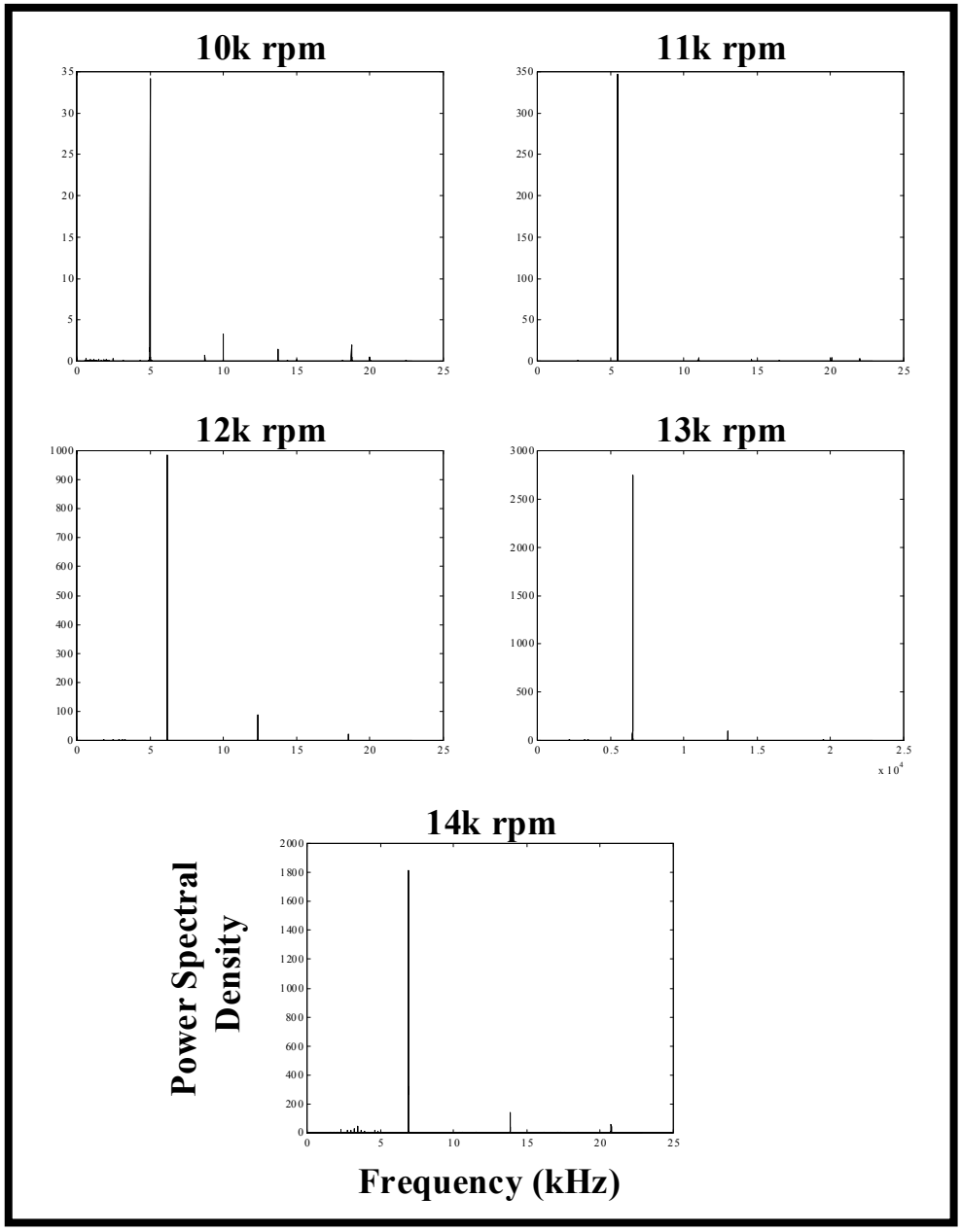

Figure 4.6 Power Spectral Density of on-blade measurements

Comparison of IGV surface pressure fluctuations relative to downstream OGV

The final objective of the on-blade measurements is to determine if the downstream OGV PFF is detectable at the IGV trailing edge, as discussed previously. Therefore, measurements were performed at each fan speed with the IGV located between two of the downstream OGV and directly upstream of an OGV. The pressure fluctuations measured on the IGV trailing edge become increasingly sporadic with increasing fan speed, making it impossible to determine if the pressure fluctuations differ at the two IGV circumferential locations. This is due to the inherent random unsteadiness in engine testing, especially for the transonic fan speeds. Therefore, it is necessary to ensemble average the unsteady data in order to determine if the PFF of the OGV is detected at the IGV trailing edge. The ensemble averaging technique is discussed in section 4.1.1. It was determined that 100 ensemble averages, averaged over one fan revolution, was adequate in removing the random pressure fluctuations in the signals. The difference between 100 and 200 ensembles was negligible.

Ensemble averaging of the unsteady pressure data removes the random unsteady content from the signals generated by local flow instabilities. The resulting ensemble averaged P-P amplitudes of the pressure signals are therefore reduced when compared to the raw data, as shown in Fig. 4.5. The reduction in amplitude is especially evident for the transonic fan speeds where ensemble averaging reduces the P-P amplitude of the signal by 35% at 14k rpm. Reductions in amplitude of the same order have been previously reported for upstream pressure measurements of subsonic and transonic rotors (Falk,

1998, Johnston and Fleeter, 1998). Figure 4.7 shows the raw unsteady pressure fluctuations compared to the 100 ensemble averaged data for the 11k subsonic fan speed. The resulting ensemble average reduces the amplitude of the raw signal, while preserving the phase and waveform well.

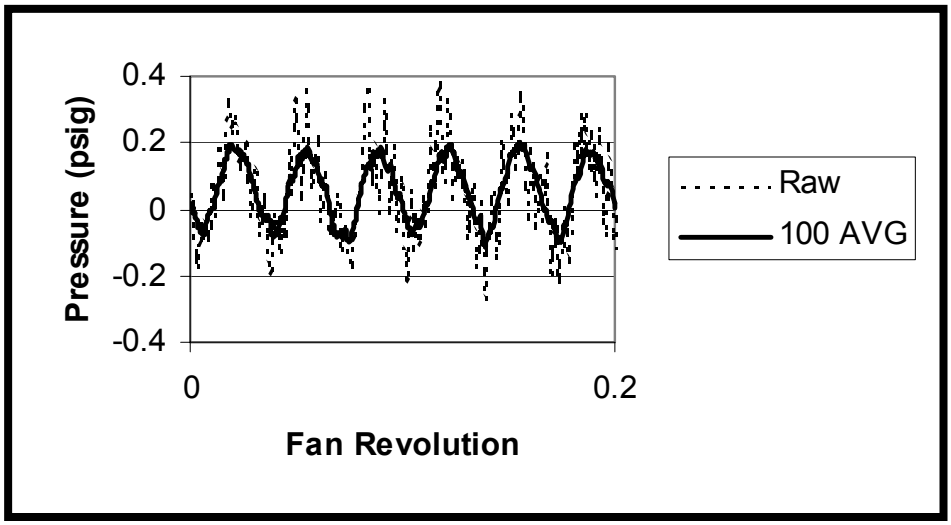

Figure 4.7 Raw versus 100 ensemble averages over 0.2 fan revolutions at 11k

Figure 4.8 shows the raw unsteady pressure fluctuations compared to the 100 ensemble averaged data for the 12k transonic fan speed. The resulting ensemble average reduces the amplitude of the raw signal, while preserving the phase well. However, the ensemble averaging does not accurately preserve the step generated by the passing shocks in the raw data, as shown in the figure. This is an unfortunate consequence of ensemble averaging pressure signals generated by transonic rotors, as the passing shocks are highly unsteady, showing slight random variance in phase for each fan blade from revolution to

revolution (Johnston and Fleeter, 1998). However, without ensemble averaging the data, a direct comparison between measurements could not be made.

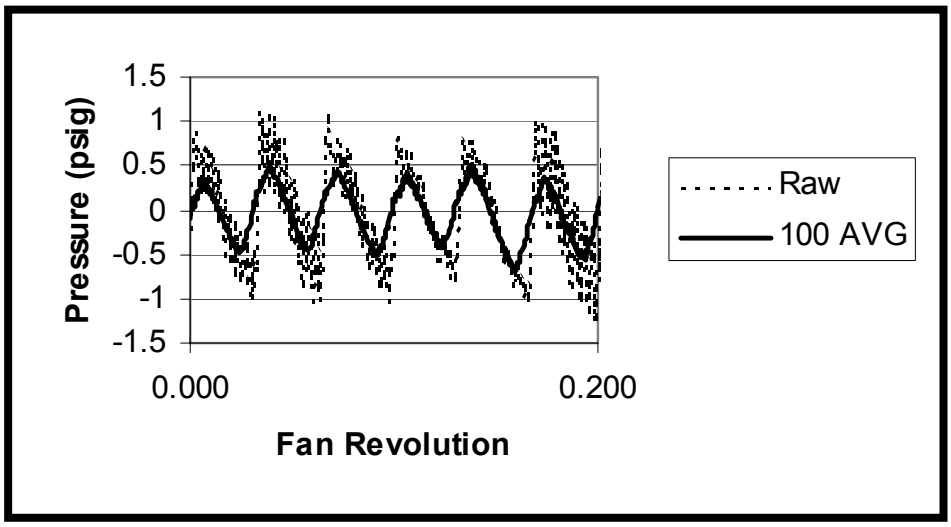

Figure 4.8 Raw versus 100 ensemble averages for 0.2 fan revolutions at 12k

The ensemble averaged pressure fluctuations at the IGV trailing edge located between (BT) and directly upstream (US) of the downstream OGV are shown in Fig. 4.9 for the entire fan revolution. Results show no detectable influence of the OGV on the upstream IGV for both subsonic and transonic fan speeds. Therefore, when the IGV is indexed in the Phase II experiments, only disturbances from the downstream fan will impact the IGV surface. Figure 4.9 also shows the repeatability of both the pressure measurements and the ensemble averaging technique. Finally, these results show distinct variations in amplitude and phase between the pressures fields generated by each fan blade. These results are consistent for each fan speed measured. For instance, the pressure signals for

the fourth and seventh blades in the figure have larger amplitudes than the neighboring blades, which is consistent for all measurements. These repeatable variations are attributed to slight geometry differences, due to the manufacturing tolerances, between each fan blade.

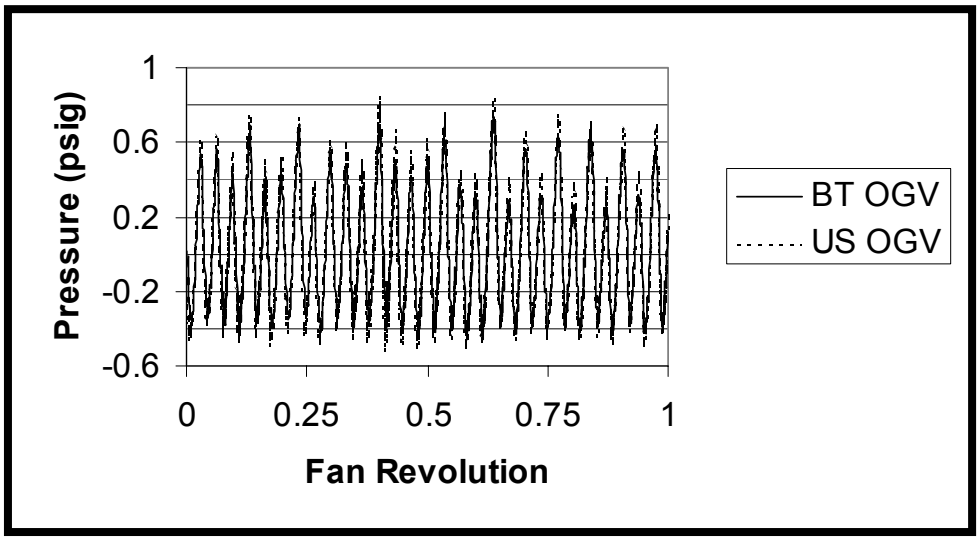

Figure 4.9 Comparison between (BT) and upstream (US) OGV at 13k rpm

4.2 High-Frequency Total Pressure Probe

High frequency total pressure measurements were performed with a Kulite pressure transducer mounted between the IGV and fan, with the measuring head facing **upstream** toward the IGV and the on-coming inlet flow, as discussed in section 2.3. The custom made 0.1 in head XWC-065 Kulite is recessed one diameter into the probe. The probe is mounted at a radial immersion of 1.1 in (2.8 cm) from the engine cowling. The probe sensor head is located 0.15 IGV chords downstream of the IGV, and 0.26 fan chords upstream of the fan leading edge, as shown in Fig. 4.10. The probe is fixed to the engine casing, therefore the IGV is circumferentially indexed between runs in order to resolve the IGV wake in the pitchwise (x) direction. The IGV trailing edge is located 0.43 fan chords upstream of the fan, which is in the typical range of IGV-fan spacings in modern military engines. The rotor leading edge is at an axial distance of 0.4 IGV chords downstream of the IGV. Total pressure measurements are performed for both the no flow control and TEB flow control cases. These measurements are performed at fan speeds of 10k and 11k rpm (subsonic), and 12k, 13k, and 14k rpm (transonic). These fan speeds correspond to 70, 77, 85, 90 and 100% maximum fan speed, respectively.

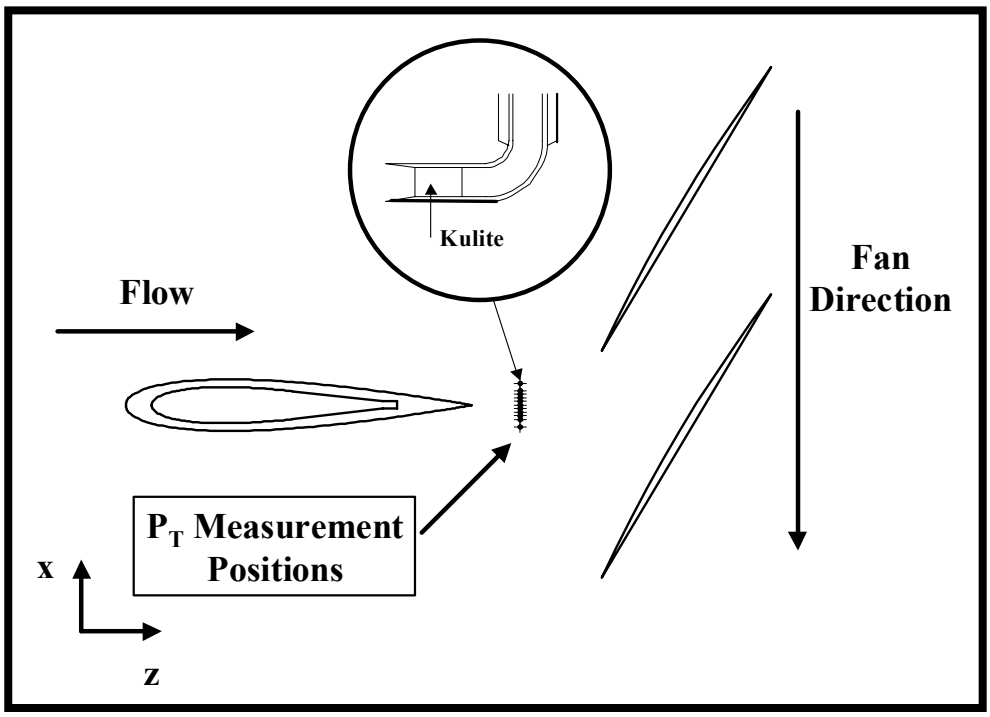

Figure 4.10 Unsteady total pressure measurements

The following sections will first present the data reduction techniques used in the Phase II investigation, which includes the description of a unique method for reducing the unsteady IGV wake profiles. The results and discussion of the time averaged and unsteady IGV wake measurements are presented in sections 4.2.2 and 4.2.3 for subsonic and transonic relative fan blade velocities, respectively.

4.2.1 Data Reduction

The voltage signals from the Kulite pressure transducer embedded in the total pressure probe are divided into the DC and AC components, as discussed in section 2.3.1. The DC component is used to determine the time averaged IGV wakes. The filtered AC

component is used to determine the unsteady total pressure fluctuations and is acquired with the high speed LeCroy Waveform DAQ system. The signal from the one-per-revolution fiber-optic trigger is acquired simultaneously with the AC signal. The data are acquired at a sampling frequency of 500 kHz, over a period of 0.262 seconds, which corresponds to approximately 50 fan revolutions per acquisition. For each measuring location and fan speed tested, four data sets are acquired. The unsteady pressure fluctuations are phase locked and ensemble averaged over 100 fan revolutions. The ensemble averaging technique is discussed in section 4.1.1.

Initial total pressure measurements were performed with a clean inlet, i.e. no IGV, for the five fan speeds tested. The time averaged inlet total pressure was obtained from the DC component of the Kulite signal, as discussed in section 2.3.1.5. Reduction of the AC signal components showed strong unsteady pressure fluctuations at the BPF, with P-P amplitudes as high as 7 psi for the highest fan speed tested. These pressure fluctuations are the result of the upstream propagating PFF and passing shocks from the subsonic and transonic fan, respectively. Therefore, the Kulite in the total pressure probe, which is facing upstream, is sensing the unsteady static pressure fluctuations of the PFF and shocks at each blade pass, as shown in Fig. 4.11.

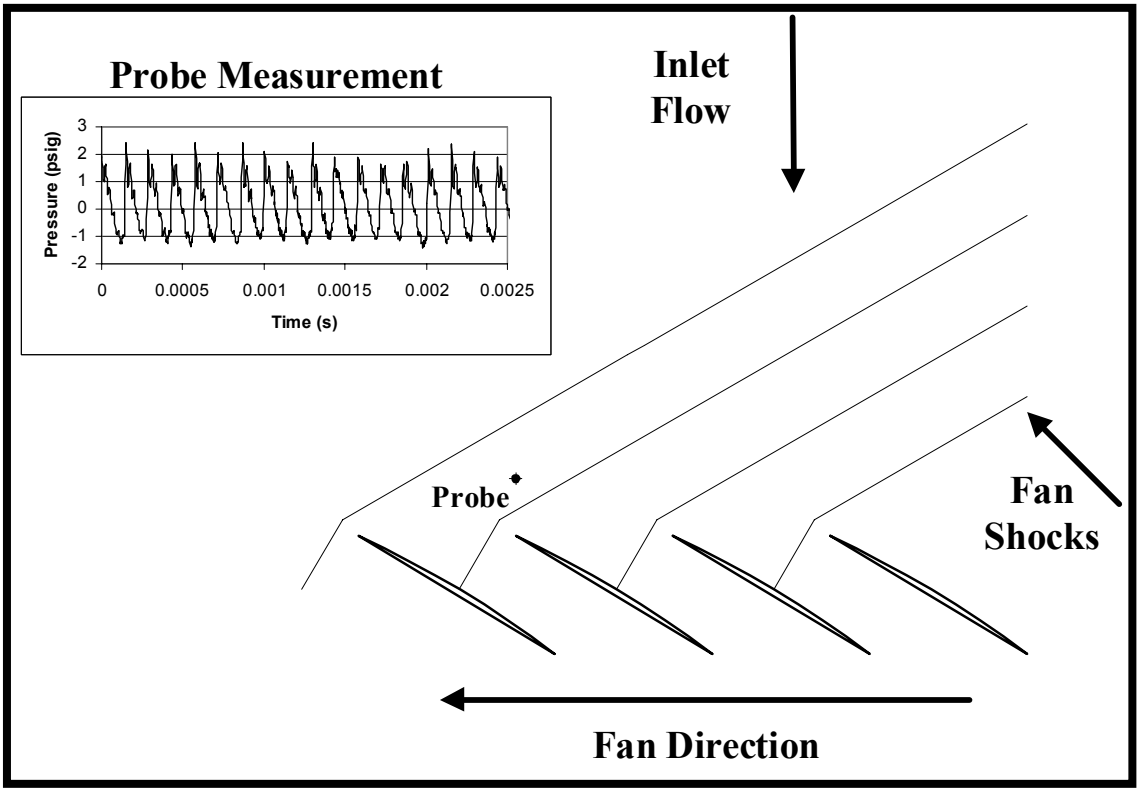

Figure 4.11 Shocks passing over total pressure probe in clean inlet

In the next step in the experiment, the IGV is placed onto the inlet and wake measurements are taken with the total pressure probe. The time averaged total pressure deficit in the IGV wake region is determined from the DC component of the Kulite signal. However, the AC component of the Kulite signal is a combination of the unsteady IGV wake fluctuations coupled with the fan passing PFF or shocks, as shown in Fig. 4.12.

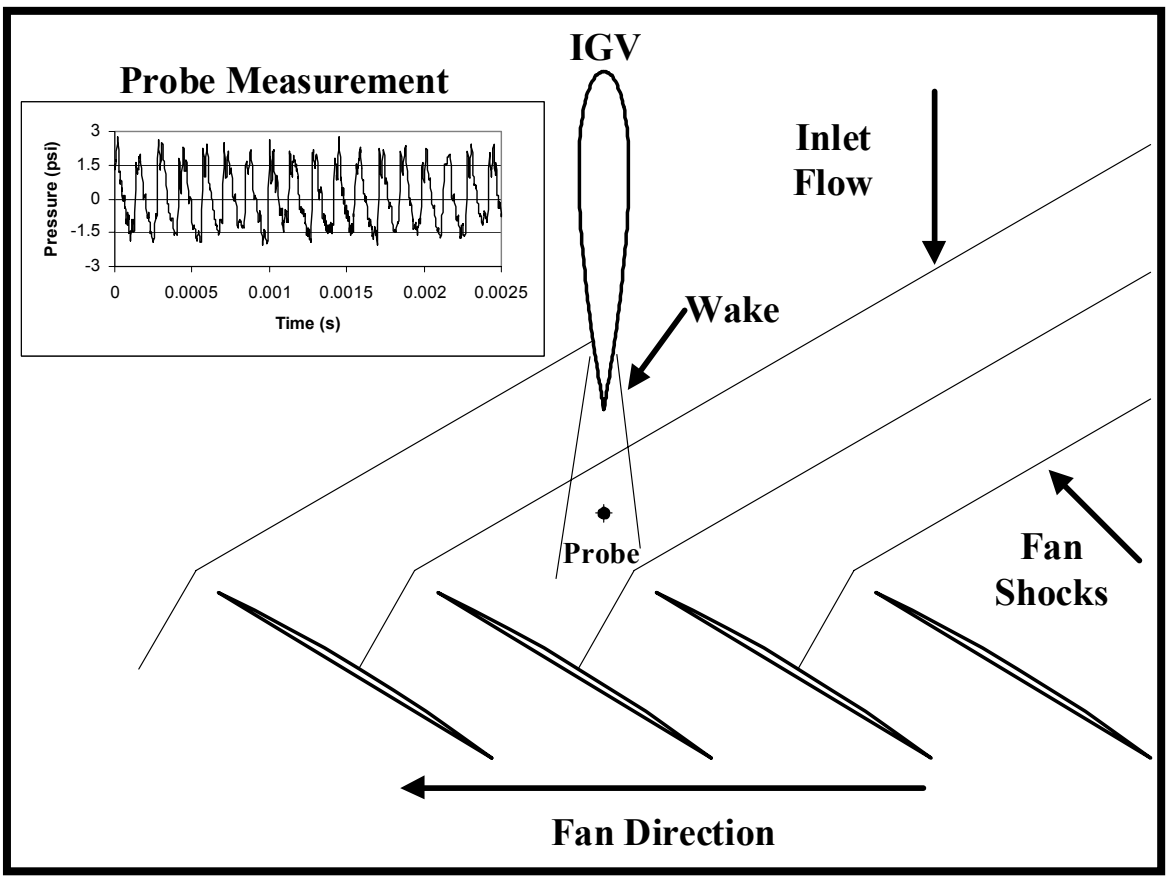

Figure 4.12 IGV unsteady wake coupled with passing rotor shocks

In order to resolve the unsteady wake profiles of the IGV, the raw signal containing the wake data and the passing shock fluctuations must be uncoupled. Previous studies have shown that the subsonic fan PFF and the transonic fan passing shocks propagate upstream at an angle relative to the rotor direction, as discussed in section 1.2. Therefore, the shock waves or potential flow waves that pass over the probe do not interfere with either the IGV surface or the IGV wake, as shown in Fig. 4.13. In other words, the probe does not obstruct the path of the passing shocks that effect the unsteady wake profile of the IGV. Therefore, the unsteady pressure fluctuations from the shock/potential waves

passing over the probe is added to the incoming unsteady wake fluctuations at each point in time.

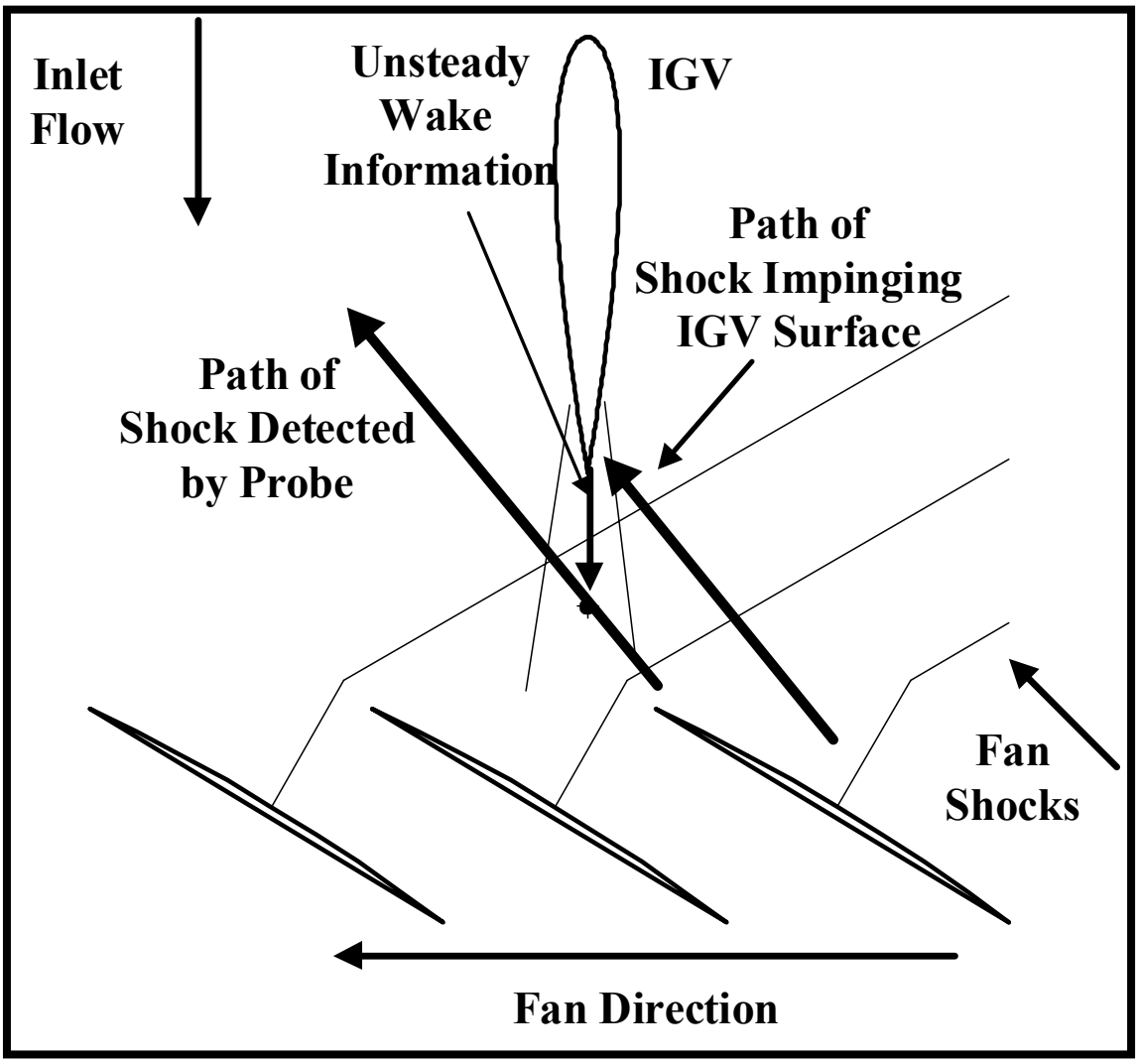

Figure 4.13 Shock and wake directions relative to total pressure probe

In order to accurately uncouple the shock/potential waves passing over the probe from the unsteady wake profile, the signals have to be ensemble averaged. The ensemble

averaging is employed for the same reasons discussed in the Phase I investigation. Since the shock/potential waves passing over the probe are independent of the information from the unsteady wake profile, the shock/potential waves can be subtracted out of the signal at each point in time for a given pressure-time trace in the wake region. Therefore, the ensemble averaged pressure fluctuations from the clean inlet measurements, as shown in Fig. 4.11, are subtracted from the ensemble averaged total pressure measurements in the wake region at each point in time for a given pitchwise measuring location, as shown in Fig. 4.14. The resulting pressure fluctuations are the unsteady wake information over one fan revolution.

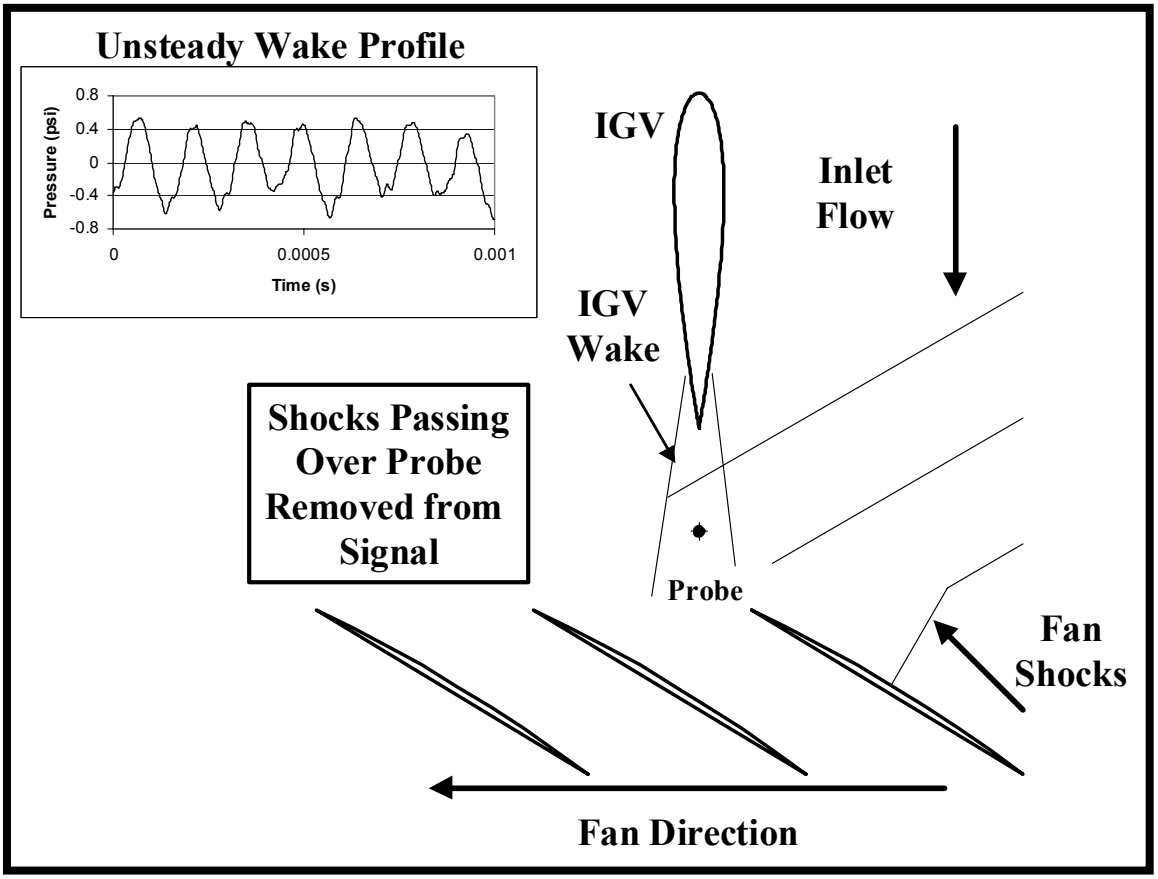

Figure 4.14 Uncoupled unsteady IGV wake at a given measuring location

In order to resolve the unsteady wake profiles spatially, the pressure signals at each measuring location are phase locked to each fan revolution. The probe and the reflective tape on the spinner (FOT) are fixed throughout the Phase II experiments. The IGV and IGV ring are indexed circumferentially between runs to measure different pitchwise locations, as shown in Fig. 4.10. At each of the pitchwise measuring locations, the FOT initiates the data acquisition at the same exact fan position, regardless of the IGV position. Therefore, at t = 0 in each data set, the fan is fixed relative to each pitchwise

measuring location. The pitchwise profile of the unsteady wake can then be resolved for each point in time relative to the fan position.

Summary of Resolving the Unsteady Wake Profiles

The unsteady pressure fluctuations for a clean inlet, with no IGV, are measured, phase locked and ensemble averaged for each fan speed tested. The IGV is then indexed to each pitchwise measuring location where the pressure fluctuations are measured, phase locked and ensemble averaged. The unsteady pressure fluctuations from the clean inlet measurements, which are comprised of passing shock/potential waves only, are subtracted from each of the pitchwise signals at each point in time over one fan revolution. The unsteady wake profiles are then obtained over the entire pitchwise measuring range for each point in time over one average blade pass.

4.2.2 Clean Inlet Investigation

Initial unsteady total pressure measurements were conducted with a clean inlet, i.e. no IGV, with the probe sensing head located 0.26 C_F upstream of the fan. Measurements were conducted at subsonic relative fan speeds of 10 and 11k rpm, and transonic relative fan speeds of 12, 13 and 14k rpm. Since there are no obstructions upstream of the probe location, the time averaged inlet total pressure is equal to the atmospheric pressure. The unsteady pressure profiles measured with the probe detect the upstream propagating potential flow and shock waves from the subsonic and transonic fan, respectively, as shown in Fig. 4.11. Results showed high amplitude pressure fluctuations with maximum P-P amplitudes of 1.4 psi and 7 psi for the 11k and 14k rpm fan speeds, respectively. These correspond to 10 and 50% of the inlet total pressure. Probasco, et. al, (1998) also found maximum pressure amplitudes as high as 7 psi for the same measuring location, relative to the rotor chord, in the transonic compressor rig at CARL, as discussed in section 1.2. **These results demonstrate how severe the upstream propagating forcing function, generated by the fan passing shocks, would be on an IGV located 0.26 C_F upstream of the fan, which is a typical IGV-fan spacing in new engine designs.**

The average P-P pressure amplitudes for the raw and ensemble-averaged data are shown in Figure 4.15, for the fan speeds tested. The average amplitudes for the raw data correspond to 3.5, 5.0, 9.8, 19.8, and 28.9% of the inlet total pressure for each fan speed. The ensemble averaging reduces the average pressure amplitudes, with a maximum

reduction of 30% at 14k rpm, which is the same as those observed in the Phase I investigation.

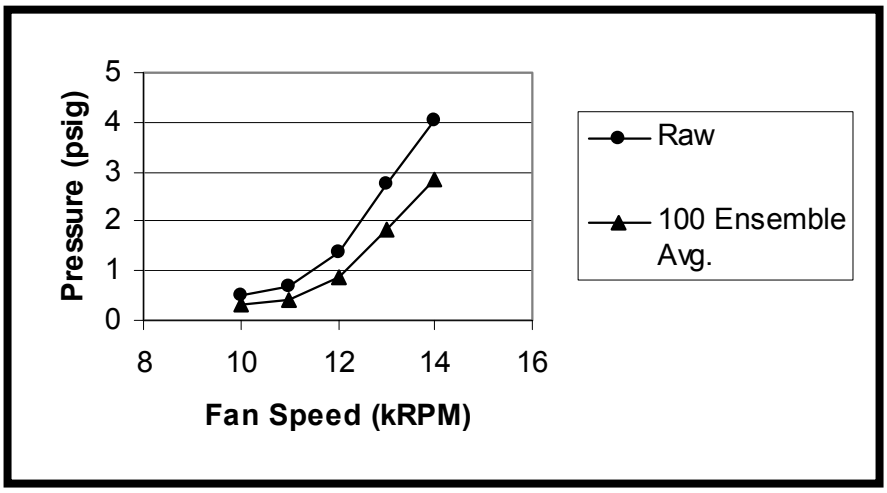

Figure 4.15 Average P-P pressure fluctuations with clean inlet

The power spectral density (PSD) of the unsteady pressure signals at 14k rpm is shown in Fig. 4.16. The fundamental frequency for the pressure signal is the blade passing frequency, with smaller higher order harmonics of the BPF, similar to the PSD figures of the on-blade measurements. This result shows that decreasing the measuring location relative to the fan does not significantly increase the higher harmonic content of the pressure fluctuations. Probasco, et. al, (1998) reported that the significance of higher harmonic content of IGV surface pressure measurements increased with decreased axial spacing. However, this study used multiple IGV, where only a single IGV is used in the current study. Therefore, the increased significance of higher order harmonics in the Probasco study is most likely the result of the increasing strength of the shock reflections

off of the adjacent vanes, and not the result of the axial measuring location upstream of the fan.

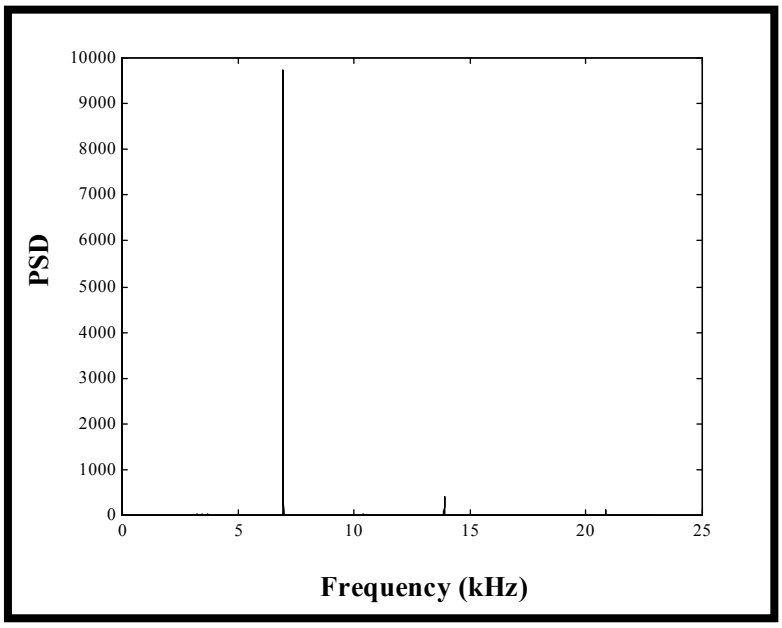

Figure 4.16 PSD at 14k rpm fan speed with clean inlet

4.2.3 Subsonic Fan

Time Averaged Wakes

The total pressure wake profiles of the IGV were measured with a high frequency P_T located between the IGV and fan, facing upstream toward the IGV, at a radial immersion of 1.1 in from the cowl for 10 and 11k rpm fan speeds. The sensing head of the probe is located 0.15 C_{IGV} downstream of the IGV trailing edge, and 0.26 C_F upstream of the fan leading edge. Since the probe was fixed to the engine casing, the IGV was

circumferentially indexed between runs to measure the wake profiles in the pitchwise direction.

The time averaged total pressure measurements of the IGV wake profiles near the fan for the subsonic fan speeds are shown in Figure 4.17. These wake profiles are compared to baseline experiments, where steady IGV wake measurements were taken with the IGV far upstream of the aerodynamic influence of the fan, which were presented in section 3.2. These results show that the wakes are compressed into the direction of the rotor by the fan's upstream propagating PFF, while the wake width of each wake is reduced by approximately 12.5% for each fan speed compared to the baseline. The maximum wake deficit for both fan speeds is 40% higher than the baseline. Furthermore, the wakes are turned approximately 0.5° into the direction of the fan when compared to the baseline. To determine the effects of the wake-PFF interaction on the average aerodynamic losses generated by the wakes, the total pressure loss coefficient is found by integrating the wake profiles, using Eq. 2.11. **The total pressure loss coefficient of the time averaged wakes was found to be 32% and 27% lower when compared to the baseline for 10 and 11k rpm, respectively.** Therefore, for subsonic relative fan speeds, close IGV-fan spacing is beneficial to the compressor stage by reducing the average aerodynamic losses generated by the IGV wakes. However, close IGV-fan spacing has a detrimental effect on the average magnitude of the forcing function (IGV wake deficit) that impinges on the downstream fan. The close spacing actually produces a 40% increase in the magnitude of the forcing function compared to the baseline, which may significantly increase rotor

blade loading, leading to HCF failures. This further demonstrates the need to investigate the effectiveness of TEB flow control for typically close IGV-rotor spacings.

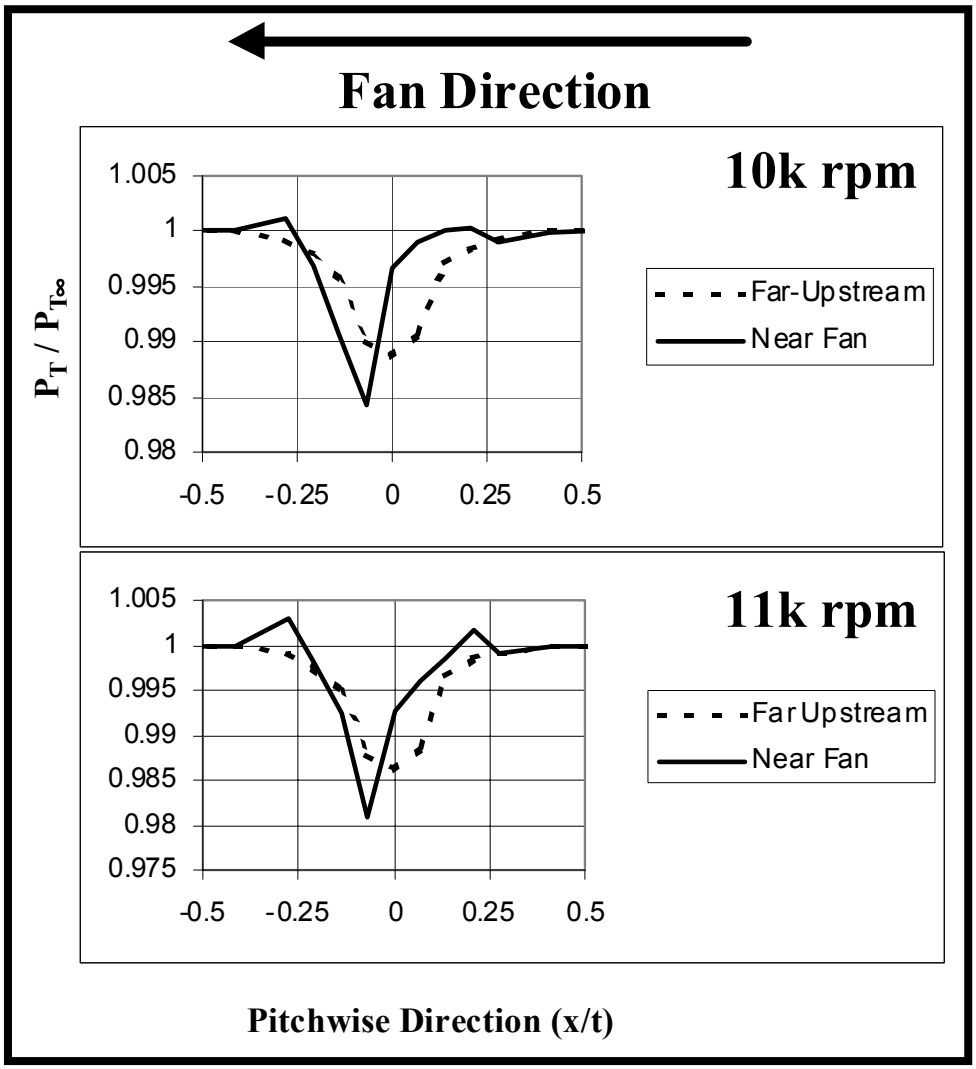

Figure 4.17 Time averaged P_T wake profiles at subsonic fan speeds

Previous investigations have shown that decreased component spacing in axial compressors with subsonic rotor speeds **increases** the isentropic efficiency of the stage, as discussed in section 1.2 (Mikolajczak, 1976; Smith 1970). Smith (1996, 1966) has attributed 25-50% of this gain to "wake recovery", the reversible inviscid wake attenuation caused by the wakes passing through (between) the downstream blade rows. The wake recovery theory characterizes the attenuated wake profiles as simultaneously being compressed in the pitchwise direction while "stretching" in the flow direction (larger wake deficit) when passing through the downstream blade row. Even though the wake deficit is increased, the compression in the pitchwise direction produces an overall wake profile with less aerodynamic losses, thereby increasing the isentropic efficiency of the stage.

The results of the current study show IGV wake attenuation **before** the wake passes through the downstream blade row. The IGV wake profile is consistent with the wake recovery theory characteristics, i.e. compressed in the pitchwise direction and stretched in the axial direction. Furthermore, the aerodynamic losses are reduced significantly compared to the baseline wake. **Therefore, these results show that reversible wake recovery is occurring due only to the fan PFF interaction with the IGV wakes.** Several previous investigations have studied the effects of the PFF from downstream stators on the wakes of upstream rotors. In the most recent study, Wo, et. al, (1999) showed that the rotor wake deficit is reduced by the downstream stator PFF in a low speed compressor rig. However, the wake attenuation was the result of axial

compression of the wake, not the pitchwise compression of the wake seen in the current study for the IGV. In the rotor-stator wake-PFF interactions, the PFF of the stator is fixed in the axial direction upstream from the stator leading edge; therefore the rotor wakes are compressed in the axial direction. However, in stator-rotor wake-PFF interactions, the rotor PFF propagates upstream along a curve in the direction of the rotor (Falk, 1998), interfering with the side of the wake facing into the rotor direction, thereby compressing the wake in the pitchwise direction. Therefore, the PFF-wake interactions between stator-rotor are not analogous to the interactions between rotor-stator. To the author's knowledge, the current study is the first to show that wake recovery occurs in the freestream due to the upstream propagating PFF interactions of a rotor with the wakes of an upstream stator. The only previous study that measured the wakes of IGV upstream of a subsonic rotor at close spacing (Johnson and Fleeter, 1996 and 1998) did not report measuring a baseline wake, i.e. outside of the rotor aerodynamic influence. Therefore, that study did not address the effects of the fan PFF on average wake shape or losses.

Unsteady Wake Profiles

This section will first compare the results of the current study with a very similar previous investigation. The method for reducing the unsteady wake profiles in that study will be employed for the current results and compared. An improved method for resolving the unsteady IGV wake profiles will then be employed for the current results, as discussed in section 4.1.1. The results of this unique method will then be presented and discussed.

The interaction of a rotor's upstream propagating PFF on upstream stators at close spacing has only recently gained attention, as discussed in section 1.2. Therefore, there is a very limited amount of information regarding the unsteady effects of the rotor PFF on the wakes generated by upstream stators. The investigations by Johnson and Fleeter (1996, 1998), discussed in section 1.2, provide the only published measurements of IGV wakes located at close proximity to a downstream subsonic rotor. That study measured the total pressure wake profiles of the IGV with a high frequency probe located between the IGV and rotor under similar conditions to the current study. Fleeter reported that the rotor unsteady PFF interacts constructively and destructively with the IGV wake over each blade pass. The constructive interference increased the wake deficit and width, while the destructive interference produced the opposite effect. This conclusion was reached by time resolving the minimum and maximum unsteady wake profiles.

Figure 4.18 shows the average level of pressure unsteadiness in the Fleeter studies for close IGV-rotor spacing as measured with as total pressure probe. The minimum and maximum wake profiles were obtained by taking the average min/max pressure observed at each of the pitchwise locations measured using the ensemble-averaged data. Using this method for the results in the current study, Fig. 4.19 shows the average maximum, mean and minimum IGV wake profiles for the 11k rpm fan speed. These results agree well with the results from Fleeter, in that the magnitude of the unsteady pressure fluctuations are increased in the wake region when compared to the fluctuations outside of the wake.

In other words, the unsteadiness in the wake region is greater than that measured in the surrounding flow.

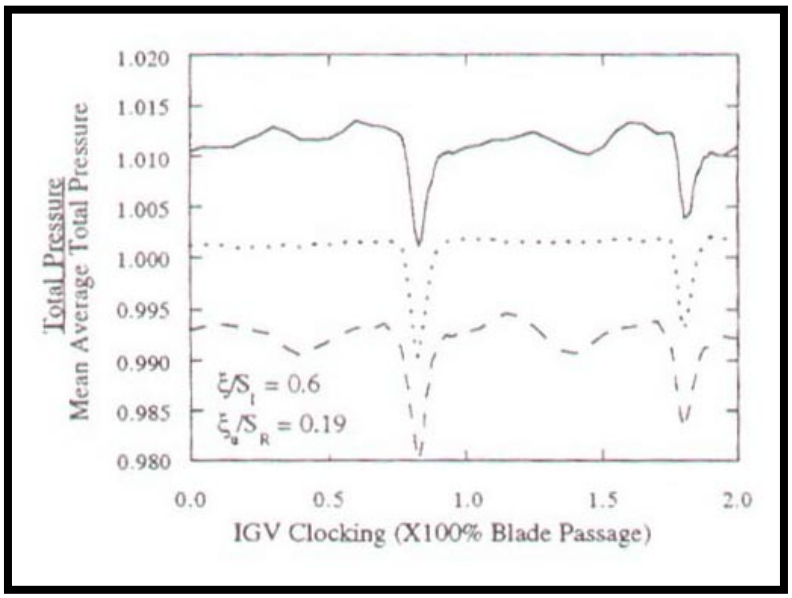

Figure 4.18 Average excursions about the mean (Johnson and Fleeter, 1996)

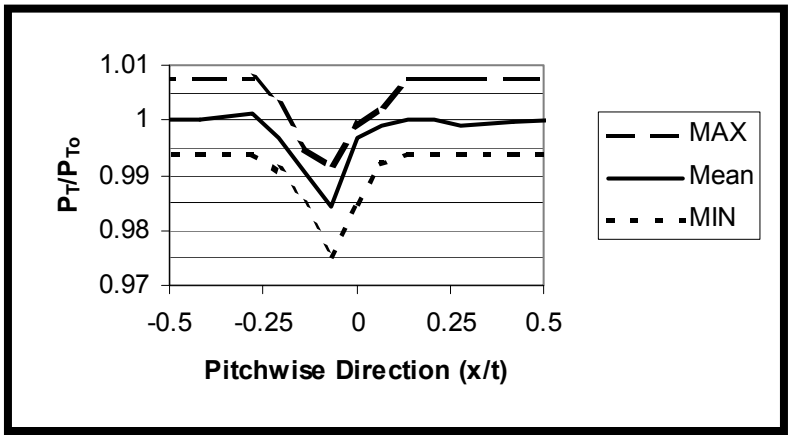

Figure 4.19 Average excursions about the mean in the current study at 11k rpm

In order to obtain the unsteady wake profiles in the pitchwise direction, the pressure signals have to be time resolved. This is done by taking one point in time from each of the pitchwise measuring locations, which are phase locked to the rotor relative position and ensemble averaged. These points are then resolved into a spatial wake profile at one point in time, an example of which is shown in Fig. 4.20. Note that the normalized total pressure signals are offset for the example and the actual number of pitchwise locations used in the study is greater than shown.

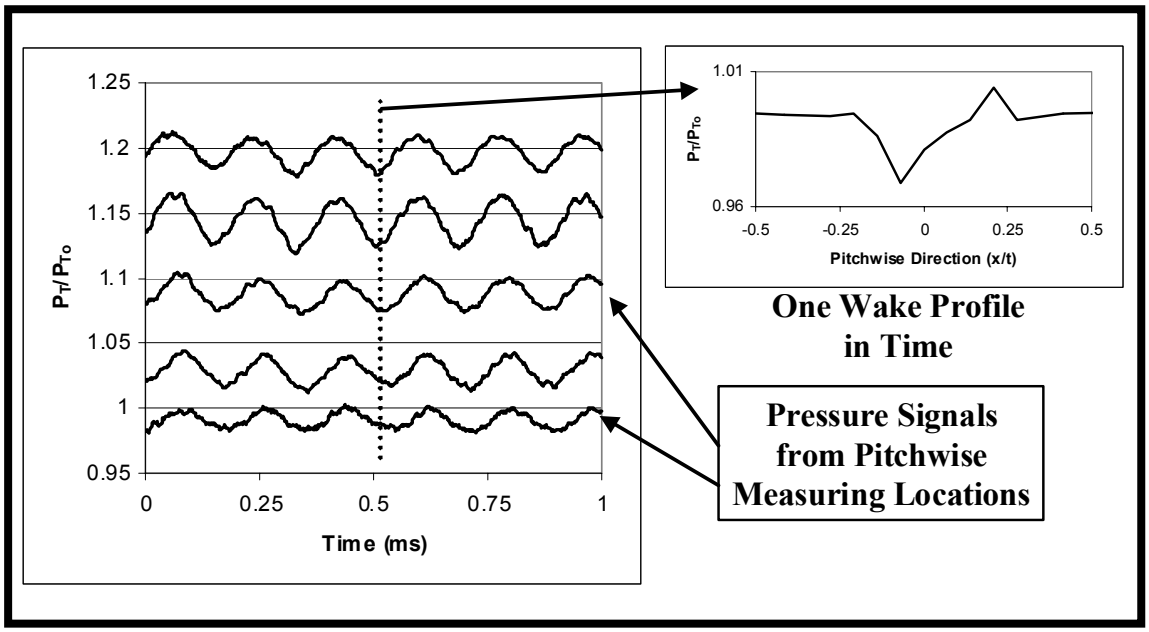

Figure 4.20 Example of time resolved wake profile at one instant in time

Fleeter's conclusion that the rotor PFF destructively and constructively interacts with the IGV wake was drawn from the time resolved wake profiles, which showed a maximum and minimum in the wake deficit over one blade pass, as shown in Fig. 4.21 from that study. Using this method, the destructive and constructive interference of the IGV wake in the current study is shown in Fig. 4.22 at 11k rpm. These results clearly show the constructive and destructive interference of the fan PFF on the IGV wakes as defined by Fleeter.

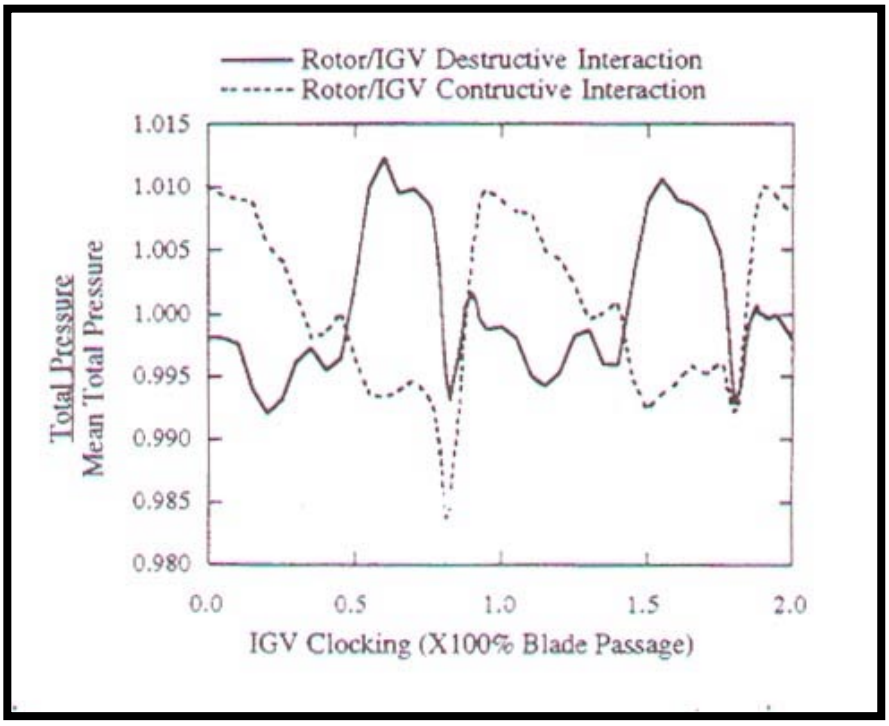

Figure 4.21 Rotor PFF destructive and constructive interaction with IGV wake (Johnson and Fleeter, 1998)

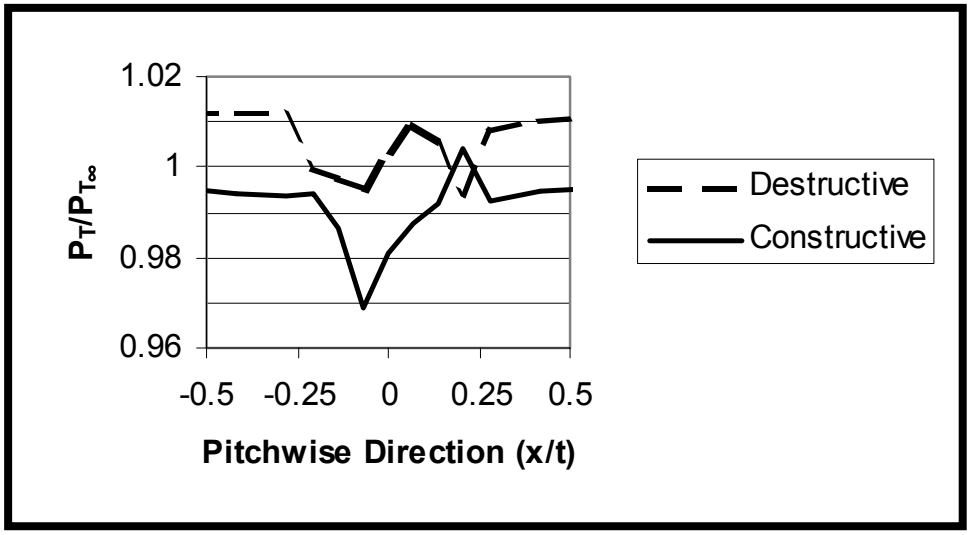

Figure 4.22 Fan PFF destructive and constructive interaction with IGV wake (Current Study)

The problem with time resolving the wake profiles in this fashion is that the static pressure from the fan's potential flow waves passing over the probe are added to the total pressure measurements in the wake region at each point in time, as discussed in section 4.1.1. The results from the clean inlet measurements, presented previously, showed that pressure fluctuations were passing over the probe at the fan BPF. Therefore, the pressure fluctuations measured by the probe in the wake region are a combination of the upstream passing PFF and the unsteady wake measurements. This is evident from Figures 4.20 and 4.22, which are from the current study. The pressure fluctuations in the freestream, outside the wake region, are identical in amplitude and phase to the pressure fluctuations measured with the clean inlet. Therefore, the freestream flow and the IGV wakes are not actually oscillating in this fashion with each blade pass. Assuming that the unsteadiness

in the clean inlet measurements is due only to the passing PFF, the normalized total pressure in the freestream should be equal to unity regardless of the fan position. This assumption is based on the fact that the amplitude of the unsteady fluctuations measured with the probe in the clean inlet agreed well with previously reported on-blade and casing mounted pressure measurements taken at the same axial location relative to the fan, as discussed in section 2.1. Therefore, in order to accurately resolve the unsteady wake profiles, the phase-locked ensemble-averaged measurements from the clean inlet are subtracted from each of the phase-locked ensemble-averaged pitchwise measurements downstream of the IGV, in each point in time, before the wakes are time resolved; as described in detail in section 4.1.1.

Figure 4.23 shows the average P-P amplitudes of the ensemble-averaged pressure fluctuations at each pitchwise location, after subtracting out the pressure fluctuations from the clean inlet, as described above. Note that the maximum P-P amplitude occurs at the x/t = +0.21 pitchwise location, and is substantially larger than the other amplitudes. It is believed that this is caused by a potential wave reflection off of the IGV surface, which will be discussed further in the following paragraph. By using the improved method, the unsteadiness of the pressure fluctuations in the freestream flow is removed and the normalized total pressure is reduced to unity. Furthermore, the unsteadiness in the wake region is well preserved. Discounting the P-P amplitude at x/t = +0.21 (wave reflection), the unsteadiness in the wake region is shown to be greatest at the pitchwise location corresponding to the largest wake deficit, x/t = -0.07. The unsteadiness then decreases to

either side of this location until it is reduced to zero outside of the wake region, i.e. in the freestream. Therefore, the unsteadiness in the wake, caused by the fan PFF, is at a maximum at the location corresponding to the maximum wake deficit, and decays at each pitchwise measuring location away from the maximum.

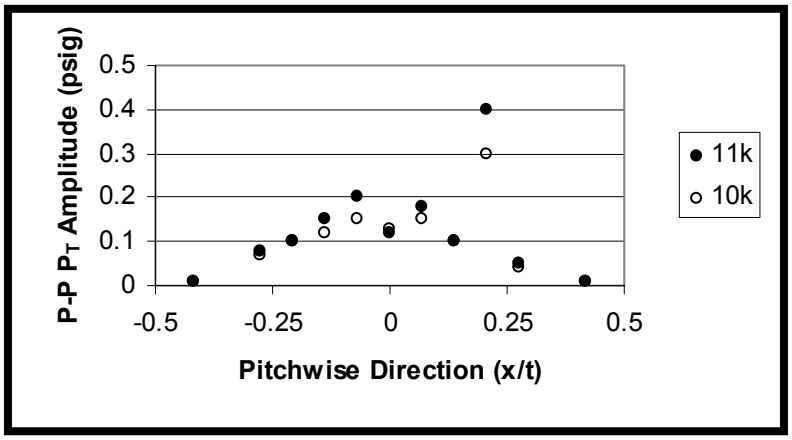

Figure 4.23 Average P-P pressure amplitude in wake region

Using the improved method for time resolving the total pressure wake profile, the wakes with the smallest and greatest wake deficit over an average blade pass are shown in Fig. 4.24 for both fan speeds tested. These results clearly show that the PFF from the fan destructively and constructively interferes with the IGV wakes with each blade pass. These results also show a fluctuation in pressure at the x/t = +2.1 pitchwise measuring location, which is consistent for both fan speeds. It is believed that this is due to a potential wave reflection off of the IGV surface at each blade pass, which is directed downstream into the probe. This assumption is based on the fact that the time averaged

normalized total pressure at this location does not indicate any losses in the flow, and that the total pressure is greater than unity at the maximum value of the fluctuation.

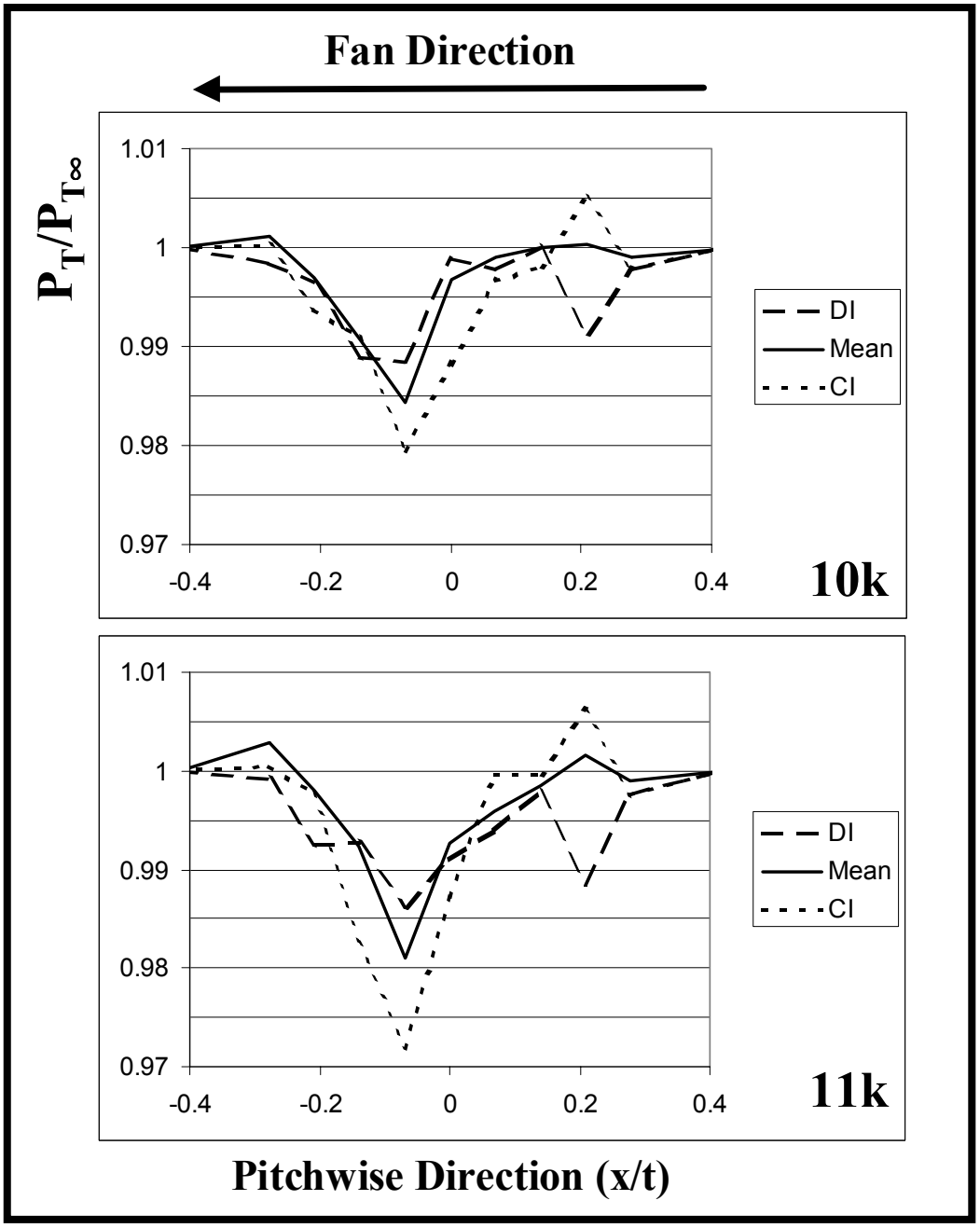

Figure 4.24 Destructive (DI) and constructive (CI) interference of the IGV wake

The results of the time resolved wakes on the previous page show that the constructive interference increases both the wake deficit and wake width. The destructive interference reduces the wake deficit, but does not substantially increase or decrease the wake width. The total pressure loss coefficient, Eq. 2.11, is reduced by 7% and increased by 40% for the destructively (DI) and constructively (CI) interfered wakes when compared to the time-averaged wake for both speeds. However, the forcing function (IGV wake deficit) is increased by 34% and 48% for the CI wakes when compared to the time-averaged wake for 10k and 11k rpm fan speeds, respectively. This corresponds to an 84% and 100% increase in the forcing function when compared to the baseline wake. The forcing function of the DI wakes is reduced by 24% and 27% when compared to the time-averaged wake for 10k and 11k. These correspond to the same magnitude as the forcing function of the baseline case, within 1%. Therefore, depending on which of these wake profiles impacts the rotor, or perhaps a profile in between, the forcing function on the downstream fan blades would be between the same and twice that of what is predicted by measuring the wake of an isolated vane.

During the placement of the fiber-optic sensor, the reflective tape was positioned on the spinner so that the trigger would initiate the DAQ when the leading edge of one particular fan blade was at the 12 O'clock position, directly downstream of the total pressure probe, as discussed in section 2.3.1.4. Therefore, the relative position of each fan blade to both the probe and IGV trailing edge was known in time for each of the measurements. In order to interpret these results, the behavior of the fan PFF must be understood.

A previous investigation of the upstream propagating PFF in the F109 engine showed that the potential waves travel upstream from the fan leading edge, along a curve, in the direction of the fan rotation, propagating upstream at the local sonic velocity, as discussed in section 1.2 (Falk, 1998). In other words, the maximum potential wave magnitude generated by a fan blade is detected upstream before that blade passes, and the minimum potential wave magnitude is detected after one-half a blade passage from the maximum. The maximum potential wave generates an increased pressure resistance to the incoming inlet flow, where the minimum potential wave produces a decreased resistance. Therefore, it is assumed that the time-resolved destructive interference of an incoming wake is due to this increased resistance of the maximum fan PFF before the potential wave-generating fan blade passes. The time-resolved constructive interference is then due to the reduced resistance after one-half a blade passage after the DI is observed.

Results from the clean inlet measurements show that the maximum pressure from the PFF occurs when the fan blade leading edge is 55.5° from the IGV trailing edge relative to the flow direction. In other words, the fan PFF is traveling into the wake at 34.5° relative to the fan direction, which is consistent for both fan speeds. Since the potential waves travel upstream along a curve in the direction of the rotor, this angle may differ when measuring at a different axial spacing. Figures 4.25 and 4.26 show the direction of the PFF, and the relative fan blade position to the IGV and probe at the instant in time

corresponding to the DI and CI wake profiles for the 10k and 11k rpm fan speeds, respectively. These results show that as the leading edge of a fan blade approaches the IGV wake, the upstream propagating potential wave destructively interferes with the wake. This is consistent for both fan speeds tested. The constructively interfered wake occurs between the maximum potential waves, after one-half a blade passage after the DI profile is observed. This is consistent for both fan speeds tested. It appears from these results that the CI wake, which has the maximum wake deficit, is ingested into the fan passage (between blades), which is the path of the least flow resistance. Therefore, it is speculated that the forcing function on the downstream fan blade suction surface is that of the time resolved wake profile with the maximum magnitude (wake deficit). If this is the case, the forcing function on the downstream fan is twice that predicted from the baseline wake measurements. This would suggest that the forcing function prediction codes based on linear cascade wake measurements and empirical wake correlations are under-predicting the magnitude of the forcing function on the fan, for typical IGV-fan spacing at subsonic relative fan speeds.

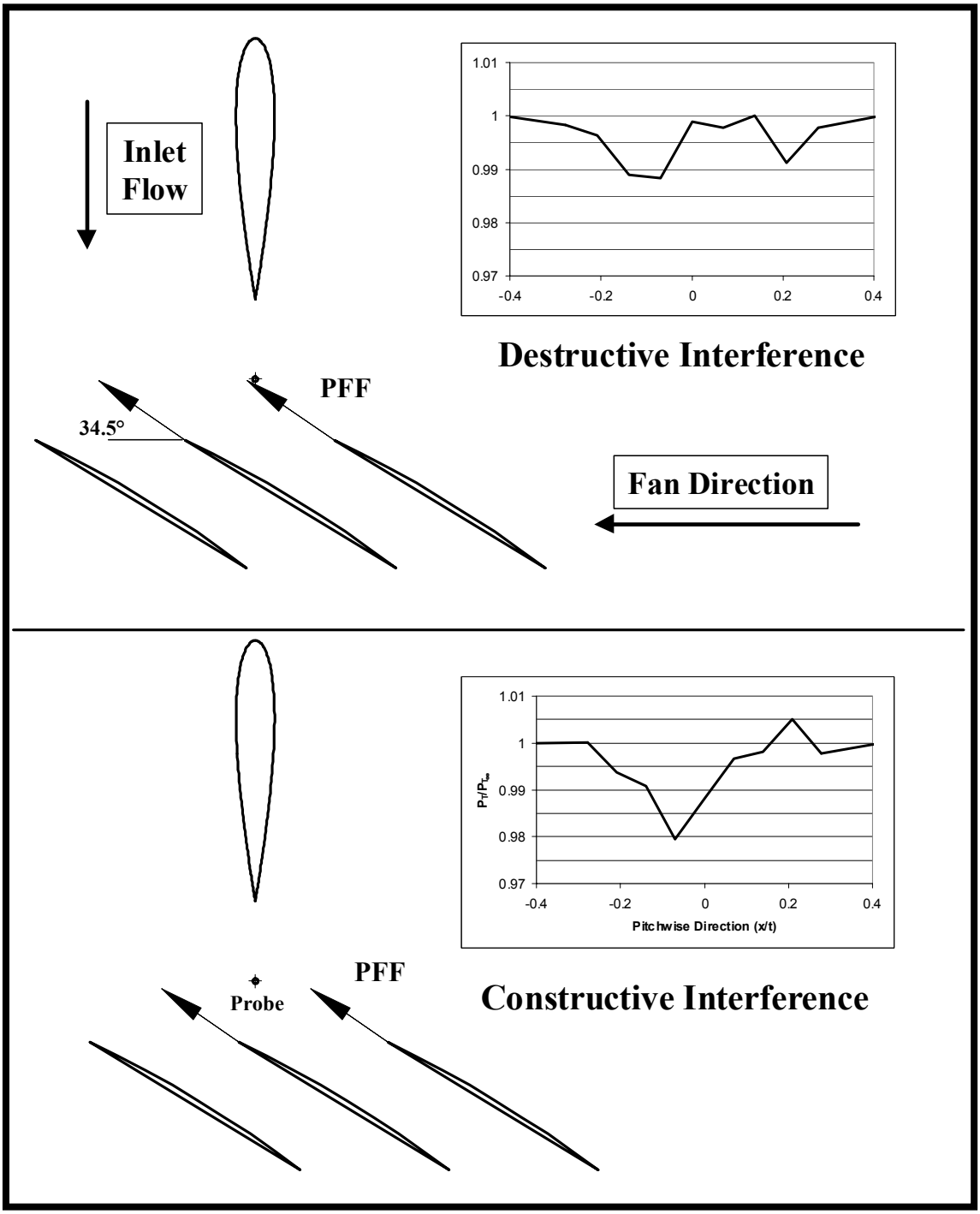

Figure 4.25 Relative position of fan for DI and CI, 10k rpm fan speed

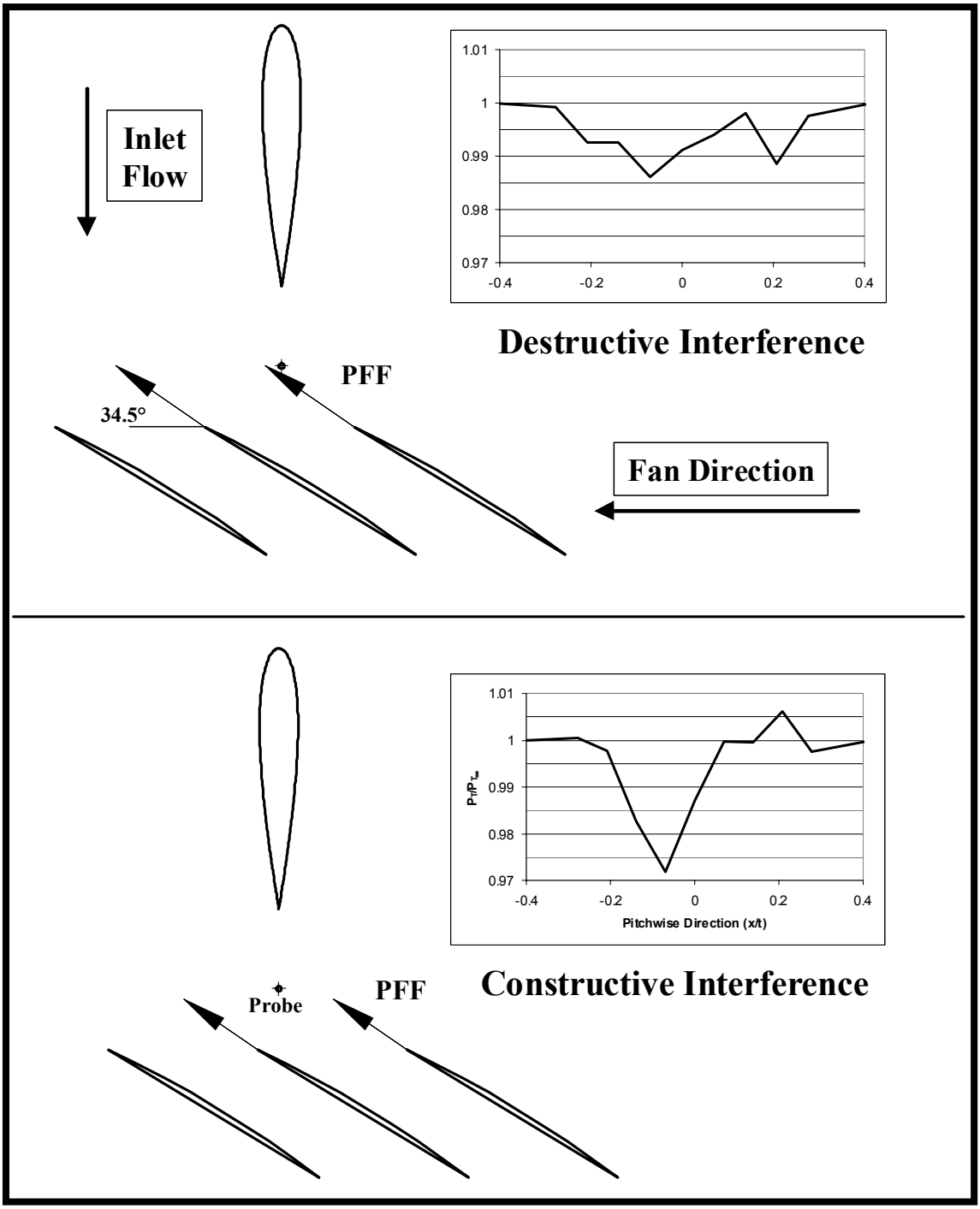

Figure 4.26 Relative position of fan for DI and CI, 11k rpm fan speed

In order to show the unsteady behavior of the wake over one fan blade pass, various points in time are chosen from the pressure-time trace at the pitchwise measuring location corresponding to the greatest wake deficit in the time-averaged wake. Figure 4.27 shows the pressure-time trace for one averaged blade pass at x/t = -0.7. Eight points in time are chosen, as indicated by the circles, which correspond to t = 0, 0.125, 0.25, 0.375, 0.5, 0.625, 0.75, and 0.875 as a fraction of one blade pass. The points t = 0.25 and 0.75 correspond to the DI and CI cases, respectively.

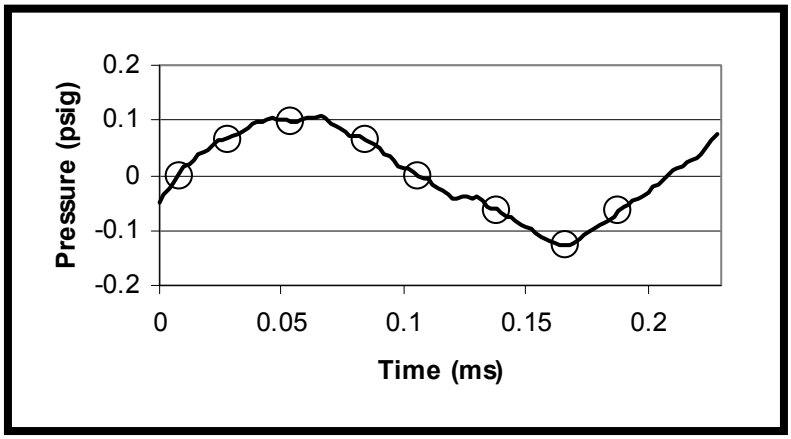

Figure 4.27 Points in time for one fan blade pass at x/t = -0.7

The time resolved wake profiles for one blade pass are shown in Fig. 4.28 over the positions in time described above for the 11k rpm fan speed. The triangle marks on the pitchwise axis represent the location of the fan blade leading edge relative to the pitchwise measuring locations at each instant in time. Note that the pitchwise axis is stretched outside of the measuring range (±0.5) in order to show the relative fan blade

positions. The normalized total pressure outside the measuring range was assumed to be unity. The same wake profiles are shown in Figure 4.29 over the actual measuring range. The wake with the minimum deficit, DI, and maximum deficit, CI, are shown at t = 0.25 and 0.75, respectively, which are the same wakes shown in Fig. 4.26. The destructive interference of the IGV wake begins at t = 0.875 as the next fan blade approaches, the wake deficit begins to decrease and the wake width begins to increase. The DI continues to reduce the wake deficit and increase the wake thickness at t = 0 and 0.125, reaching a maximum interference at t = 0.25 where the wake deficit is at the minimum value and the wake width is at a maximum. The wake profile at t = 0.125 is a combination of the IGV wake and the assumed potential wave reflection off of the IGV surface, and therefore is not a split wake. The constructive interference of the wake begins at t = 0.375 where the wake deficit begins to increase and the wake width begins to decrease. Even though the fan blade is still approaching the IGV wake measured upstream, the strength of the potential wave is waning. In other words, at this point the maximum potential wave has passed the wake region in the direction of the fan. The wake deficit growth continues for t = 0.5 and 0.625. At t = 0.75 the CI reaches a maximum, where the wake deficit is at the maximum level and the wake thickness is at a minimum. At t = 0.875, the process begins to repeat for the next blade pass. These results clearly show that the IGV wake is highly unsteady over each fan blade pass due to the interaction of the wake with the fan PFF. Both the wake deficit and wake widths are shown to vary over the fan blade pass.

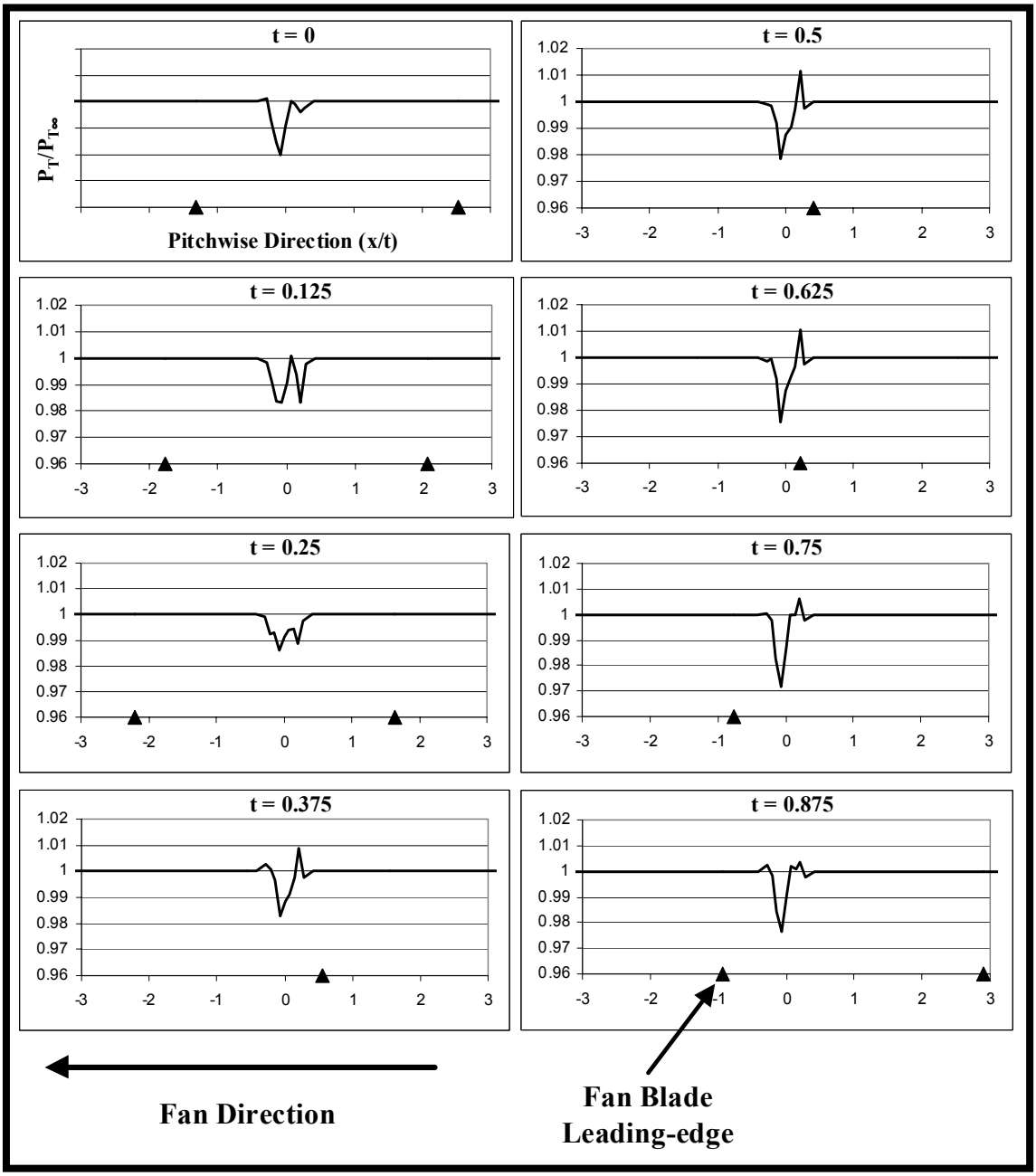

Figure 4.28 Time resolved wake profiles over one fan blade pass at 11k rpm with fan blade relative position

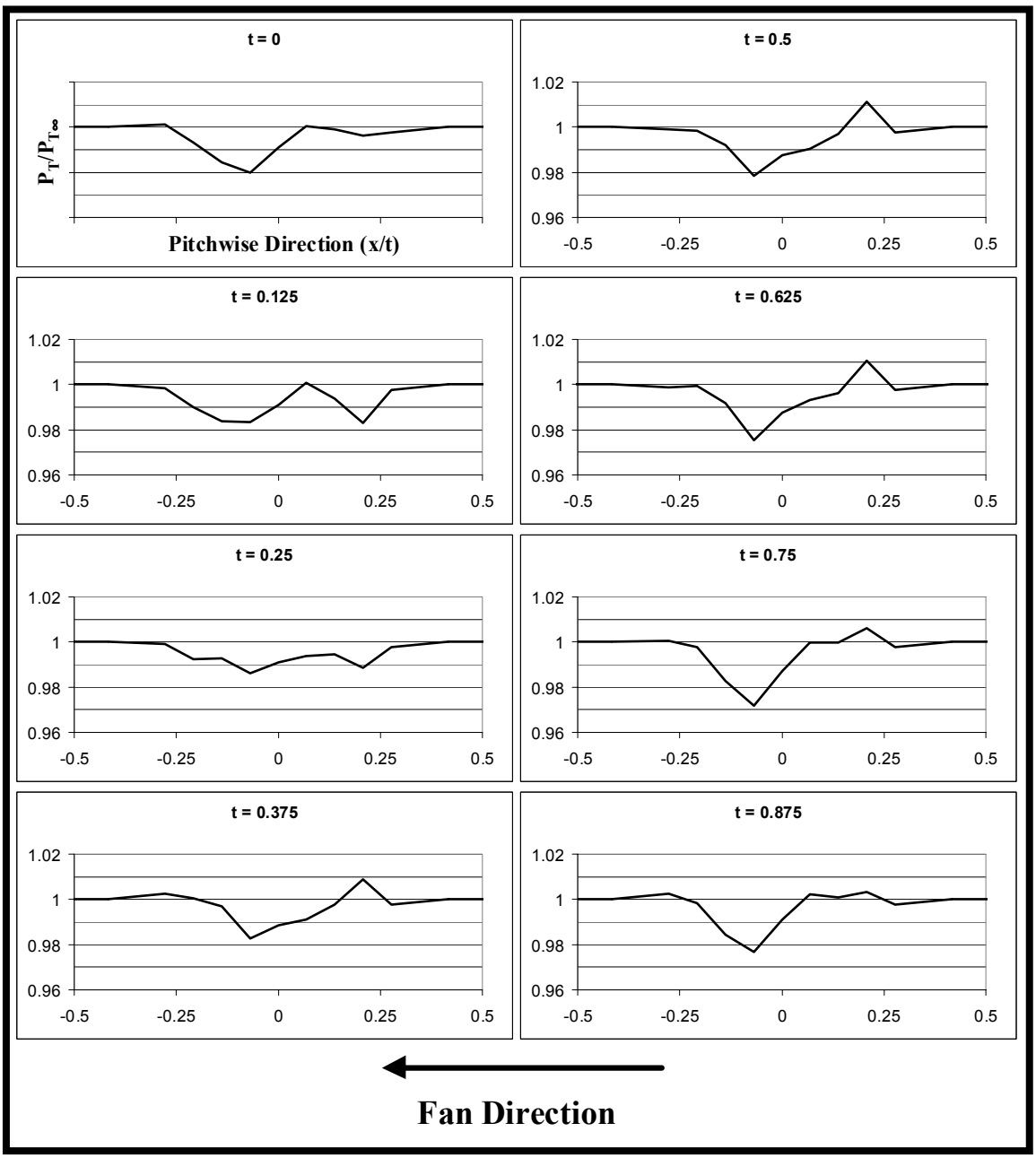

Figure 4.29 Time resolved wake profiles over one fan blade pass at 11k rpm

Since one of the goals of the current study is to investigate TEB flow control between a closely spaced IGV-fan, the results presented in this section suggest possible limiting factors in the effectiveness of TEB to reduce the total pressure deficit in the IGV wake. The fan PFF has been shown to compress the time-averaged wake in the pitchwise direction and turn the wake in the direction of the rotor. Therefore, the direction of the TEB jets may deviate from the direction of the wake. Furthermore, the time resolved wake profiles show that the fan PFF destructively and constructively interferes with the IGV wake width and deficit. The IGV wake has been shown to be unsteady over each fan blade passing. Therefore, it is not known whether the TEB jets will respond to this unsteadiness.

4.2.4 Transonic Fan

Using the same set-up and procedures at the subsonic fan measurements, both time averaged and unsteady wake measurements were performed for fan speeds of 12k, 13k and 14k rpm, which are transonic relative to the fan blade velocity. These correspond to 85, 90 and 100% of the maximum fan speed, respectively. The testing set-up and procedures are found in section 2.3.3. To the author's knowledge, this is the first published experimental study to investigate the unsteady wake profiles of an IGV placed at a typical spacing to a downstream transonic fan.

Time Averaged Wakes

The time averaged total pressure measurements of the IGV wake profiles near the fan for the transonic speeds are shown in Fig. 4.30. These wake profiles are compared to the baseline experiments, where the IGV wake measurements were performed with the IGV far upstream of the aerodynamic influence of the fan, which were presented in section 3.2. These wake profiles clearly show that the IGV wake is considerably different in shape and size when compared to the baseline and those at the subsonic fan speeds, discussed previously. These results show that the fan shock interaction with the IGV wakes and surface results in IGV wake profiles with considerable increases in wake deficit and width when compared to the baseline. The maximum total pressure deficit in the time-averaged wakes is 81, 93 and 100% greater than the baseline for the 12, 13, and 14k fan speeds. The wake width is increased by 25% for each fan speed when compared to the baseline. Furthermore, the wakes are turned approximately 1° into the direction of

the fan rotation. To determine the effects of the IGV-shock and wake-shock interactions on the average aerodynamic losses generated by the wakes, the total pressure loss coefficient is found by integrating the wake profiles using Eq. 2.11. **The total pressure loss coefficient of the time averaged wakes are found to increase by a factor 1.60, 1.74 and 2.04 when compared to the baseline for 12, 13 and 14k fan speeds, respectively.** Therefore, for transonic relative fan speeds, close IGV-fan spacing is detrimental to the performance of the compressor stage by increasing the average aerodynamic losses generated by the IGV wakes. The IGV-shock and wake-shock interactions produce the opposite effect at the same close spacing as compared to the wake-PFF interactions at the subsonic fan speeds, where the aerodynamic losses were substantially reduced. The close IGV-fan spacing also has a detrimental effect on the average magnitude of the forcing function (wake deficit) for the transonic fan speeds. The close spacing produces a 100% increase in the average forcing function magnitude when compared to the baseline. A discussion of the plausible flow physics that generate these wake profiles is discussed later with the presentation of the unsteady wake profiles.

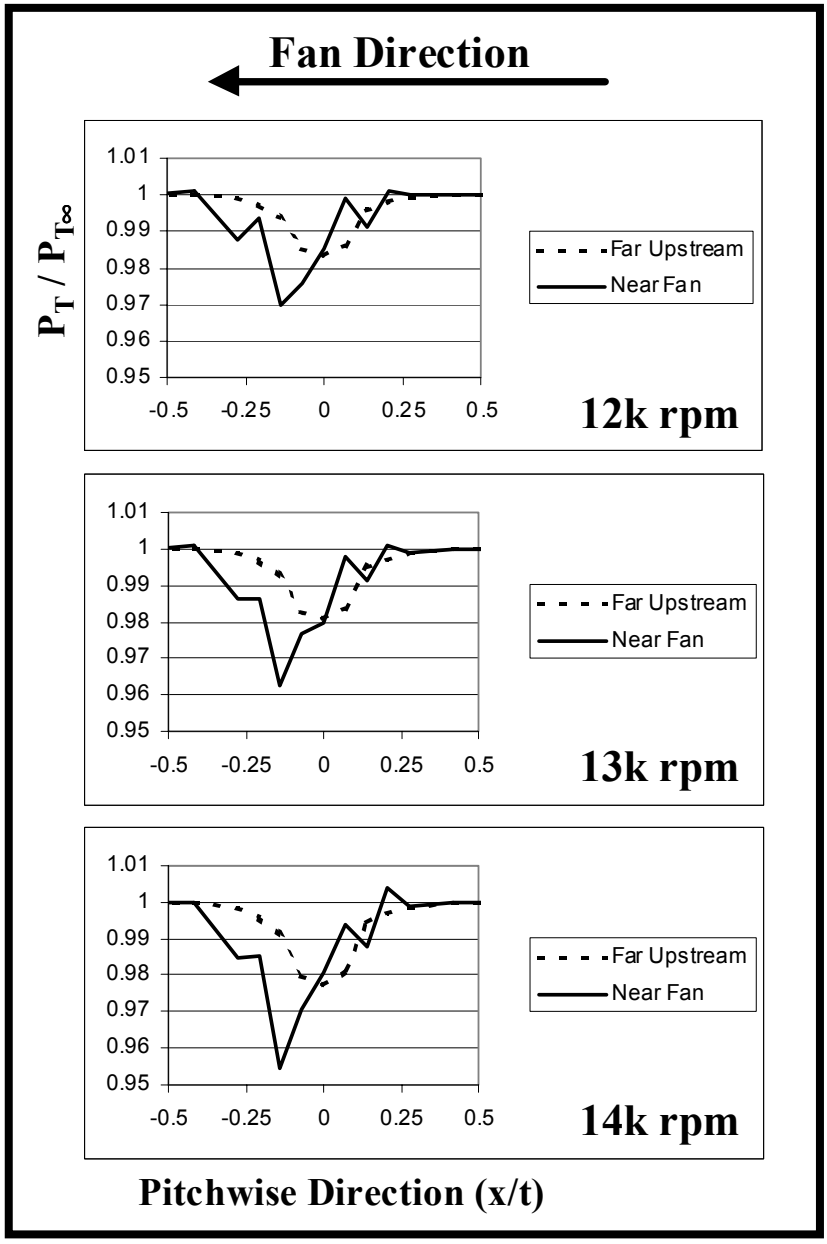

Figure 4.30 Time averaged P_T wake profiles at transonic fan speeds

As discussed in section 1.2, Gorrell and Copenhaver (1997) found that the isentropic efficiency of a 1.5 stage transonic compressor rig was significantly **decreased** with increased axial spacing between the IGV-rotor rows. These results were very surprising, drawing an incredulous response. Up until this time it was commonly believed that decreasing component spacing in axial compressors **increased** the isentropic efficiency of the stage. This belief was based on the work by Smith (1970; 1966) and others, which was previously discussed in section 2.1 and the subsonic results section. However, all of these studies were performed in compressor rigs with subsonic relative blade velocities. Therefore, after ruling out other possible sources for the decreased efficiency, Copenhaver speculated that the IGV wake-rotor shock interaction must be the cause. However, that study did not investigate the IGV wake profiles. The current study shows that the IGV wake-shock interactions with the downstream fan result in a time-averaged wake profile with total pressure loss coefficients that are a factor of 2 greater than the baseline profiles and a factor of 5 greater than those in the subsonic investigation. Therefore, this study conclusively shows that the IGV wake-shock interactions produce significantly higher aerodynamic losses in the wake region compared to the same vane location upstream of a subsonic rotor, which would subsequently reduce the stage isentropic efficiency. Although the Copenhaver study did not mention it, it should be noted that another contributing factor in the decreased efficiency might be the result of shock reflections off of the IGV surface back into the downstream rotor.

Unsteady Wake Profiles

The time resolved unsteady wake profiles were obtained using the same methods described in section 4.1.1 and were also presented with the subsonic fan results. The results of the time resolved IGV wakes will first be presented, followed by a discussion of the plausible flow physics generating these wake profiles.

Figure 4.31 shows the average P-P amplitudes of the ensemble-averaged pressure fluctuations at each pitchwise location, after subtracting out the pressure fluctuations from the clean inlet, for each of the transonic fan speeds tested. By using the improved method, the unsteadiness of the pressure fluctuations in the freestream flow is removed and the normalized total pressure is reduced to unity. Furthermore, the unsteadiness in the wake region is well preserved. The unsteadiness in the wake region is shown to be greatest at the pitchwise location corresponding to the largest wake deficit, x/t = -0.14. The unsteadiness decreases to either side of this location until it is reduced to zero outside of the wake region, i.e. in the freestream. The amplitude of the pressure fluctuations is shown to increase substantially in the wake region with increasing fan speed. Furthermore, the P-P amplitudes at the location of the maximum wake deficit, x/t = -0.14, are 10 times greater than those observed at the location of maximum wake deficit at the subsonic speeds. Therefore, the IGV wake-shock interactions generate unsteadiness in the wake that is an order of magnitude greater than the unsteadiness generated by the IGV wake-PFF interactions.

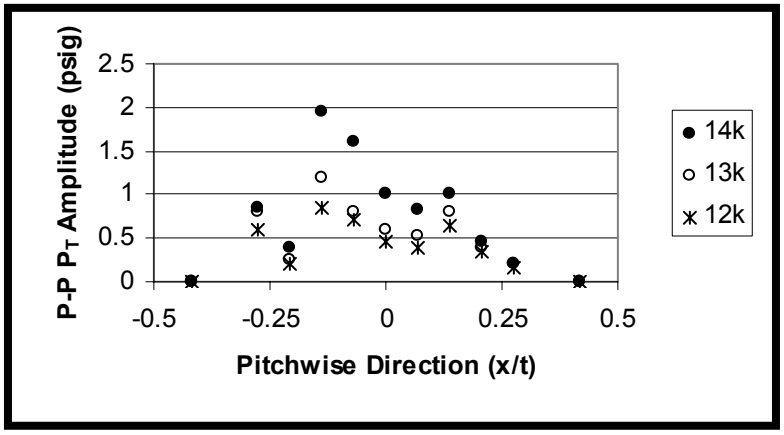

Figure 4.31 Average P-P pressure amplitudes in the IGV wake for transonic fan

Using the improved method for time resolving the total pressure wake profile, the wake profiles with the minimum and maximum wake deficit over an average blade pass are shown in Fig. 4.32 for each fan speed tested. These results show that the maximum wake profiles are substantially wider and deeper than the time averaged wake. For the 14k fan speed, the wake width is increased by 35%, and the wake deficit is increased by almost three times. Interestingly, the minimum wake profiles show very little evidence of a wake at all, with small variations in normalized total pressure about unity. A plausible explanation for this is provided in a discussion following the presentation of the results. These results also show possible shock reflections off of the IGV surface at x/t = +0.28 at 13 and 14k fan speeds.

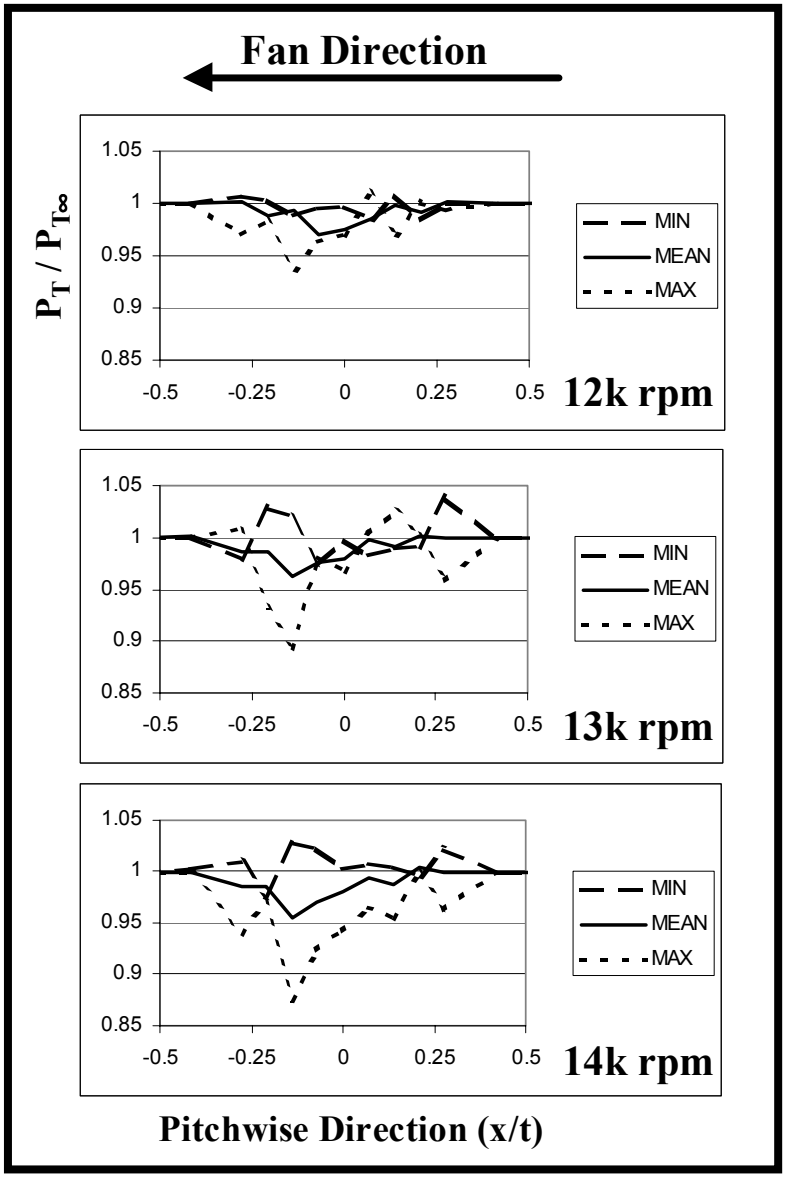

Figure 4.32 Minimum and maximum time resolved wake profiles

The time resolved wake profiles over one average fan blade pass are shown in Fig. 4.33 for the 14k rpm fan speed. The triangle marks on the pitchwise axis represent the location of the fan blade leading edge relative to the pitchwise measuring locations at each instant in time. Note that the pitchwise axis is stretched outside of the measuring range in order to show the relative fan blade positions. The normalized total pressure outside the measuring range was assumed to be unity. The same wake profiles are shown in Figure 4.34 over the actual measuring range. The profiles at t = 0.25 and t = 0.75 correspond to the points in time where the wake profiles show a minimum and maximum wake deficit, respectively, and are the same as those shown in Fig. 4.32. After the time of the maximum wake profile, t = 0.75, the wake begins to attenuate at t = 0.85. The wake continues to attenuate at t = 0 and 0.125, reaching a minimum profile at t = 0.25. After this point in time, the wake begins to either grow or develop again at t = 0.375. The wake deficit and width continue to increase until the maximum is reached again at t = 0.75. A discussion of these results follows.

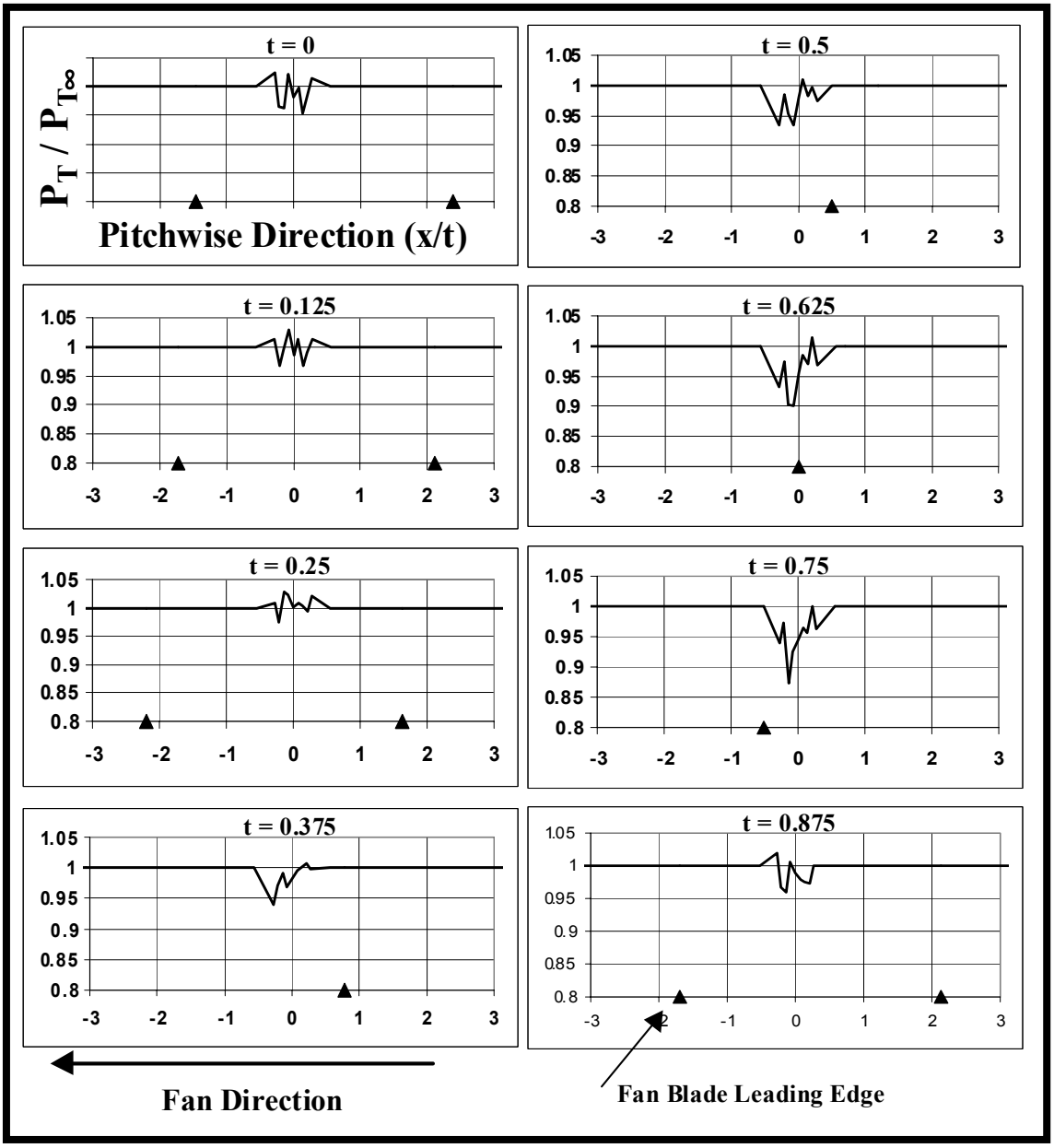

Figure 4.33 Time resolved wake profiles over one fan blade pass at 14k rpm with fan blade relative position

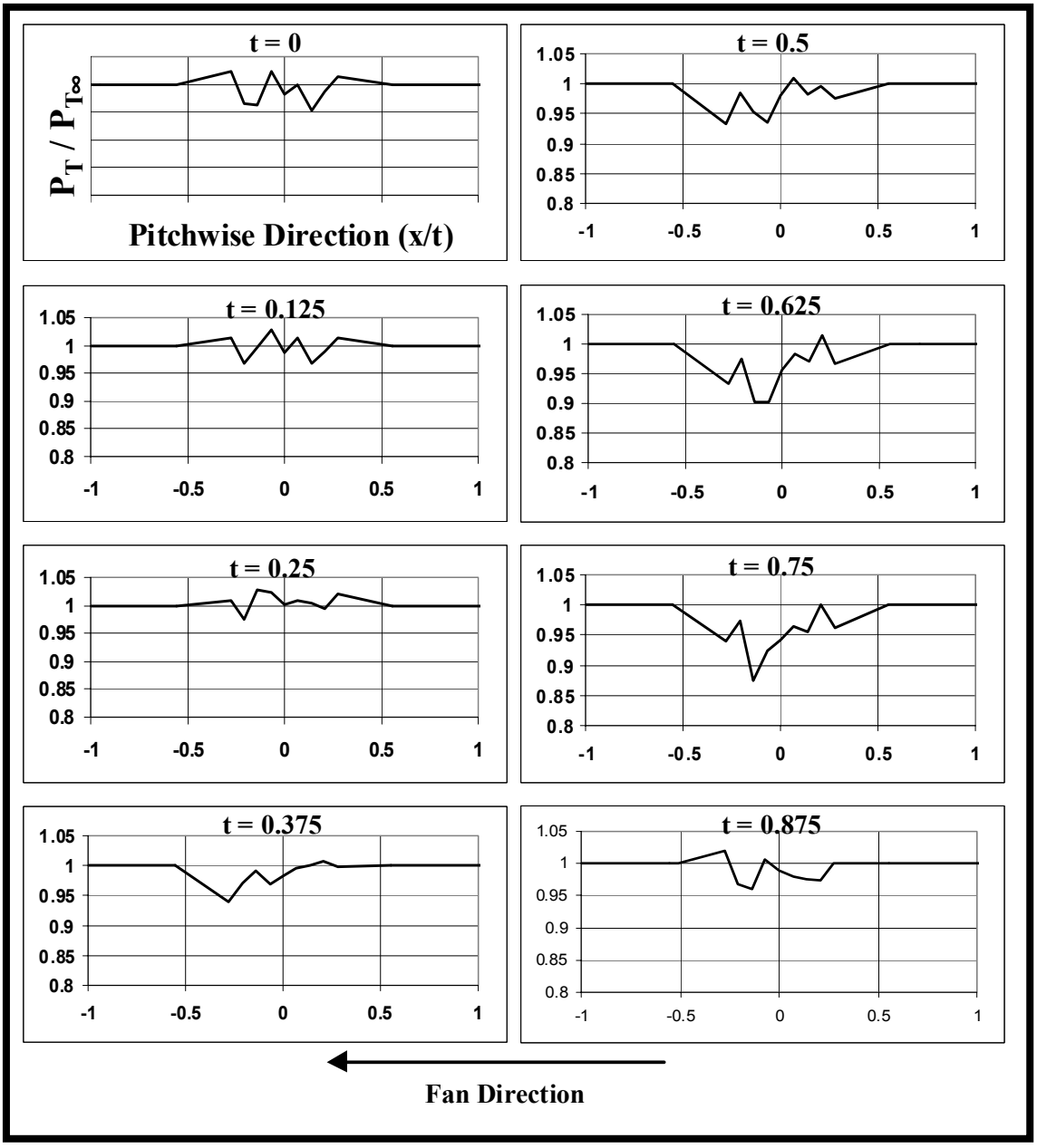

Figure 4.34 Time resolved wake profiles over one fan blade pass at 14k rpm

Discussion of Unsteady Wake Profiles

When the inlet flow is subsonic and the relative velocity of the fan blades is transonic, bow shocks form just upstream of the fan blade leading edges, extending both upstream into the inlet flow, and downstream into the neighboring blade passage, as shown in Fig. 4.11. The upstream portion of the shock wave propagates upstream at the local sonic velocity, passing at the fan BPF (Sanders and Fleeter, 1999). These shock waves have been shown to produce high amplitude pressure variations on the surface of an upstream stator, as shown in this study, Sanders and Fleeter (1999), and Probasco (1998). Pressure fluctuations as high as 4.7 psig P-P were found at the IGV trailing edge in the current study. Unlike the subsonic fan PFF, which is believed to only interact with the IGV wake, fan shock waves interact with both the IGV wake and the IGV surfaces. Unfortunately, the interactions between these shock waves and the upstream IGV surface are not well understood. Furthermore, the interaction of these shock waves with the wakes of an upstream IGV has not previously been investigated.

In a very recently published article, Sanders and Fleeter (2000) provide a brief discussion of the plausible affects of the upstream passing shock interactions on the boundary layer of an upstream IGV, based on the 1999 paper. In the 1999 study, surface pressure measurements were performed along the chord of both the suction and pressure surfaces of an IGV placed at an axial distance upstream of a transonic rotor under similar conditions as the current study, as discussed in section 1.2. The resulting pressure fluctuations were phase-locked ensemble-averaged and time-resolved. These results

seemed to indicate that once the shock wave impacts the IGV pressure surface (surface facing into rotor direction), it continues to move upstream along the IGV surface, increasing in magnitude until a maximum is reached at about 10% chord upstream from the trailing edge. At this point in time, a minimum pressure magnitude is observed at the same chord location on the suction surface, 180° out of phase with that on the suction surface. Sanders speculated that this was due to a pressure wave developing at the IGV trailing edge periodically at the fan BPF. Sanders described this pressure wave as forming at the point the shock wave reflects off of the IGV pressure surface, where a significant increase in static pressure occurs on the surface. Since the flow field around the IGV is subsonic, a pressure wave develops which "equalizes this over-pressurized zone".

An example of this is shown in Fig. 4.35 using the geometry of the current study. In the region aft of the reflection point on the IGV surface, the static pressure increases substantially, $P_2 > P_1$. The pressure wave described by Sanders would then develop in the region surrounding P_2, as shown in the figure. In the next instances in time, the shock continues to propagate upstream along the IGV surface. Although it was not mentioned in the study, in personal communication with the author, Fleeter (2000) speculates that this pressure wave separates from the trailing edge of the IGV and propagates downstream as a vortex, shedding off the vane at the fan BPF.

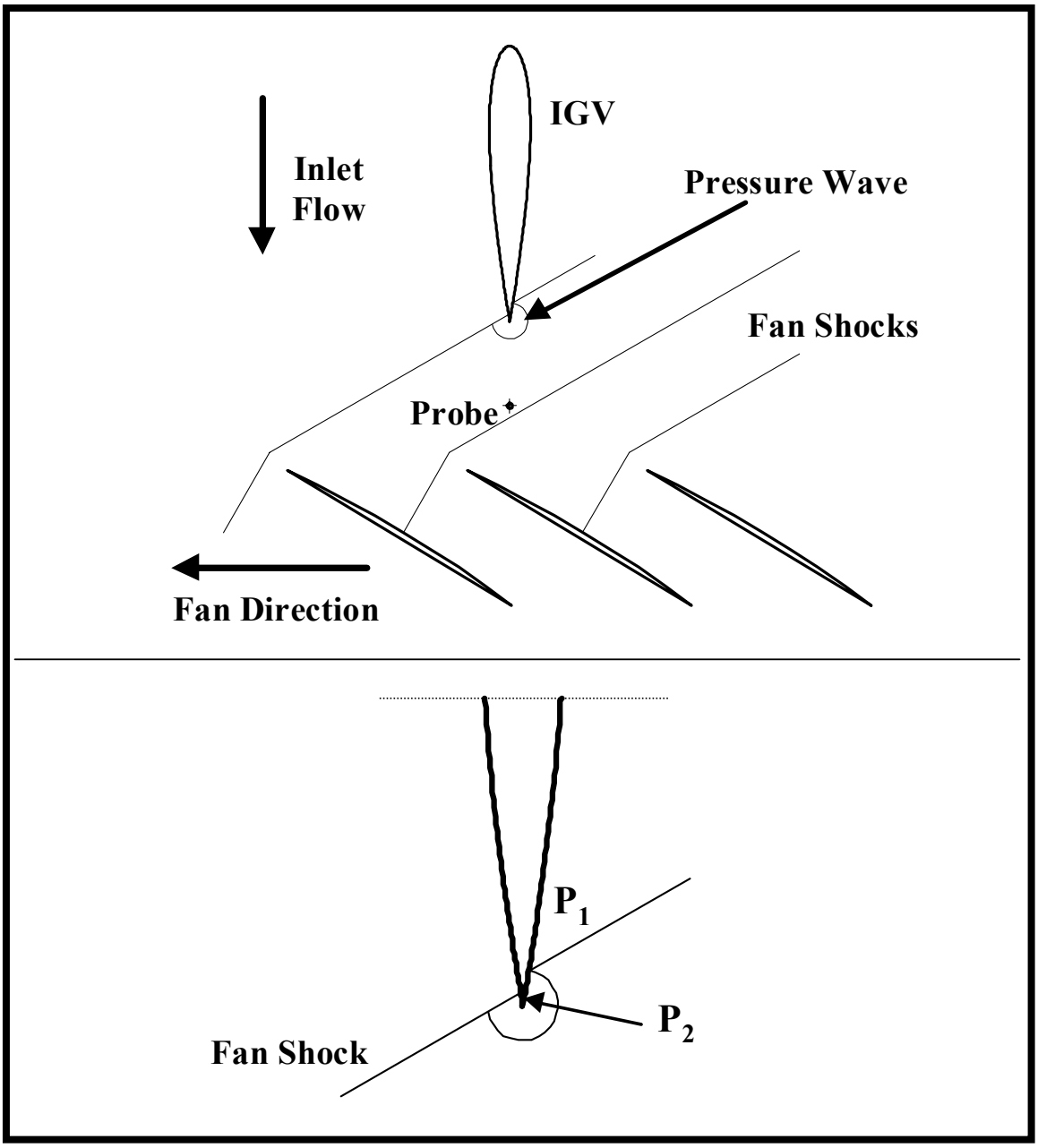

Figure 4.35 IGV trailing edge pressure wave

In recent communications with Gorrell and Copenhaver (2000), an unpublished study was recently performed where PIV measurements were taken in the transonic compressor rig at CARL, Wright-Patterson AFB. Preliminary results seemed to indicate that the passing rotor shocks generated visible flow separation at the trailing edge of the upstream IGV. This separation then appeared to propagate downstream as a vortex, shedding off the vane at the rotor BPF.

The results of the current study give credence to the pressure wave theory and the Copenhaver observations. The time resolved wakes of the IGV appear to shed off of the IGV at the fan blade passing frequency, as shown in Fig. 4.33 and 4.34. Furthermore, the time averaged IGV wakes were shown to have much higher aerodynamic losses than the baseline and subsonic wake profiles, which is symptomatic of fan shock induced boundary layer separation on the IGV, thereby generating a larger wake profile.

Besides the fan shock interactions with the IGV surface, the fan shocks also periodically interfere with the resulting wake. Therefore, it is possible that the minimum wake profile, which shows little evidence of a wake, is due to complete destructive interference by a passing shock and not a vortex separating from the vane at the BPF. In order to determine if this is the case, measurements of the shocks passing over the probe must be looked at carefully. The angle of the bow shocks could not be determined from the measurements in the current study. However, the spacing between fan blades, coupled with the spacing between the fan blades, probe and IGV, suggest that as one shock wave

is impacting the IGV surface, the next shock wave will interfere with the resulting wake, as shown in Fig. 4.35. Therefore, the time resolved wake profiles are a result of the combination of shock-IGV and shock-wake interactions. From the clean inlet and wake measurements, it was determined that a shock wave passes over the total pressure probe just prior to the occurrence of the **maximum** time resolved wake profile. Therefore, the **minimum** wake profile is not caused by the destructive interference of a passing shock. This further reinforces the assumption that the measured wake is shedding off of the vane at the fan BPF.

The results of the time averaged and time resolved IGV wake profiles of the IGV located at close proximity to a downstream transonic fan, present possible limiting factors in the effectiveness of TEB. First, the time-averaged wakes are shown to be turned approximately 1° into the rotor direction when compared to the baseline wakes. Therefore, it is not known whether the TEB jets will follow or deviate from the turned wake, as is the concern with the subsonic results. Furthermore, the minimum wake profile in the time resolved results show little evidence of a wake at this point in the fan blade pass. Therefore, it is not known whether the TEB jets will "over-blow" at this point, generating a forcing function equal to the maximum wake deficit, but in the opposite direction.

5.0 Results and Discussion:

Unsteady Trailing Edge Blowing Flow Control

The results from the unsteady wake measurements in the previous chapter demonstrated some possible limiting factors for the effectiveness of TEB flow control to reduce the IGV wake when the IGV is in close coupling with the downstream fan. The results from the subsonic relative fan speeds showed that the time averaged IGV wake is compressed in the pitchwise direction and is turned slightly into the direction of the fan rotation, when compared to the baseline. Therefore, it is not known whether the TEB jet will follow or deviate from the wake direction. Furthermore, the time resolved wake profiles showed that the fan PFF destructively and constructively interferes with the IGV wake, causing the wake to fluctuate in width and depth over each blade pass. Therefore, it is not known whether the TEB jets will respond in the same manner to the fan PFF as the IGV wakes. The results from the transonic relative fan speeds showed that the time averaged IGV wake is turned into the fan rotation, and is considerably wider with a significantly larger wake deficit when compared to the baseline. Therefore, it is not known whether the TEB jets will expand in the pitchwise direction to fill this thicker wake, and whether the TEB holes will choke since a higher momentum flow would be needed to fill in the deeper wake. The time resolved wake profiles for the transonic fan case indicate that the IGV wake is shedding off of the vane at the fan BPF due to the boundary layer shock interactions, where the minimum wake profile over each fan blade pass is near unity. This presents the greatest possible limiting factor of TEB. Even if the TEB fills in the

maximum wake shed off of the vane during the blade pass, the TEB jet may over-blow when the minimum wake is encountered over the blade pass. Therefore, even though the maximum wake is filled, the jet would produce a forcing function on the rotor in the opposite direction of the wake when the wake profile is at the minimum. Finally, pressure fluctuations as high as 4.7 psi were detected on the IGV trailing edge in the Phase I investigation. These high amplitude pressure fluctuations may generate a periodic resistance on the TEB jets at the fan BPF, thereby reducing the effectiveness of the wake filling. This final section in the presentation of the results of this study will attempt to answer these questions.

A series of experiments were conducted to determine if trailing edge blowing (TEB) flow control in an IGV could eliminate the low pressure and velocity wake profiles (deficits) in the wakes of an IGV placed in close proximity to a downstream fan. Experiments were conducted for both subsonic and transonic relative fan speeds. Unsteady total pressure measurements of the IGV wake region were repeated with IGV TEB flow control. This investigation used the same testing set-up and measuring procedures which were used in the unsteady wake investigation, with the addition of the flow control scheme, discussed in section 2.1.5. For each fan speed tested, the IGV was circumferentially indexed so that the total pressure probe was at the pitchwise location, relative to the IGV, which corresponds to the location where the maximum wake deficit was observed in the time-averaged wake profiles of the previous section. After the engine was brought to the desired speed, the TEB air supply pressure was adjusted so that

the time averaged pressure signal from the total pressure probe, the DC component, was equal to the inlet total pressure. The supply air pressure was then recorded and the DAQ was made. Since the IGV is indexed, the engine is shut off between runs. When the IGV is indexed to another measuring location and the engine is run up, the TEB supply air pressure is set to the value determined from the initial test for a given fan speed.

5.1 Subsonic Fan

Time Averaged Effectiveness of TEB

The effectiveness of TEB flow control for a typical IGV-fan spacing at a relative subsonic fan blade velocity was investigated for a fan speed of 11k rpm, corresponding to 79% of the engine maximum speed. The time-averaged effectiveness of TEB is shown in Fig. 5.1, compared to the case of no blowing, which was presented earlier. These results show that TEB is effective in reducing the total pressure deficit in the time averaged IGV wake, which was altered by the wake-PFF interactions. These results clearly show that the TEB jet follows the turned wake, and does not deviate from the path of the wake, which was a concern discussed previously. The total pressure loss coefficient, Eq. 2.11, of the TEB flow is reduced by 91.2% compared to the case with no blowing. The TEB flow parameters, discussed in section 2.2.1.5 and 3.3, are shown in Table 5.1. Recall that 8 TEB holes are used in the modified IGV used in the unsteady experiments, compared to 21 TEB holes for the full span IGV used in the steady experiments, as discussed in section 2.3.1.1. Therefore, so that a direct comparison can be made with the steady

baseline experiments, the mass flow required for TEB in the unsteady experiments was determined for one hole and multiplied by 21. This represents the mass flow required for a full span IGV with the same span as the F109 fan blades. This result is listed in Table 5.1.

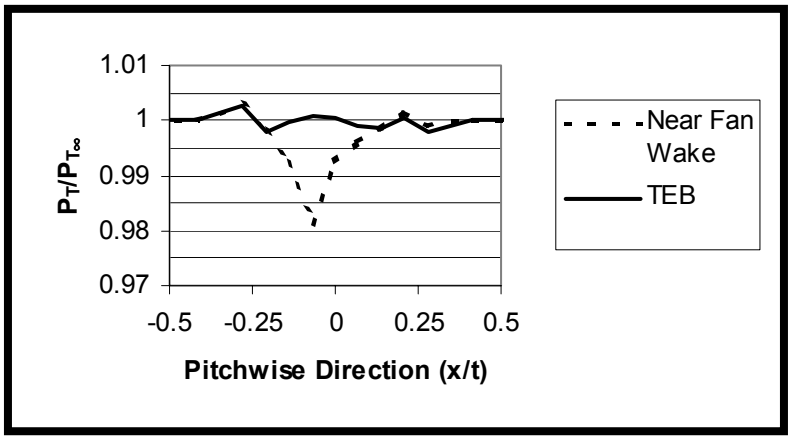

Figure 5.1 TEB flow control compared to wake—subsonic fan

Mass Flow ($m^{\bullet}_{TEB}/m^{\bullet}_{\infty}$) 8 holes	**0.0088% per modified IGV**
Mass Flow ($m^{\bullet}_{TEB}/m^{\bullet}_{\infty}$) 21 holes—full span	**0.023% per IGV**
TEB Line Pressure ($P_{T(TEB)}/P_{T\infty}$)	**1.19**
Avg. TEB Jet Velocity (u_j/U_∞)	**1.043**
Max. TEB Jet Velocity (u_{jmax}/U_∞)	**1.782**
Blowing Coefficient, C_B $[(\rho u)_j/(\rho U)_\infty]$	**1.085**
Momentum Coefficient, C_μ $[(\rho u^2)_j/(\rho U^2)_\infty]$	**1.132**
Discharge Coefficient, C_o	**0.64**

Table 5.1 TEB flow parameters for subsonic fan—11k rpm

The results of the TEB flow parameters for the subsonic fan experiment compare well with those of the steady experiments at the same axial measuring station, discussed in section 3.3. The same mass flow is required in both cases for the wake filling, within 1%. The other flow parameters also agree within 1%. **Therefore, the time averaged interactions between the close spacing IGV wake—fan PFF do not alter the properties of TEB compared to that of the IGV located upstream of the aerodynamic influence of the fan.** However, the total pressure loss coefficient of the TEB wake filling is 91.2% for the subsonic fan case, compared to 75% for the baseline case. This is most likely due to the reversible "wake recovery" observed in the IGV wakes due to the wake-PFF interactions, as discussed in Chapter 4. Since the IGV wake is compressed in the pitchwise direction, the subsequent wake is shown to have reduced aerodynamic losses compared to the baseline wake. Therefore, the measured effects of the TEB behind the IGV subsequently show reduced aerodynamic losses compared to the baseline. Recall from the discussion of the steady state experiments that the limiting factor at this axial measuring station, $z/C_{IGV} = 0.15$, in completely filling in the IGV wake was the TEB hole diameter. The wake-PFF interaction in the unsteady experiments appears to compensate for this limiting factor by reducing the time averaged losses.

These results show that the IGV-fan interactions for subsonic relative fan speeds most likely only generate wake-PFF interactions, as opposed to IGV surface-PFF interactions. There are two arguments for this conclusion. First, the same TEB mass flow and flow parameters are observed for both the unsteady and steady state cases. If the fan PFF

interaction generated either a loss or gain by interacting with the IGV boundary layer, a greater or less amount of mass flow and momentum, respectively, would be required for wake filling. Second, the unsteady pressure fluctuations measured at the IGV trailing edge for the subsonic fan speeds were quite small, ~0.2 psi P-P. Therefore, it is unlikely that these pressure fluctuations would prematurely separate the boundary layer on the IGV, or delay the separation when compared to the baseline study.

Unsteady TEB Profiles

Using the improved unsteady wake reduction method, section 4.1.1, the average P-P amplitudes of the ensemble-averaged pressure fluctuations at each pitchwise location, after subtracting out the pressure fluctuations from the clean inlet, for TEB flow control is shown in Fig. 5.2. These results are compared to the unsteady pressure fluctuations observed in the wake region with no blowing**. These results show that in the portion of the wake reduced by TEB, the unsteadiness of the pressure fluctuations is effectively removed.** This is not to say that the TEB removes the unsteadiness in the flow, just that the probe is measuring a near constant total pressure in the IGV wake region, which is equal to the inlet total pressure. In other words, the portion of the wake reduced by TEB produces the same unsteadiness as the freestream flow. In the portion of the wake in the pitchwise direction that was not effected by TEB, $x/t < -0.28$ and $x/t > 0.14$, the unsteadiness of the pressure fluctuations remained the same as the case with no blowing. **Therefore, in terms of the forcing function (wake deficit) on the downstream rotor,**

TEB produces a uniform pressure distribution in the filled portion of the wake that does not vary with the fan BPF, which is the same as the freestream flow.

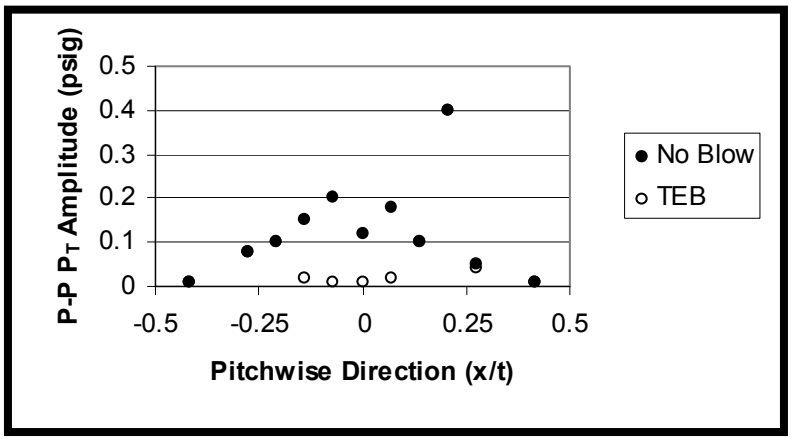

Figure 5.2 Average P-P pressure amplitudes in the TEB wake—subsonic fan

To demonstrate these results in another way, Figure 5.3 shows the original unsteady pressure fluctuations of the clean inlet and TEB signals over 1 ms, 0.18 fan blade passes, and the resulting pressure fluctuations after the clean inlet fluctuations are subtracted from the TEB fluctuations at each point in time. The TEB signal is from the pitchwise location corresponding to the maximum wake deficit, x/t = -0.07. Note that the pressure scales are different on each plot in order to view the subtracted signal. The results show that the phase locked ensemble-averaged pressure fluctuations for the clean inlet (freestream flow) and TEB are nearly identical. The resulting subtraction shows very small amplitude pressure fluctuations that are not preserved at the fan BPF. Therefore, these fluctuations are residuals from the ensemble averaging technique.

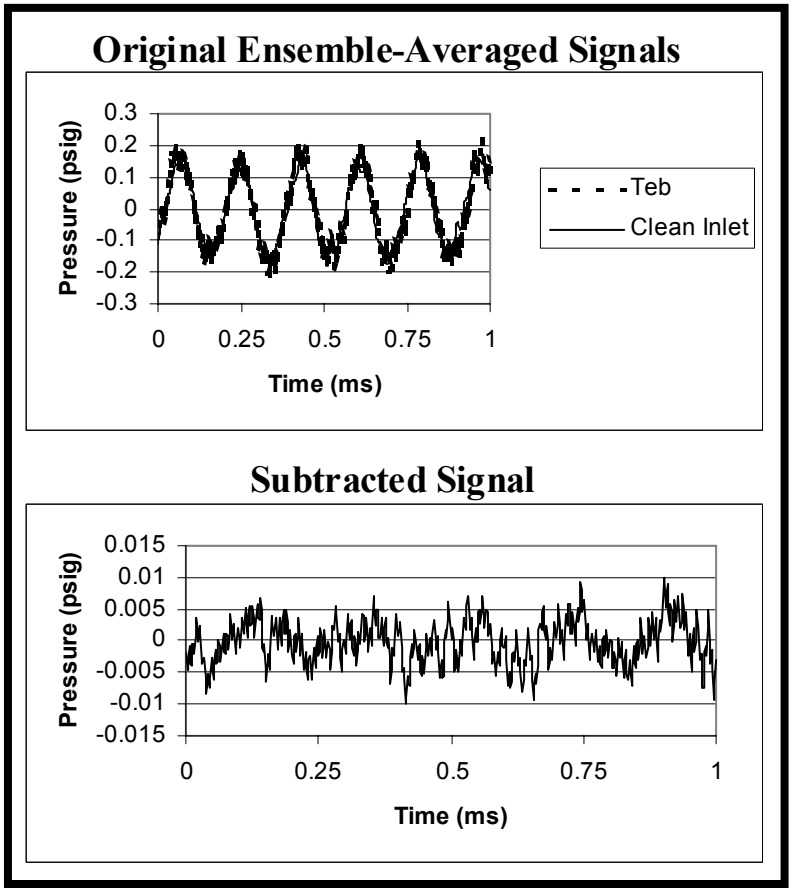

Figure 5.3 Subtracted TEB signal at location of maximum wake deficit

Figure 5.4 shows the destructive, mean and constructive interference of the TEB flow profile downstream of the IGV. As discussed above, the region of the wake effected by the TEB flow control shows negligible pressure fluctuations. The region outside of this shows the same pressure fluctuations observed in the wake measurements, including the assumed potential wave reflection.

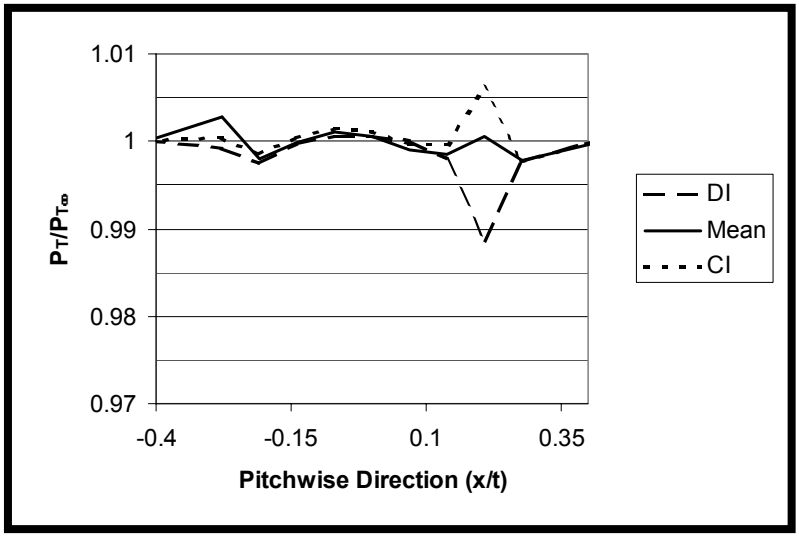

Figure 5.4 Destructive (DI) and constructive (CI) interference of TEB flow profile

The results of the time resolved TEB flow profiles downstream of the IGV demonstrate that the TEB flow control generates the same amount of unsteadiness as the freestream flow. However, this does not mean that the unsteadiness in the flow is removed by TEB, simply that the total pressure profile in the axial direction remains constant in the effected IGV wake region over each fan blade pass as measured by the total pressure probe. Therefore, the interference generated by the wake-PFF interaction does not cause the TEB jets to respond differently to each fluctuation, as was a concern discussed previously. In fact, the wake-PFF interactions do not appear to generate an adverse affect on the TEB jet development.

In conclusion, TEB is effective in reducing the total pressure deficit in the wake of an IGV placed at a typical spacing upstream of a subsonic fan. Furthermore, the

total pressure loss in the wake was reduced from that seen in the baseline while using the same amount of mass flow. Finally, the unsteadiness observed in the wake profiles with no blowing generated by the destructive and constructive interference of the IGV wake, do not adversely affect the TEB jet development. In fact, the total pressure, as measured by the probe, contains a negligible amount of unsteadiness when compared to the freestream.

5.2 Transonic Fan

Time Averaged Effectiveness of TEB

The effectiveness of TEB flow control for a typical IGV-fan spacing at relative transonic fan blade velocities was investigated for fan speeds of 12k and 14k rpm, corresponding to 85 and 100% of the engine maximum speed, respectively. The time-averaged effectiveness of TEB is shown in Fig. 5.5, compared to the case of no blowing, which was presented earlier. These results show that TEB flow control eliminates the wake region with the maximum total pressure deficit, but does not have an effect outside the core of the wake. However, the TEB jets do appear to following the turning of the wake in the direction of the rotor, which was a concern addressed earlier. The TEB flow control reduces the total pressure loss coefficient, Eq. 2.11, by 68.8 and 68.4% compared to the wakes with no blowing, at 12 and 14k rpm fan speeds, respectively. The TEB flow parameters, discussed in section 2.2.1.5 and 3.3, are shown in Table 5.2. The mass flow required for TEB is shown for the modified 8 hole IGV used in the unsteady experiments, and the 21 hole IGV used in the steady baseline. The mass flow required for the reduced

wake filling of the time averaged IGV wake near a transonic fan is 2.3 and 2.65 times that required for the baseline and subsonic investigations, for 12 and 14k fan speed, respectively. To put this into perspective, a fan with 30 blades would typically have around 24 IGV. For 24 IGV, the baseline and subsonic results showed complete wake filling would be achieved with using only 0.8% of the total engine mass flow. However, the transonic results show that the mass flow required for 24 vanes would be at least 1.9 and 2.16% of the total engine mass flow, at 12 and 14k rpm, respectively. In the actual implementation of TEB flow control in a military turbofan, the TEB supply air will have to be bled from one of the downstream compressor stages, producing a cost to the compressor. Therefore, 2% of the total engine mass flow might be undesirable to engine designers, thereby making the concept of TEB less attractive. However, it should be noted that relative transonic fan blade speeds usually exist only at the upper 1/3 span of the blade near the tip (Cumpsty, 1989). Therefore, the IGV plenum could be partitioned between the TEB supply air needed for the upper 1/3 of the fan (transonic) and the lower 2/3 of the fan (subsonic). **This would result in a required mass flow of 1.2% of the total engine flow, which is in the range of acceptable cost to the compressor.**

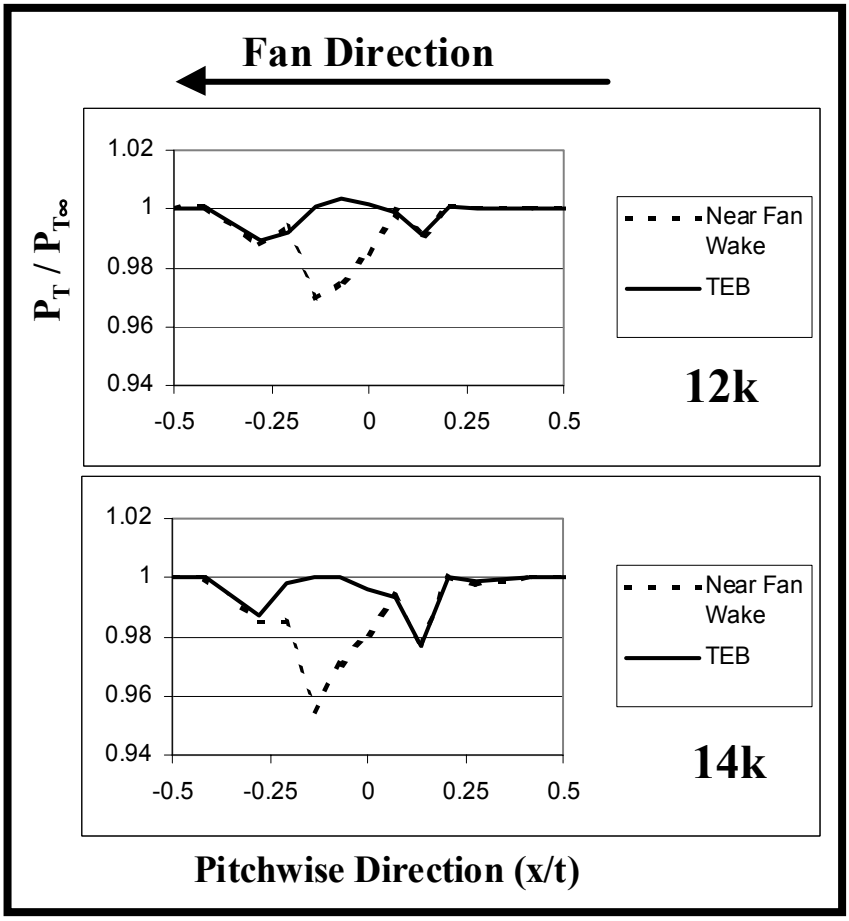

Figure 5.5 TEB flow control compared to wake—transonic fan

Fan Speed	12k rpm	14k rpm
Mass Flow ($\dot{m}_{TEB}/\dot{m}_{\infty}$) 8 holes	0.031% per modified IGV	0.035% per modified IGV
Mass Flow ($\dot{m}_{TEB}/\dot{m}_{\infty}$) 21 holes—full span	0.078% per IGV	0.09% per IGV
TEB Line Pressure ($P_{T(TEB)}/P_{T\infty}$)	2.24	3.55
Avg. TEB Jet Velocity (u_j/U_{∞})	3.4	2.85
Max. TEB Jet Velocity (u_{jmax}/U_{∞})	3.5	2.85
Blowing Coefficient, C_B $[(\rho u)_j/(\rho U)_{\infty}]$	3.85	4.41
Momentum Coefficient, C_{μ} $[(\rho u^2)_j/(\rho U^2)_{\infty}]$	13.09	13.04
Discharge Coefficient, C_o	0.65	0.65

Table 5.2 TEB flow parameters for transonic fan—12k and 14k rpm

The mass flow required for TEB flow control for the transonic speeds increases between 12 and 14k rpm. The baseline results showed that for the same measuring locations, the TEB mass flow to total engine mass flow ratio was constant for all fan speeds. Therefore, this result shows that the IGV wake deficit near a transonic fan increases disproportionately when compared to an isolated IGV. This is most likely due to the increased strength of the shock waves with engine speed that interact with the IGV surface.

The TEB flow parameters also show that the jet velocity to inlet velocity ratio has increased substantially compared to the baseline and subsonic results. This increase is due to the significant increase in the wake total pressure deficit due to the IGV boundary layer—shock interactions, discussed in the case without flow control. The jet velocity at

12k rpm is just under the local sonic speed, while the jet velocity at 14k rpm is choked. This is evident by observing the TEB line pressure, velocity ratios, and blowing and momentum coefficients. The density of the TEB supply air in the IGV plenum increased by 30% between the 12 and 14k rpm cases. However, the velocity ratio decreased between these two cases. Therefore, even though the holes are choked in the 14k case, thereby limiting the TEB jet velocity to the local sonic velocity, the increased line pressure increased the air density, subsequently increasing the mass flow even though the velocity was not increased. Throughout the baseline results and discussion, it was pointed out that TEB hole choking might reduce the effectiveness of wake filling because the jet velocity could not be increased. This was also suggested in previous studies (Naumann, 1997; Waitz, 1996). However, the current results show that TEB effectiveness was the same at 12 and 14k rpm, even though the holes were choking at 12k. This is explained by observing the momentum coefficients for both fan speeds, which are identical. Therefore, the effectiveness of TEB to fill in the wake is a first order function of the jet momentum, and not the jet velocity, as has been previously reported. Furthermore, these results seem to indicate that the TEB hole choking is not a limiting factor, as long as the density of the TEB supply air can be increased accordingly. In the baseline results, the hole diameter to downstream measuring location ratio was shown to be a limiting factor in TEB effectiveness. Therefore, these results show that smaller holes can be used to improve TEB effectiveness at closer axial spacings to the IGV trailing edge.

Finally, the effectiveness of IGV TEB near a transonic fan was reduced when compared to the baseline and the subsonic results. This is most likely due the thicker wakes caused by the IGV surface boundary layer—shock interactions, as discussed in Chapter 4.

Unsteady TEB Profiles

Using the improved unsteady wake reduction method, section 4.1.1, the average P-P amplitudes of the ensemble-averaged pressure fluctuations at each pitchwise location, after subtracting out the pressure fluctuations from the clean inlet, for TEB flow control is shown in Fig. 5.6. These results are compared to the unsteady pressure fluctuations observed in the wake region with no blowing**.** The unsteady pressure fluctuations in the wake region are reduced by 81% and 79% with TEB compared to those of the wake with no blowing, for the 12k and 14k cases, respectively. This is not as large as reduction as the subsonic cases, where the unsteadiness was effectively reduced to zero in the TEB effected region of the wake. Furthermore, the fluctuations in the TEB region occur at the fan BPF. Again, this does not mean that the unsteadiness in the flow is reduced by TEB, simply that the total pressure profile in the axial direction contains smaller pressure fluctuations in the effected IGV wake region over each fan blade pass as measured by the total pressure probe. In the portion of the wake in the pitchwise direction that was not effected by TEB, $x/t < -0.21$ and $x/t > 0$, the unsteadiness of the pressure fluctuations remained the same as the case with no blowing. **Therefore, in terms of the forcing function (wake deficit) on the downstream rotor, TEB produces a substantially reduced total pressure fluctuation in the filled portion of the wake.**

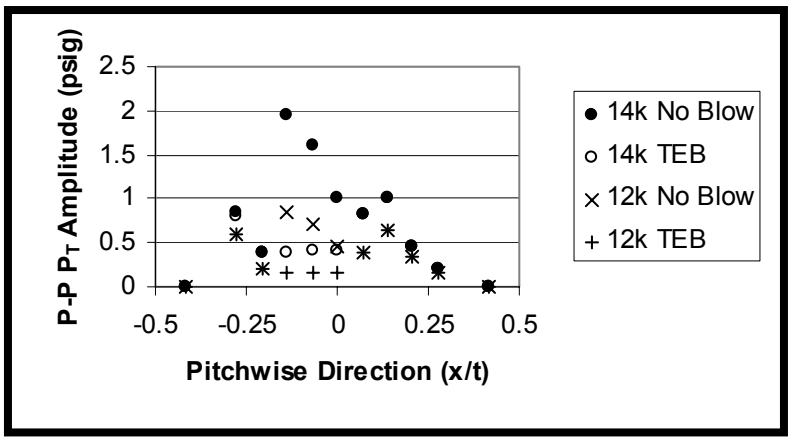

Figure 5.6 Average P-P pressure amplitudes in the TEB wake—transonic fan

The minimum, mean and maximum TEB flow profiles over one averaged fan blade pass is shown in Fig. 5.7. These results show that even though the pressure fluctuations in the TEB effected region of the wake are higher in amplitude to those in the subsonic case, the pressure fluctuations are still small compared to the region of the IGV wake not affected by TEB. Furthermore, these results show that over-blowing is not occurring at the time when the minimum wake is observed. Recall from the transonic results without blowing, that the minimum wake profile produced very little evidence of a wake profile. Therefore, the primary concern with implementing TEB flow control was that the wake would be filled-in at the time of the wake maximum, but would over-blow at the time of the minimum wake. Thereby producing a forcing function on the downstream fan that was equal in magnitude, but opposite in direction as the IGV wake. These results clearly show that over-blowing in this region is not a concern. There are two plausible

explanations for this. First, if the fan passing shocks destructively interfere with the IGV wake enough to eliminate its detection downstream, at a blade pass location between the shock induced vortex shedding, then the TEB jets would also be attenuated. Second, measurements made with the pressure transducer inside one of the TEB holes, Phase I, showed pressure fluctuations on the IGV trailing edge with amplitudes as high as 4 psig at the 14k rpm fan speed. Therefore, when the shock passes over the hole, at the time of the minimum wake profile, the jet may experience resistance or blockage in between the vortex shedding off the IGV.

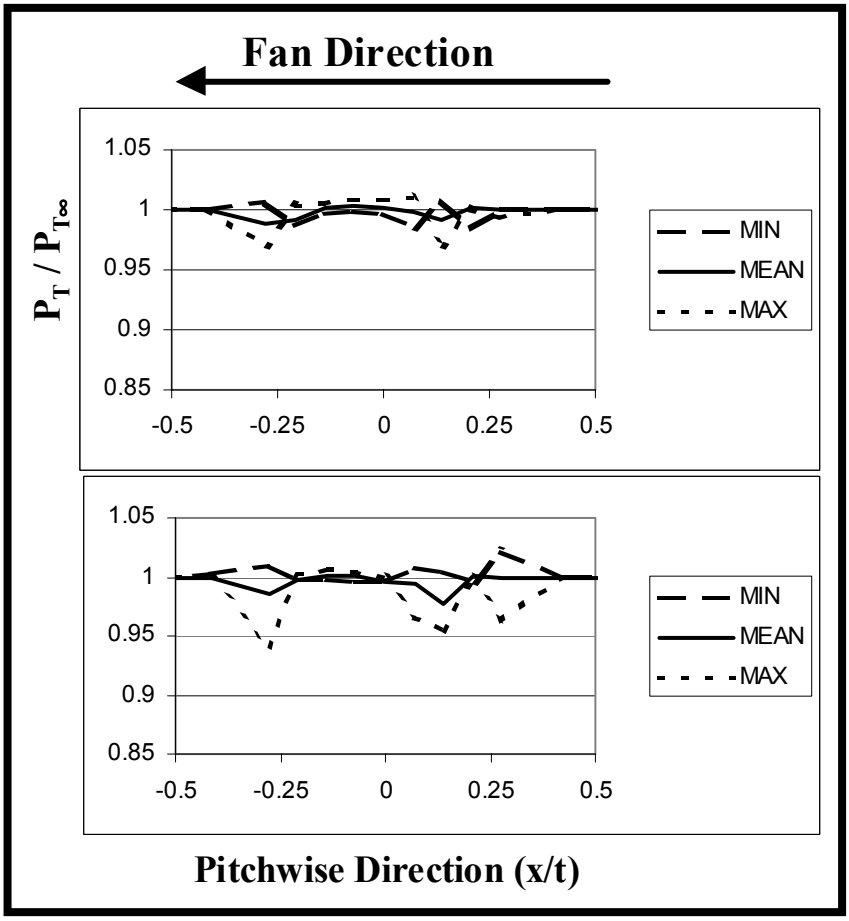

Figure 5.7 Minimum and maximum TEB flow profiles over one blade pass

In conclusion, TEB is effective in reducing the magnitude of the forcing function, the total pressure deficit in the wake, of an IGV placed at a typical spacing upstream of a transonic fan. Furthermore, the total pressure loss in the wake was reduced by 68% when compared to the case without flow control. However, in order to achieve this wake reduction, 2.5 times more mass flow was required when compared to the subsonic fan and baseline TEB results. Finally, the unsteadiness observed in the wake profiles with no blowing generated by the IGV-shock and

wake-shock interactions, do not adversely affect the TEB jet development. In fact, the total pressure, as measured by the probe, contains a reduced amount of unsteadiness when compared to the freestream.

6.0 Conclusions

In order to achieve the aggressive goals of the Department of Defense IHPTET program, the component spacing in new axial compressor designs has been significantly reduced. The close spacing between the IGV and first stage fan has produced many unexpected results. Aerodynamic interactions between the IGV and fan, that were until recently thought to have a second order effect, have been shown in the last three years to have a first order effect on IGV blade loading, IGV wake profiles, and stage efficiency. The effects of a transonic fan on the IGV wake have not been studied. Therefore, the first objective of this study is to determine the effects of the fan PFF and passing shocks on the aerodynamic losses generated by the IGV wakes. The second objective was to determine the effects of the upstream passing shocks of a transonic fan on the wake profiles shed by an upstream IGV.

High cycle fatigue failures of the fan blades in the first stage of axial compression in modern military turbofan engines have been shown to be a result of the unsteady blade loading generated by the wakes of the upstream inlet guide vanes (IGV). The best way to reduce or eliminate these failures is to remove the forcing function itself, i.e. the IGV wakes. Previous studies have shown the effectiveness of trailing edge blowing (TEB) flow control in reducing the total pressure (forcing function) and velocity deficits in the wakes of isolated stators. However, all of the previous studies have measured TEB effectiveness at axial distances downstream of the stator that are not representative of a

rotor leading edge in a typical military engine. Therefore, the third objective of this study was to investigate the effectiveness of TEB at closer axial measuring locations downstream of an isolated IGV trailing edge. The effectiveness of IGV TEB flow control in the harsh unsteady environment of close IGV-fan spacing has not been examined. The fourth objective of the current study was to demonstrate the effectiveness of TEB in reducing the wakes of an IGV placed at a typical distance upstream of a fan operating at realistic conditions.

In order to achieve these objectives and demonstrate that TEB flow control is feasible in modern military turbofan engines, the investigation was performed in a running full-scale military turbofan engine, the Allied Signal F109. Since the objectives of this study focus on the first stage of axial compression, the engine inlet and front fan are the only relevant components in this investigation.

This research effort is separated into two categories, steady state and unsteady aerodynamic investigations. The steady state investigation consists of time averaged wake measurements of an isolated IGV, with and without TEB flow control, at closer measuring distances downstream of the IGV than have been previously studied. These steady experiments were also used for a baseline comparison in the unsteady experiments. Therefore, in order to provide an analogous comparison, the steady experiments are conducted in the F109 turbofan engine under the same inlet flow conditions used in the unsteady experiments. In the steady experiments the IGV is placed

far upstream from the fan, well outside of any upstream propagating disturbances generated by the fan. For this investigation, the engine is essentially being used as a wind tunnel.

The unsteady experiments are divided into two separate phases: Phase I) High frequency IGV surface pressure measurements; Phase II) High frequency IGV wake total pressure measurements. Since previous investigations have shown substantial wave reflections off of adjacent IGV blades, which interfere with the surrounding flow, the current study uses a single IGV so that the unsteady wake profile can be determined without the pollution of wave reflections. In the unsteady experiments, the IGV is placed at a typical spacing upstream of the fan. Surface pressure measurements were performed on the IGV trailing edge, and time averaged and unsteady IGV wake profiles were measured for subsonic and transonic relative fan speeds.

This chapter will first summarize the conclusions reached in the steady state and unsteady investigations. The contributions of this study to the field of turbomachinery will then be presented. Finally, recommendations for future investigations will be discussed.

6.1 Steady-state Experiment Conclusions

A series of experiments were conducted to measure the baseline IGV wake profiles, with and without TEB flow control, with the IGV placed well upstream of the aerodynamic influence of the fan. Measurements were performed at various fan speeds at measuring

locations downstream of the IGV trailing edge equal to 0.15, 0.25, 0.5 and 0.75 IGV chords. This measuring location represents the location of a fan leading edge at typical IGV-fan spacings. Results showed that complete pitchwise and spanwise wake filling in was achieved through TEB at the 0.5 and 0.75 measuring locations, while requiring only 0.032% of the total engine inlet mass flow. Integrating the mass flow deficit in the wake confirmed this result. To put these results into perspective, an engine with 24 IGV would require only 0.8% of the engine mass flow for TEB. This is significant because in the actual implementation of TEB, the supply air will have to be bled from a downstream compressor stage, thereby inducing a cost to the engine. A mass flow of ~1% of the total engine flow is deemed acceptable by engine designers.

TEB flow control showed a reduced effectiveness at the two axial measuring stations closest to the IGV trailing edge. At the 0.25 measuring station, the limiting factor was the TEB hole spacing along the IGV span, as only partial wake filling was observed in the spanwise direction. However, it was estimated that the mass flow required would be 0.032%, as the mass flow deficit in the wake region showed negligible change at each axial measuring location. This closer axial spacing was found to be beneficial by reducing the TEB jet velocity required for complete pitchwise wake filling, when compared to the further spacings. This was attributed to increased jet dissipation at the further spacings. At the 0.15 measuring location, TEB had a reduced effectiveness in the pitchwise direction and no effect in the spanwise direction. The reduced effectiveness in the pitchwise direction was attributed to the TEB hole diameter to axial measuring

location ratio, which was determined to be at least 12 for complete pitchwise filling. The reduced effectiveness in the spanwise direction was attributed to span hole spacing, as found for the 0.25 location.

6.2 Unsteady Experiment Conclusions

A series of experiments were conducted to investigate the effectiveness of TEB flow control in an IGV placed at a typical distance upstream of a fan operating at both subsonic and transonic relative blade speeds. The IGV was located 0.43 fan chords upstream of the fan leading edge. Phase I experiments were first conducted to measure the unsteady pressure fluctuations at the IGV trailing edge generated by the fan's upstream propagating PFF and shock waves at subsonic and transonic relative fan speeds, respectively. A high frequency pressure transducer was flush mounted into an IGV TEB hole at a 1.1 in immersion. Phase II experiments consisted of measuring the time averaged and unsteady IGV wake profiles with located 0.43 fan chords upstream of a subsonic and transonic fan. Measurements were performed for both no blowing and TEB flow control. These measurements were compared with the baseline results in the steady state experiments. The unsteady IGV wake profiles were measured with a high-frequency total pressure probe, facing upstream toward the IGV and the incoming inlet flow, at a radial immersion of 1.1 in, which is located directly downstream of the TEB hole used in the Phase I investigation. All of the resulting pressure signals were phase locked with the fan rotation and ensemble averaged.

The results of the Phase I on-blade pressure measurements showed conclusively that the F109 fan operates at both subsonic and transonic relative fan speeds. The amplitudes of the pressure fluctuations measured at the IGV trailing edge increased substantially between the subsonic and transonic fan speeds. The passing shock waves generated P-P pressure amplitudes that were 10 times those measured by the fan PFF, with maximum pressure fluctuations of 4.7 psi P-P on the IGV surface at the highest fan speed tested. This demonstrates the severity of the forcing function generated by the fan on the upstream IGV. Both the fan PFF and passing shocks were found to occur at the fan BPF, with less significant higher harmonic content.

Results of the Phase II upstream total pressure measurements in a clean inlet, i.e. no IGV, showed significantly higher amplitude pressure fluctuations when compared to the Phase I results at the same fan speeds, with maximum P-P pressure fluctuations of 7 psi at the highest fan speed. These fluctuations were determined to be generated by the passing fan PFF and shock waves for the subsonic and transonic fan speeds, respectively. It was determined that the total pressure probe was measuring the static pressure fluctuations of these passing waves. Therefore, an improved data reduction method was presented which eliminated these pressure fluctuations from the unsteady wake measurements.

The time averaged wake profiles for the subsonic fan speeds showed that the wake was compressed in the direction of the fan rotation and turned approximately 0.5° when compared to the baseline wakes. The maximum wake deficit was found to be slightly

higher than the baseline. **The total pressure loss coefficient of these wakes was found to be 30% lower when compared to the steady baseline results.** Therefore, for subsonic relative fan speeds, close IGV-fan spacing is beneficial to the compressor stage by reducing the average aerodynamic losses generated by the IGV wakes. The time resolved unsteady IGV wake profiles showed that the PFF from the fan destructively and constructively interferes with the IGV wakes with each blade pass.

The time averaged wake profiles for the transonic fan speeds showed that the fan shock interaction with the IGV wakes and surface results in IGV wake profiles with considerable increases in wake deficit and width when compared to the baseline. The wake width is increased by 25% and the wake is turned approximately 1° into the direction of the fan rotation, when compared to the baseline. **The total pressure loss coefficient of the time averaged wakes was found to increase by a factor 2 when compared to the steady baseline results.** Therefore, for transonic relative fan speeds, close IGV-fan spacing is detrimental to the performance of the compressor stage by increasing the average aerodynamic losses generated by the IGV wakes. The close IGV-fan spacing also has a detrimental effect on the average magnitude of the forcing function (wake deficit) for the transonic fan speeds. The close spacing produces a 100% increase in the average forcing function magnitude when compared to the baseline. The time resolved unsteady wake profiles showed that maximum wake width across a fan blade pass is increased by 35%, and the wake deficit is increased by almost three times. The minimum wake profiles show very little evidence of a wake at all, with small variations

in normalized total pressure about unity. The behavior of the time resolved wakes was attributed to a combination of shock induced boundary layer separation on the IGV surface, coupled with the shock interactions of the corresponding IGV wake.

The time averaged profiles of the subsonic relative fan speeds showed that TEB is effective in reducing the total pressure deficit in the wake of an IGV placed at a typical spacing upstream of a subsonic fan. Furthermore, the total pressure loss in the wake was reduced from that seen in the baseline while using the same amount of mass flow. Finally, the unsteadiness observed in the wake profiles with no blowing generated by the destructive and constructive interference of the IGV wake, do not adversely affect the TEB jet development. In fact, the total pressure, as measured by the probe, contains a negligible amount of unsteadiness in the effected wake region when compared to the freestream.

The time averaged profiles of the transonic relative fan speeds showed that TEB flow control eliminates the wake region with the maximum total pressure deficit, but does not have an effect outside the core of the wake. However, the TEB jets do appear to following the turning of the wake in the direction of the rotor. The TEB flow control reduces the total pressure loss coefficient by 68% compared to the wakes with no blowing. The mass flow required for the reduced wake filling of the time averaged IGV wake near a transonic fan is 2.6 times that required for the baseline and subsonic investigations. The effectiveness of TEB to fill in the wake was shown to be a first order

function of the jet momentum, and not the jet velocity, as has been previously reported. The time resolved wake profiles showed that TEB reduces the unsteadiness in the effected wake region by 80% when compared to the case with no blowing. Therefore, in terms of the forcing function (wake deficit) on the downstream rotor, TEB produces a substantially reduced total pressure fluctuation in the filled portion of the wake.

In conclusion, TEB was found to be very effective in reducing the total pressure deficits generated by IGV wakes when the IGV was placed at a typical spacing upstream of a subsonic fan. TEB was found to be less effective in reducing the total pressure deficits for transonic fan speeds due to the increased wake losses generated by shock-boundary layer interactions on the IGV surfaces. However, the maximum magnitude of the forcing function was eliminated and the total pressure deficits were reduced by almost 70%. Therefore, this study shows that inlet guide vane TEB flow control is a feasible method for reducing the IGV wake forcing function on the downstream fan in the harsh environment of close component spacing in modern military turbofan engines.

References

Air Force Research Laboratory, "IHPTET: Air Dominance Through Propulsion Superiority", *Brochure*, April 2000.

Behnken, R.L., Leung, M., Murray, R.M., "Characterizing the Effects of Air Injection on Compressor Performance for Use in Active Control of Rotating Stall", ASME Paper 97-GT-316, June 1997.

Breugelmans, F.A.E., "The Effect of Leading-Edge Thickness on the Bow Shock in Transonic Rotors", Transonic Flow Problems in Turbomachinery, Edited by T.C. Adamson and M.F. Platzer, Hemisphere Publishing Co., 1978.

Cimbala, J.M., and Park, W.J., "An Experimental Investigation of the Turbulent Structure in a Two-Dimensional Momentumless Wake", Journal of Fluid Mechanics, Vol. 213, pp. 479-509, 1990.

Corcoran, Timothy, "Control of the Wake from a Simulated Blade by Trailing Edge Blowing," Masters Thesis, Mechanical Engineering Department, Lehigh University, 1992.

Cousins, W., Personal communication, Honeywell/Allied-Signal, 1999.

Cumpsty, N.A., "Vibration and Noise—Compressor Aerodynamics", *Longman Scientific and Technical*, 1st Edition, 1989.

Cunningham, T., and Bruce, T., "Installation Manual for the TFE109-1 Turbofan Engine", Allied-Signal Aerospace Company, Dec. 1992.

Davenport, O.B., "Operational Readiness and High Cycle Fatigue", Presented at t the 1998 IHPTET Conference, Wright-Patterson AFB, Sept. 1998.

Day, I.J., "Active Suppression of Rotating Stall and Surge in Axial Compressors", *Journal of Turbomachinery*, Vol. 115, pp. 40-47, 1993.

Fabian, M.K., and Jumper, E.J., "Rearward Forcing of an Unsteady Compressible Cascade", *J. of Propulsion and Power*, Vol. 15, No. 1, pp. 23-30, 1999.

Falk, E.A., Jumper, E.J., and Fabian, M.K., "Upstream Propagating Potential Waves in the F109 Turbofan Engine Inlet Flow", AIAA Paper 98-3294, 1998.

Fleeter, S., Personal communication, Purdue University, June 2000.

Gorrell, S.E., Copenhaver, W.W., and Randall, M.C., "Effects of Upstream Wakes on the Performance of a Transonic Compressor Stage", ISOABE Paper 97-7070, 1997.

Haines, MGEN D., "Sustaining AF Engines", Presented at the 1998 IHPTET Conference, Wright-Patterson AFB, Sept. 1998.

Hamed, A. And Numbers, K., "Inlet Distortion Considerations for High Cycle Fatigue in Gas Turbine Engines", 3rd High Cycle Fatigue Conference, San Antonio, TX, Feb. 1998.

Harvell, J.K., Internal F109 Document, United States Air Force Academy, 1994.

Hiller, K.W., Batterton, P.G., Bustadt, P.L., and Szuch, J.R., "Propulsion Systems Technology," NASA SP-259, Capter XIII, pp. 387-388, 398, Nov. 1970.

Hsu, S.T., and Wo, A.M., "Reduction of Unsteady Blade Loading by Beneficial use of Vortical and Potential Disturbances in an Axial Compressor with Rotor Clocking", *ASME J. of Turbomachinery*, Vol. 120, pp. 705-713, Oct. 1998.

Johnson, R., and Fleeter, S., "Time Resolved Variations of an IGV Flow Field in the Presence of a Rotor Potential Field", AIAA Paper 96-2670, July 1996.

Johnson, R., and Fleeter, S., "Three-Dimensional Time Resolved Measurements of IGV-Rotor Potential Interactions", AIAA Paper 98-3896, July 1998.

Johnston, R., and Fleeter, S., "High-Speed Rotor Wake Features and Inherent Flow Unsteadiness", AIAA Paper 98-3297, July 1998.

Kerrebrock, J.L., and Mikolajczak, A.A., "Intra-Stator Transport of Rotor Wakes and its Effect on Compressor Performance", *ASME J. of Engineering for Power*, Vol. 92, pp. 359-368, 1970.

Kielb, R.E., Personal communication, GE Aircraft Engines, January 1997.

Kobayashi, H., Leger, T., Wolff, J.M., "Experimental and Theoretical Frequency Response of Pressure Transducers for High Speed Turbomachinery", AIAA Paper 98-3745.

Lakshiminarayana, B., and Davino, R., "Mean Velocity and Decay Characteristics of the Guidevane and Stator Blade Wake of an Axial Flow Compressor", *ASME Journal of Engineering for Power*, Vol. 102, Jan. 1980, pp. 50-60.

Leitch, Thomas., "Reduction of Unsteady Stator-Rotor Interaction by Trailing Edge Blowing", M.S. Thesis, Virginia Polytechnic Institute and State University, Blacksburg, VA, 1997.

Leitch, T.A., Saunders, C.A., and Ng, W.F., "Reduction of Unsteady Stator-Rotor Interaction Using Trailing Edge Blowing", AIAA Paper 99-1952, May 1999.

Majjigi, R.K. and Gliebe, P.R., "Development of a Rotor Wake/Vortex model," Vol. 1 – Final Report, NASA Contract Report 174849, 1984, pp. 6-21.

Manwaring, S.R., and Fleeter, S., "Rotor Blade Unsteady Aerodynamic Gust Response to Inlet Guide Vane Wakes", *ASME J. of Turbomachinery*, Vol. 115, pp. 197-206, Jan. 1993.

Manwaring, S.R., and Wisler, D.C., "Unsteady Aerodynamic and Gust Response in Compressors and Turbines", *ASME J. of Turbomachinery*, Vol. 115, pp. 724-740, Oct. 1993.

Mikolajczak, A.A., "The Practical Importance of Unsteady Flow", AGARD CP-144, April 1976.

Morris, R.J., Benedict, B.K., Cowles, B.A., Stange, W.A., and Scheuren, W.J., "Active Structural Control for Gas Turbine Engines", ASME Paper 98-GT-514, IGTI, June 1998.

Morris, R.J., Personal Communication, Pratt & Whitney, 1999.

Naumann, R. Georg, "Control of the Wake from a Simulated Blade by Trailing Edge Blowing", Masters Thesis, Mechanical Engineering Department, Lehigh University, 1992.

Park, W.J., and Cimbala, J.M., "The Effects of Jet Injection Geometry on Two-dimensional Momentumless Wakes," Journal of Fluid Mechanics, Vol. 224, pp. 29-47, 1991.

Popp, Oliver, "Steady and Unsteady Heat Transfer in a Film Cooled Transonic Turbine Cascade", Doctoral Dissertation, Mechanical Engineering Department, Virginia Tech, 1999.

Pratt and Whitney,
http://www.pratt-whitney.com/engines/gallery/lg.f119.cut.html, 2000.

Probasco, D.P., Wolff, J.M., Copenhaver, W.W., and Chriss, R.M., "Unsteady Blade Row Potential Interaction in a Compression Stage", AIAA Paper 97-3285, July 1997.

Probasco, D.P., Wolff, J.M., Copenhaver, W.W., and Chriss, R.M., "Axial Spacing Effects in a Transonic Compressor on the Upstream Vane Loading", AIAA Paper 98-3431, 1998.

Richardson, S., "The High Cycle Fatigue (HCF) S&T Plan", *Status Report*, Turbine Engine Division, Wright Laboratories, 1995.

Ritchie, R.O., Boyce, B.L., Campbell, J.P. and Roder, O., "High-Cycle Fatigue of Turbine Engine Alloys", *Presented at the Fatigue Symposium*, The Society of Materials Science, Japan, 1998.

Roa, N.M., Feng, J.F., Burdisso, R.A., and Ng, W.F., "Active Flow Control to Reduce Fan Blade Vibration and Noise", AIAA Paper 99-1952, May 1999.

Sanders, A.J., and Fleeter, S., "Vane Row Indexing for Passive Vibration Control of Axial Flow Turbomachine Rotors", AIAA Paper 95-2656, July 1995.

Sanders, A.J., and Fleeter, S., "Transonic Axial-Flow Compressor IGV-Rotor Interactions", HCF Conference, Monterey, CA, March 1999.

Sanders, A.J., and Fleeter, S., "Experimental Investigation of Rotor-Inlet Guide Vane Interactions in Transonic Axial-Flow Compressor", *AIAA Journal of Propulsion and Power*, Vol. 16, No. 3, pp. 421-430, May-June 2000.

Saunders, C.A., "Noise Reduction in an Axisymmetric Supersonic Inlet using Trailing Edge Blowing," M.S. Thesis, Virginia Polytechnic and State University, Blacksburg, VA 1998.

Sell, Julian, "Cascade Testing to Assess the Effectiveness of Mass Addition/Removal Wake Management Strategies for Reduction of Rotor-Stator Interaction Noise", MS Thesis, Massachusetts Institute of Technology, Cambridge, MA 1997.

Sheldahl, R.E. and Klimas, P.C., "Aerodynamic Characteristics of Seven Airfoil Sections Through 180 Degrees Angle of Attack", SAND80-2114, Sandia National Laboratories, March 1981.

Smith, L.H., "Wake Dispersion in Turbomachines", *J. of Basic Engineering*, pp. 688-690, Sept. 1966.

Smith, L.H., "Casing Boundary Layers in Multistage Axial Flow Compressors", Flow Research in Blading, edited by L.S. Dzung, Elsevier Publishing Co., 1970.

Smith, L.H., "Wake Ingestion Propulsion Benefit", *J. of Propulsion and Power*, Vol. 9, No. 1, pp. 74-82, 1993.

Thomson, D.E. and Griffin, J.T., "The National Turbine Engine High Cycle Fatigue Program", Memo describing the National HCF Program, 1999.

Waitz, I.A., Brookfield, J.M., Sell, J., and Hayden, B.J., "Preliminary Assessment of Wake Management Strategies for Reduction of Turbomachinery Fan Noise", *Journal of Propulsion and Power*, Vol. 12, No. 5, pp. 958-966, 1996.

Weigl, H., Paduano, J., Epstein, A., Greitzer, E., Bright, M., and Strzisar, A., "Active Stabilization of Rotating Stall in a Transonic Single Stage Axial Compressor", ASME IGTI Paper 97-GT-316, June 1997.

Wo, A.M., Chung, M.H., Chang, S.J., and Lee, S.F., Wake Vorticity Decay and Blade Response in an Axial Compressor with Varying Axial Gap", ASME IGTI Paper 99-GT-451, June 1999.

Appendix A

Uncertainty Analysis

There are two types of errors in measurement uncertainty, bias and precision errors (Beckwith, 1993). Bias uncertainty is defined as errors that occur consistently for each different measurement in an experiment, such as DC offsets. Precision uncertainty is defined as random errors that vary from measurement to measurement in the experiments. If more than one measurement is used to determine a given property, the error is compounded. For example, in determining the flow velocity from the Pitot-static probe, the engine inlet total pressure, static pressure and total temperature are used. Therefore, the errors from each of these measurements result in an uncertainty in the velocity calculation that is different than the uncertainty of the individual measurements. This compounded uncertainty is determined from the propagation of uncertainty, given by:

$$u_y = \sqrt{\left(\frac{\partial y}{\partial x_1}u_1\right)^2 + \left(\frac{\partial y}{\partial x_2}u_2\right)^2 + \ldots + \left(\frac{\partial y}{\partial x_n}u_n\right)^2} \qquad \textbf{(A.1)}$$

Where y is the given equation derived from measurements x_n with uncertainty u. The total uncertainty is then given by:

$$U_n = \sqrt{B_n^2 + P_n^2} \qquad \textbf{(A.2)}$$

Where B and P represent the bias and precision uncertainty, respectively.

Far Upstream IGV Wake Measurements (Steady-State)

The pressure transducers used in the steady experiments have a nominal precision error of ± 0.1%, as discussed in section 2.2.1.3. Bias errors, such as the DC offset, were accounted for in the calibration and data reduction techniques. For all wake measurements, 1000 samples were averaged for each data point, as discussed in section 2.2.1.5. The total pressure wake measurements were all acquired with the 5 pisg pressure transducer. **Therefore, the total pressure wake measurements have a total uncertainty of ± 0.1%, which corresponds to ± 0.005 psig, within a 95% confidence interval (CI).**

The velocity in the IGV wakes is determined from Eq. 2.7 using the total pressure and static pressure measurements from the Pitot-static probe and the inlet total temperature. Both pressures were measured with a 5 psig transducer with a nominal error of ± 0.1 %. The transducers were calibrated with a dead weight tester which was checked with a ± 0.1 % high precision Fluke calibrator. The total temperature was obtained from the local weather service at the Virginia Tech airport, and is assumed to have an error of ± 1 %.

Therefore, the total uncertainty of the IGV wake velocity measurements is ± 0.514% within a 95% CI.

The total pressure loss coefficient of the IGV wake was determined using Eq. 2.12. This coefficient is determined by integrating the wake total pressure profile over a fixed pitchwise distance. The nominal error of the 5 psig pressure transducers and the probe traversing mechanism is ± 0.1%. **Therefore, the total uncertainty of the total pressure loss coefficient calculation is ± 3.16%.**

The momentum thickness of the IGV wake was determined using Eq. 2.14. Using the resulting uncertainty of the velocity calculation and the nominal error of the traverse, **the total uncertainty of the momentum thickness calculation is ± 7.9%.**

Trailing Edge Blowing (TEB) Parameters

The mass flow of the TEB supply air was obtained from Equation 2.2, as a function of the differential pressure across the orifice plate and the total pressure and total temperature of the TEB supply line. **The total uncertainty of the TEB mass flow measurements is ± 0.714%.**

The TEB blowing coefficient was obtained from Equation 2.17, as a function of total and static pressure measured with the Pitot-static probe, the total (ambient) temperature, and the total pressure and total temperature in the IGV plenum. The pressure measurements

were performed with the 5 psig pressure transducers. **The total uncertainty of the blowing coefficient is ± 1.02%.**

The momentum coefficient was obtained from Equation 2.18 as a function of the total and static pressure measured with the Pitot-static probe, and the plenum total pressure. Each of these measurements was made with the 5 psig pressure transducers. **The total uncertainty of the momentum coefficient is ± 0.107%.**

The average TEB hole jet velocity was obtained by dividing the TEB supply mass flow by the total area of the TEB holes and the local static density. **The total uncertainty of the average TEB jet velocity is ± 1.23%.** The maximum TEB hole jet velocity was obtained from Equation 2.16, as a function of the total and static pressure from the Pitot-static probe, the total (ambient) temperature, and the total pressure and total temperature in the IGV plenum. **The total uncertainty of the maximum TEB jet velocity is ± 1.01%.**

The discharge coefficient of the TEB holes was obtained from Equation 2.19, as a function of the measured mass flow from the mass flow meter divided by the total TEB hole area, the average TEB jet velocity, and the local static density. **The total uncertainty of the discharge coefficient is ± 1.33%.**

Unsteady On-Vane Pressure Measurements

The on-vane pressure measurements were performed with a 5 psig high frequency Kulite pressure transducer, which has a precision error of 0.1%. The Kulite transducer was routed through the signal amplifier, as discussed in Chapter 2.0. An uncertainty analysis of the amplifier is found in Popp, 1999. **The total uncertainty of the on-vane pressure measurements is ± 1.06%.**

Unsteady Total Pressure Probe Measurements

The total pressure in the IGV wake, with the IGV placed close to the downstream fan, was obtained with a 5 psig Kulite high frequency total pressure probe. **The total uncertainty of the total pressure measurements in the IGV wake region is ± 1.05%.**

The total pressure loss coefficient of the IGV wakes for both subsonic and transonic relative fan blade speeds was obtained from Equation 2.12. **The total uncertainty of the loss coefficient calculation for the high frequency probe is ± 3.32 %.**

Ensemble Averaging

The unsteady on-vane and total pressure probe measurements were phase locked with the fan revolution, and then ensemble averaged over one fan revolution, as discussed in Chapter 4.0. One-hundred ensemble averages for each measurement was determined to be sufficient in removing the random pressure fluctuations caused by local flow

unsteadiness with each blade pass and blade revolution. The typical method for determining the standard deviation of the ensemble averages at each instant in time is given by (Falk, 1999):

$$S_{x_k} = \sqrt{\frac{1}{N-1}\sum_{i=1}^{N}(\overline{P_k} - P_{k_i})^2} \qquad \textbf{(A.3)}$$

Where N is the number of ensembles (100), k is one instant in time over the fan revolution, and P is the on-vane or probe pressure measurement. The precision error of the ensemble-mean value at each instant in time is provided by the standard deviation of the means, given by (Falk, 1999):

$$S_{\overline{x_K}} = \frac{S_{x_k}}{\sqrt{N}} \qquad \textbf{(A.4)}$$

From this, the minimum, mean, and maximum standard deviation of the means is shown in Table A.1 for each of the fan speeds tested. The standard deviation of the subsonic relative fan speeds is nearly identical. However, the standard deviation for the transonic relative fan speeds is greater than the subsonic speeds. Furthermore, the standard deviation increases with increasing fan speed for the transonic fan. This behavior can be observed in Figures 4.5 and 4.15 which show the peak to peak pressure fluctuations for the raw and ensemble averaged data for each fan speed tested. The reasons for this behavior can be found with above mentioned figures in Chapter 4.0.

	Standard Deviation of the Means (%)		
Fan Speed (kRPM)	**Min**	**Mean**	**Max**
10	1.04	1.25	1.54
11	1.05	1.30	1.57
12	1.42	1.82	2.14
13	1.38	2.04	2.63
14	1.64	2.28	2.79

Table A.1 Standard deviation of ensemble averages

Appendix B

Design Drawings

This appendix provides the design drawings of the primary equipment used in the current study. The design drawings for the IGV used in the far upstream steady state experiments are shown in Fig. B.1-6. The modified IGV design used in the near fan unsteady experiments, discussed in section 2.3.1.1, are shown in Fig. B.7-12. The design drawings of the IGV inlet ring are shown in Fig. B.13-17. Finally, the drawings of the traverse inlet ring are shown in Fig. B.18-20.

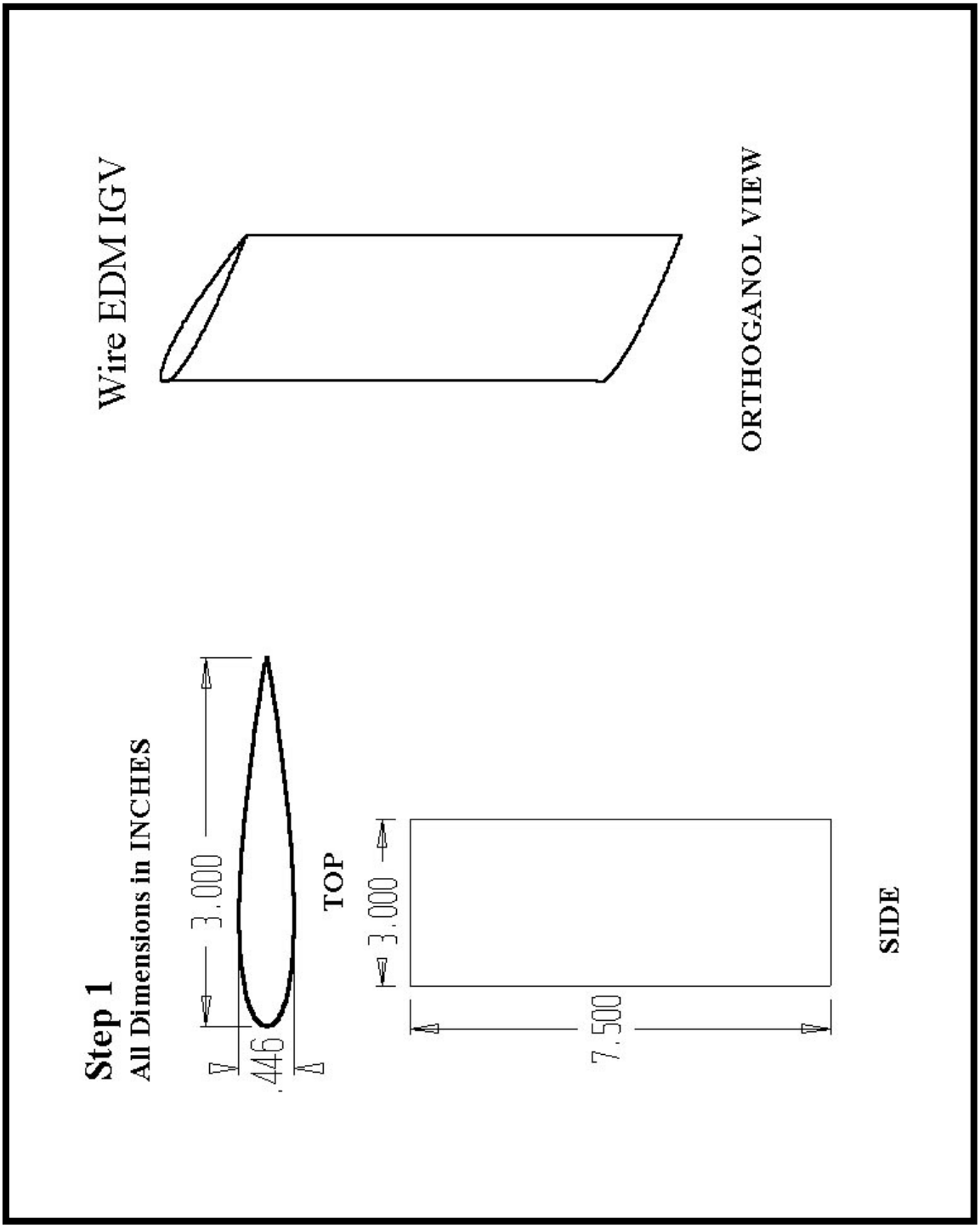

Figure B.1 IGV Design Step 1—Wire EDM

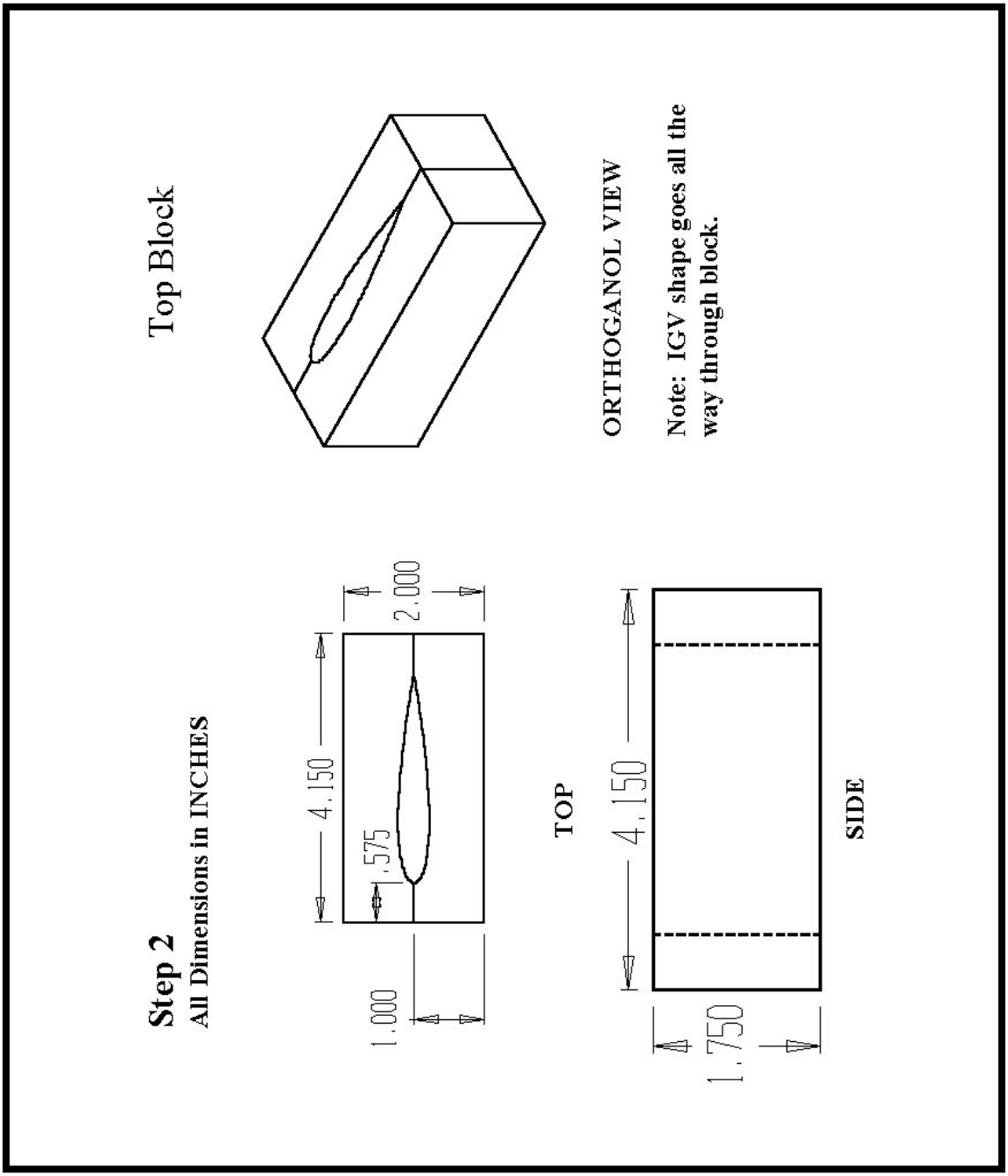

Figure B.2 IGV Design Step 2—Top Clamp/Block

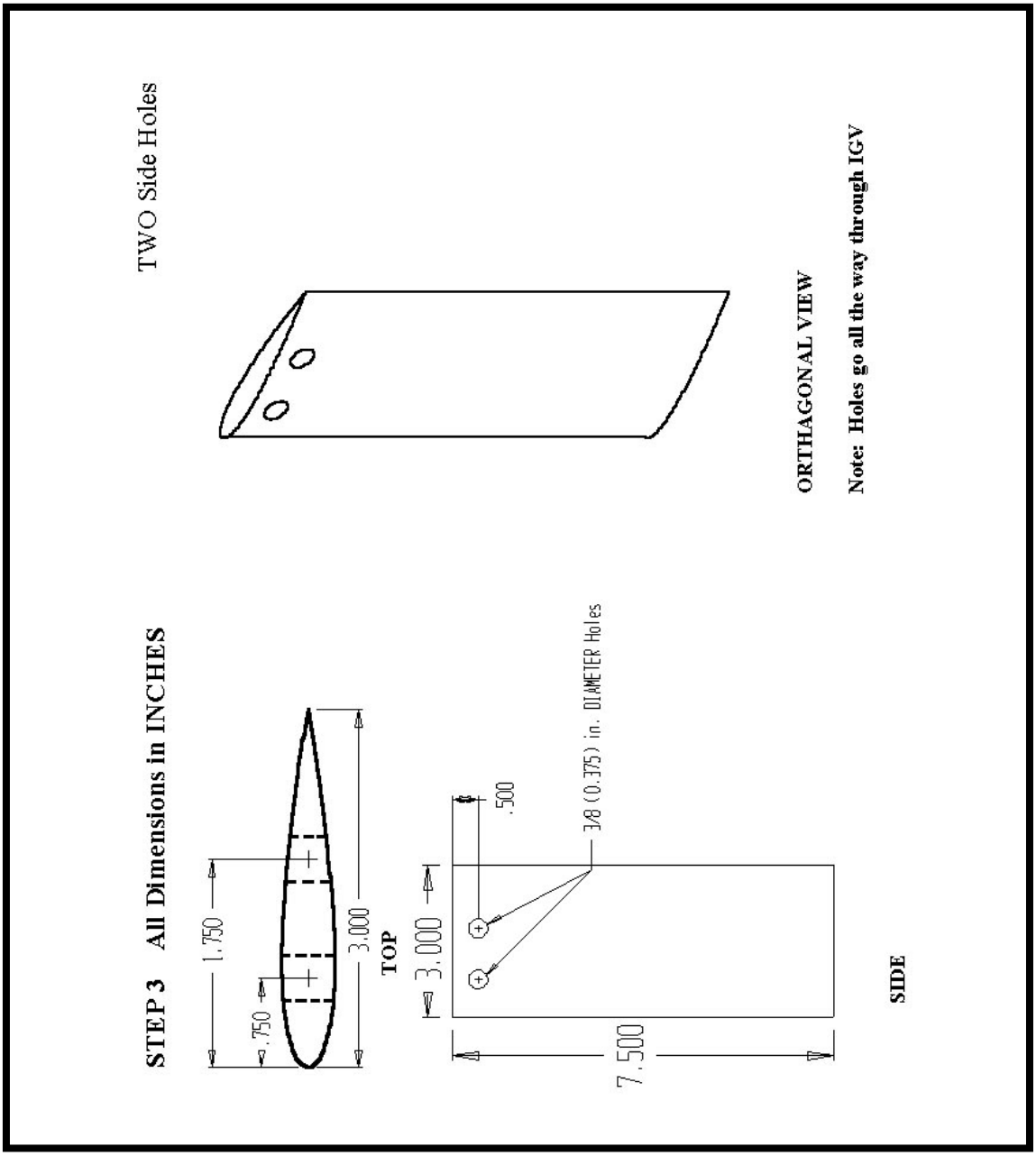

Figure B.3 IGV Design Step 3—Holes for Shoulder Bolts

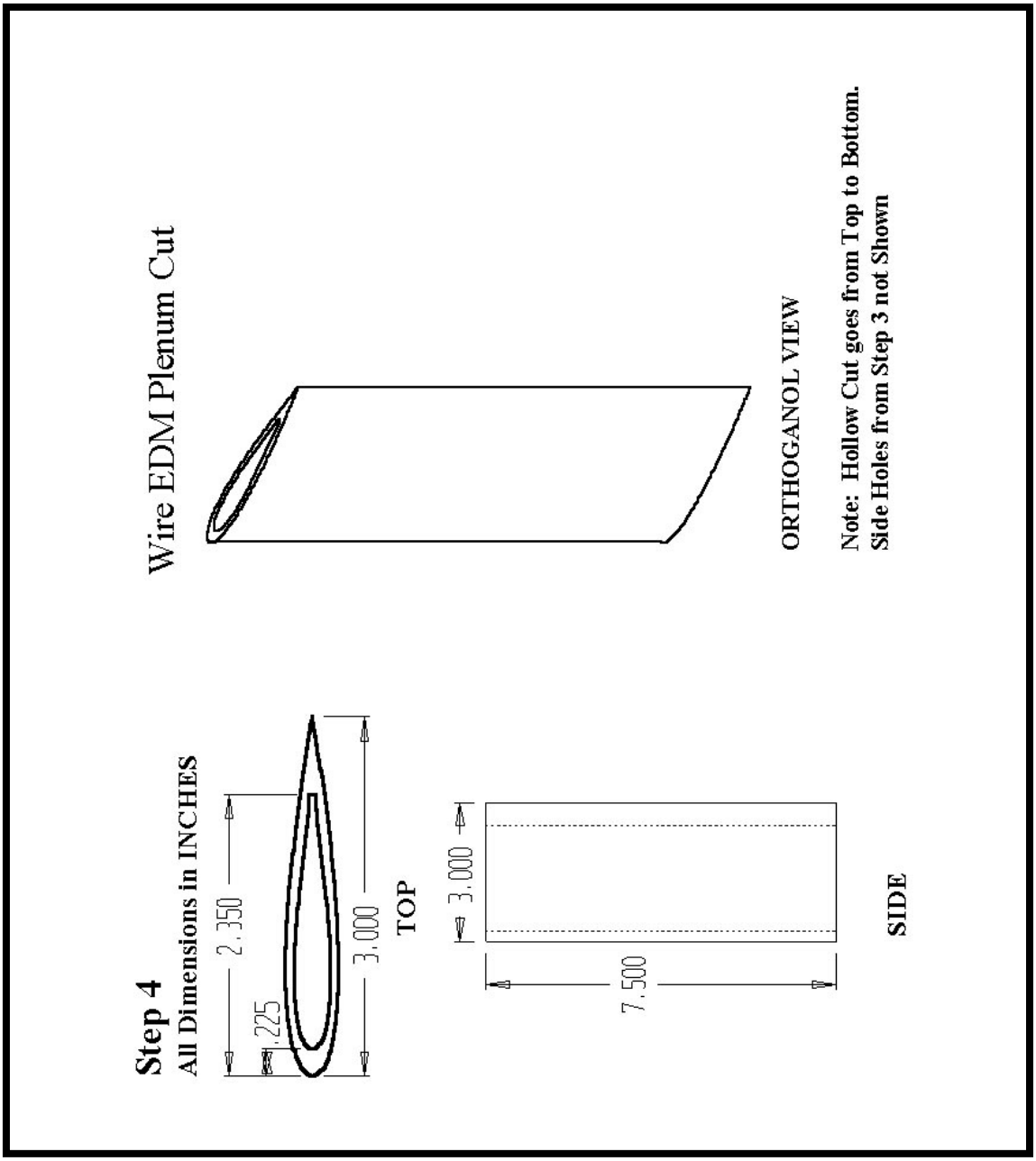

Figure B.4 IGV Design Step 4—EDM Plenum Cut-out

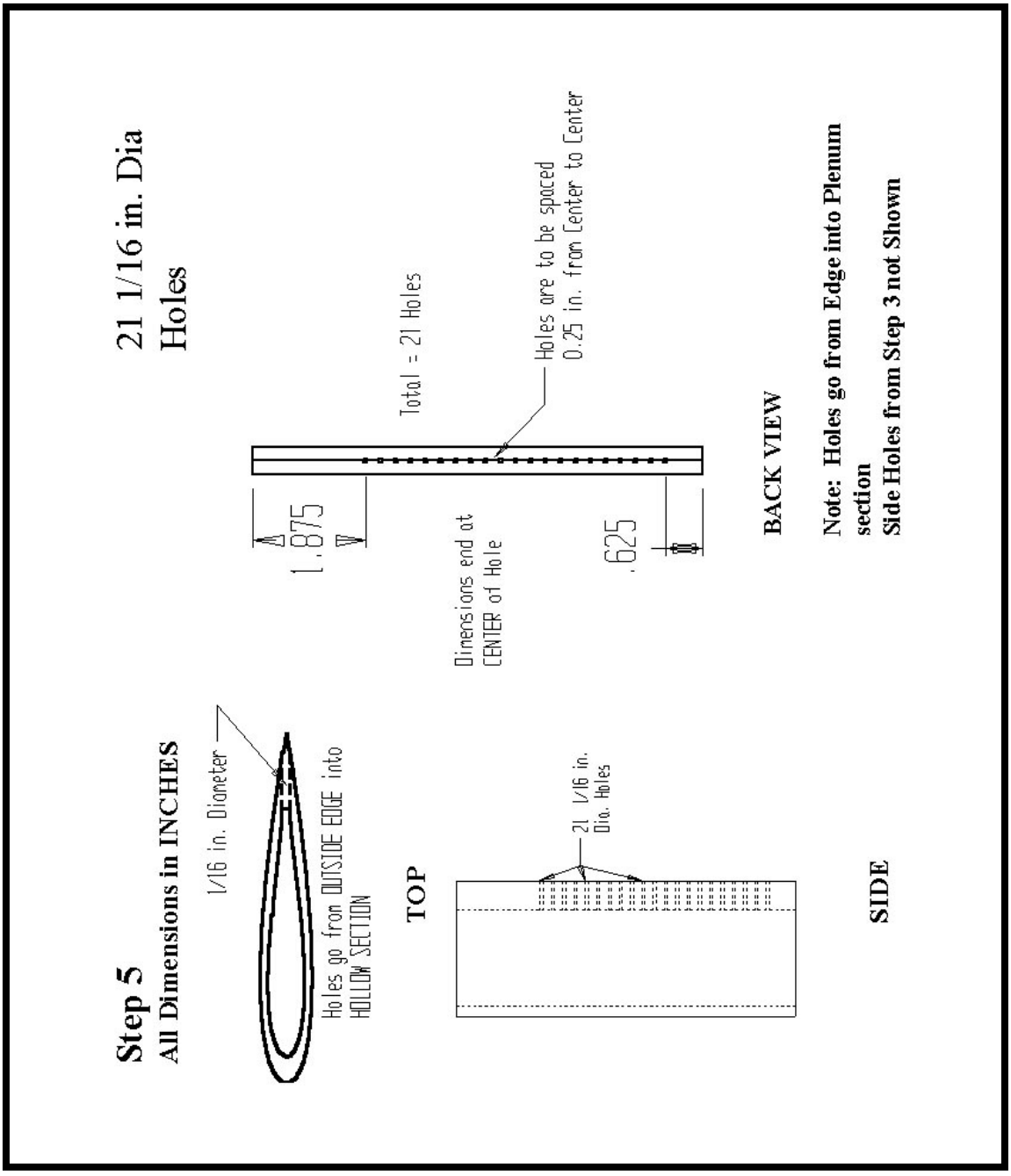

Figure B.5 IGV Design Step 5—TEB Holes

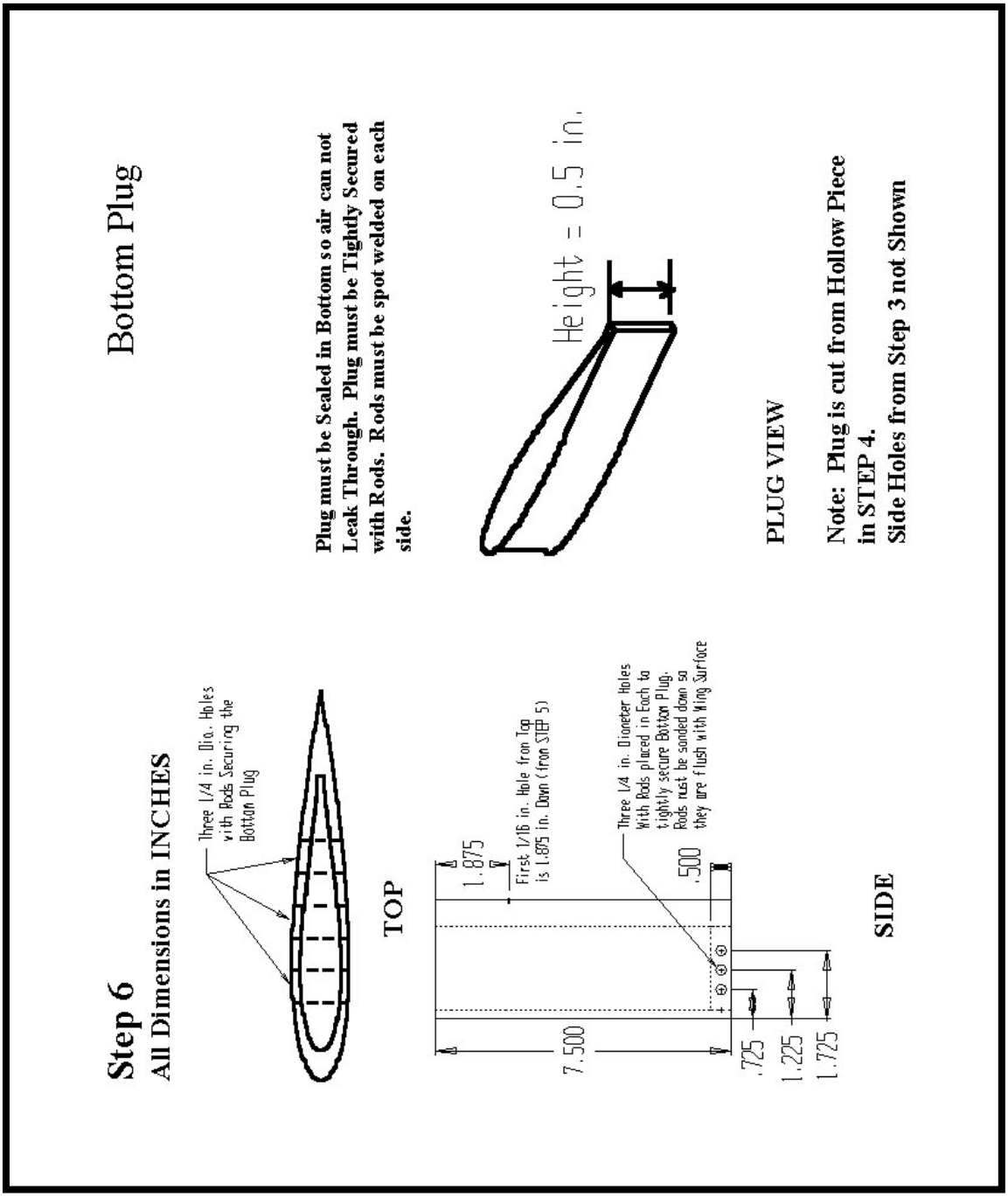

Figure B.6 IGV Design Step 6—Bottom Plenum Plug

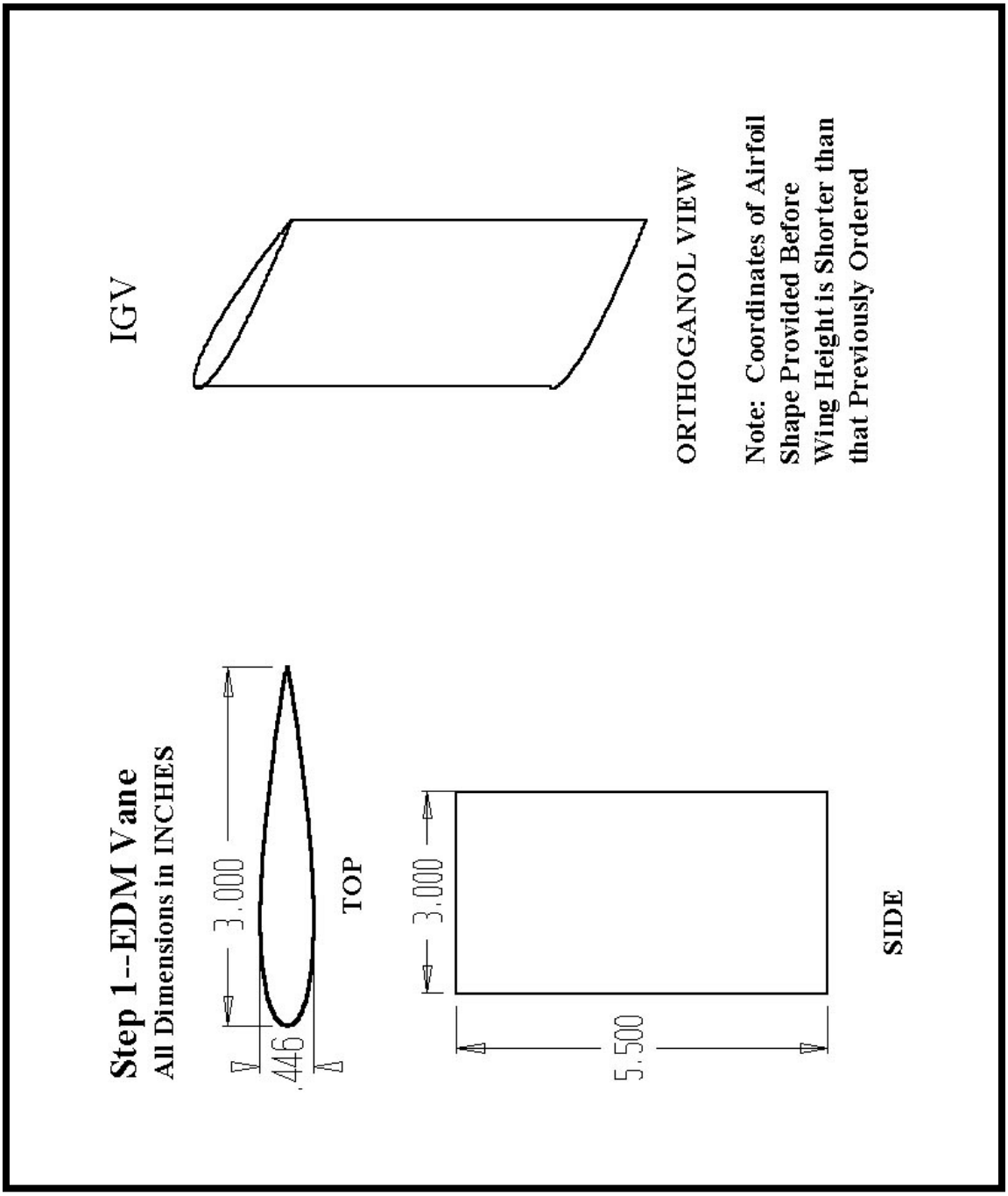

Figure B.7 Modified IGV Design Step 1—Wire EDM

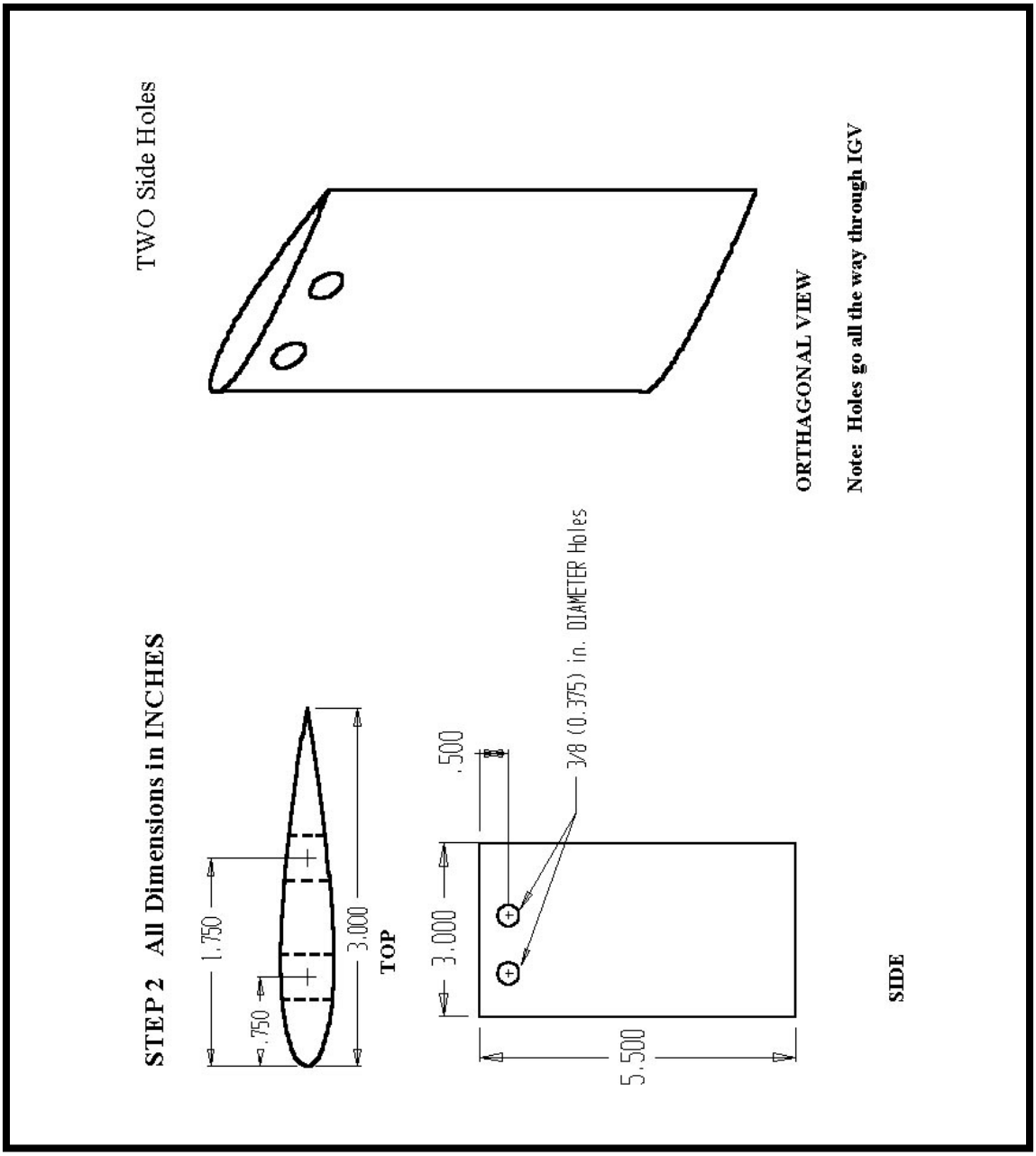

Figure B.8 Modified IGV Design Step 2—Holes for Shoulder Bolts

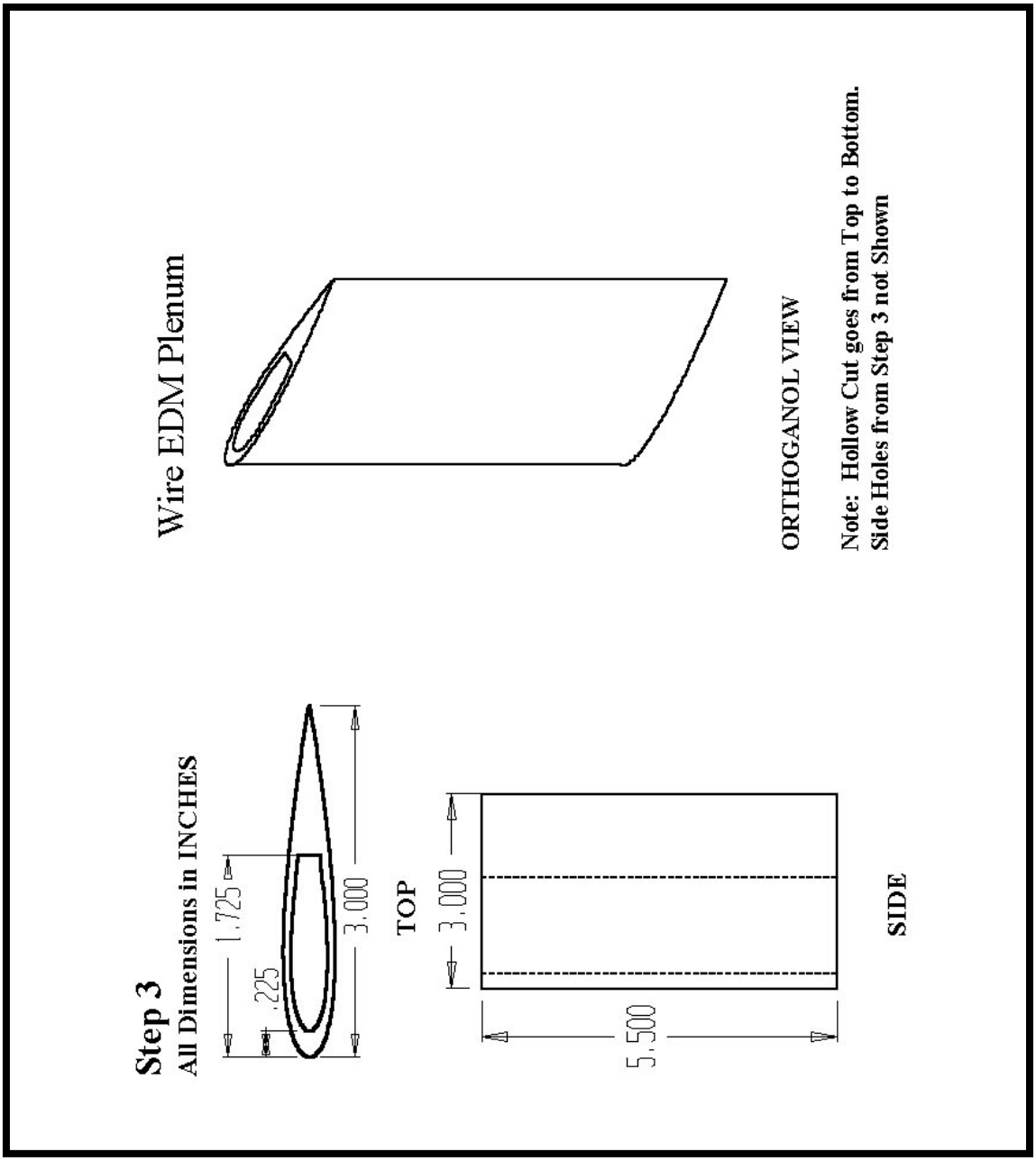

Figure B.9 Modified IGV Design Step 3—EDM Plenum Cut-out

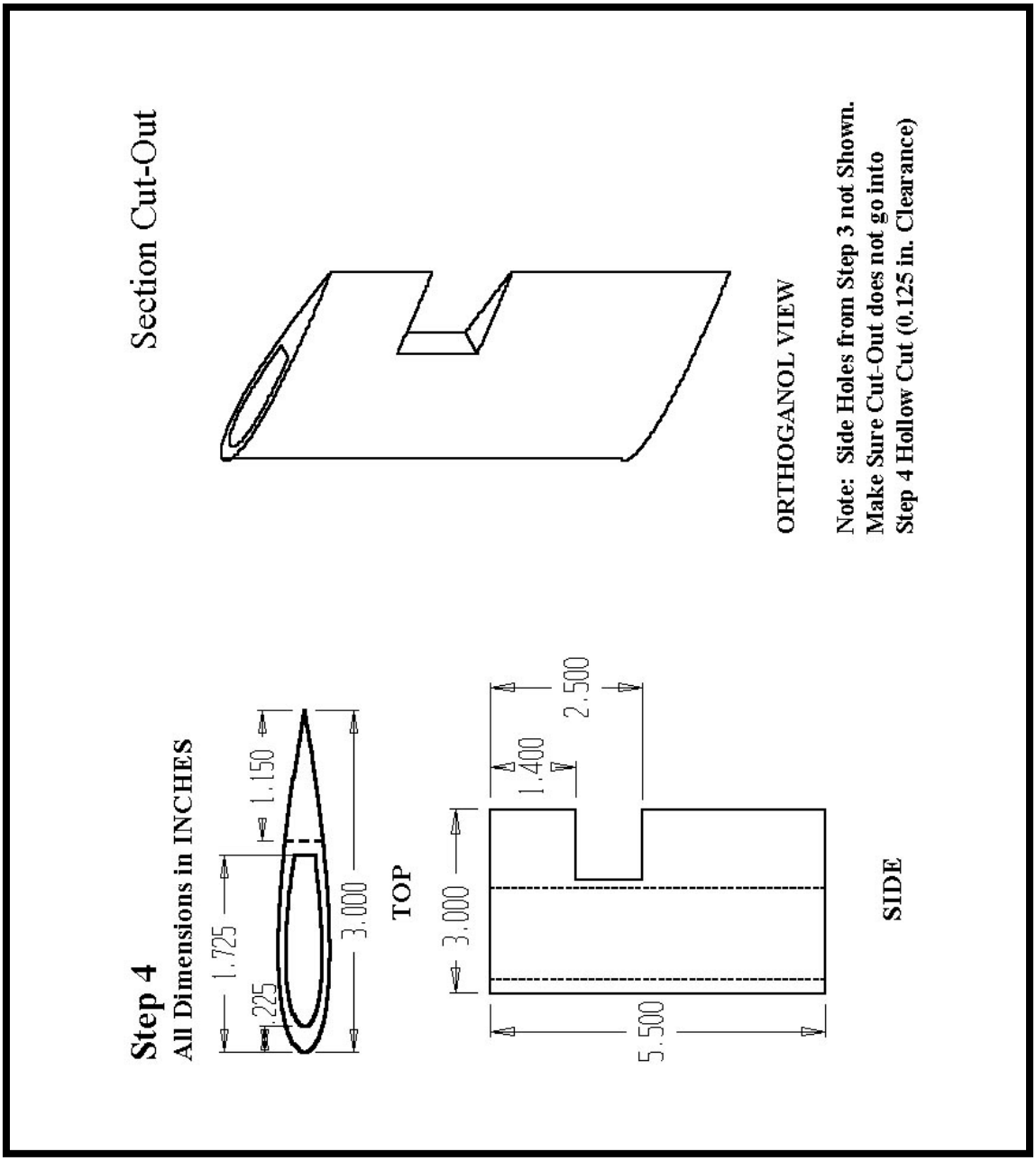

Figure B.10 Modified IGV Design Step 4—Notch Cut-out

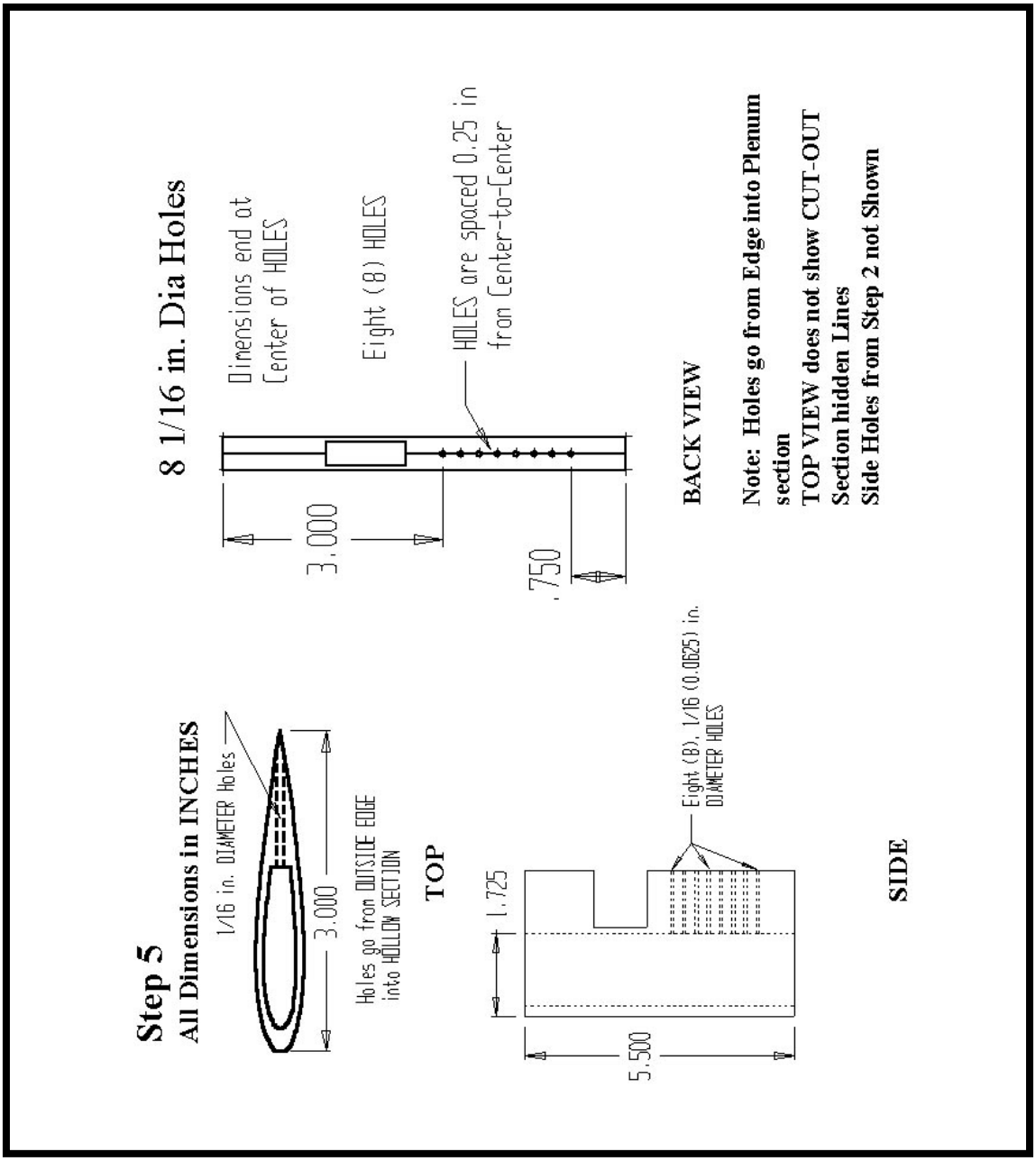

Figure B.11 Modified IGV Design Step 5—TEB Holes

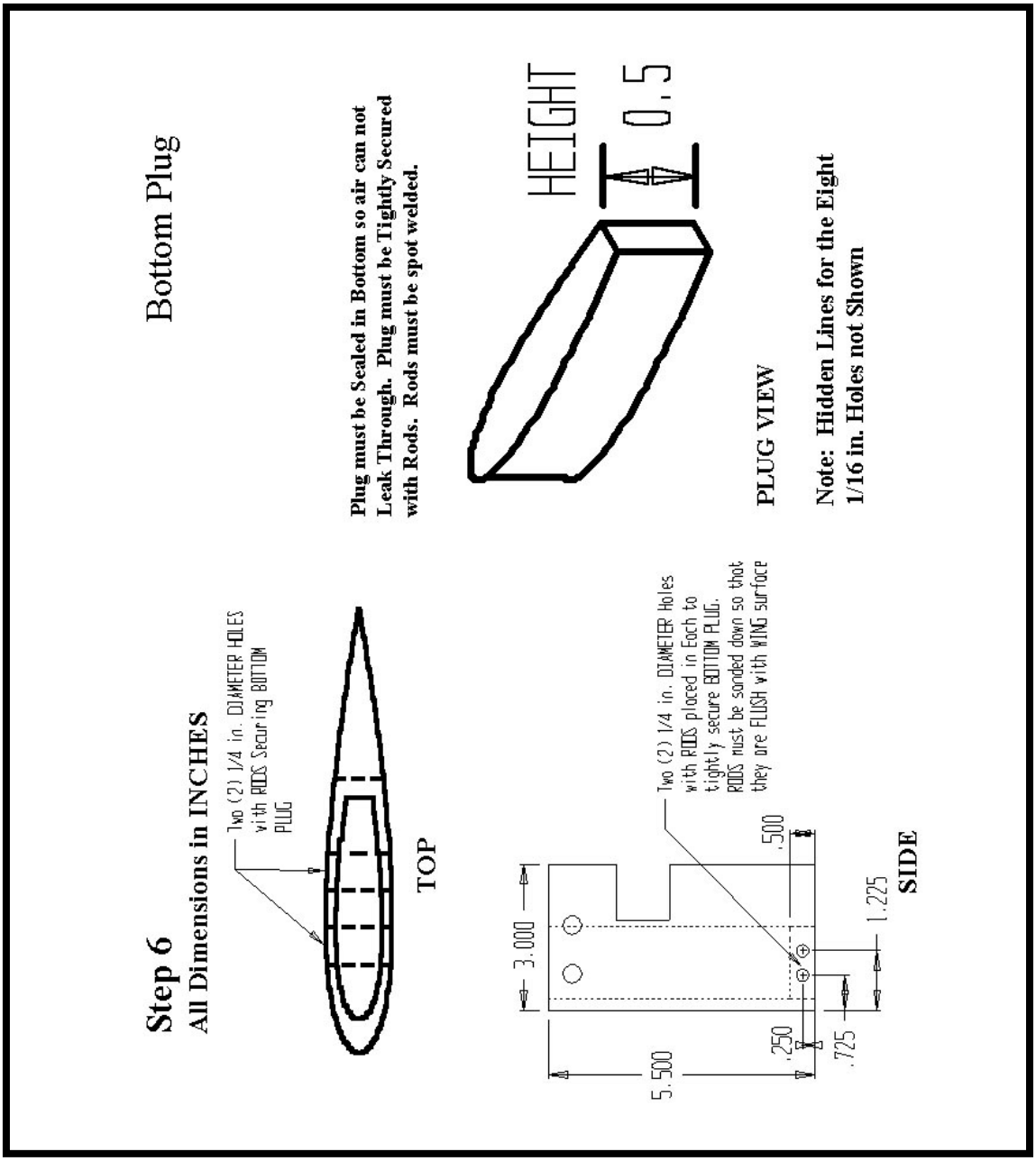

Figure B.12 Modified IGV Design Step 6—Bottom Plenum Plug

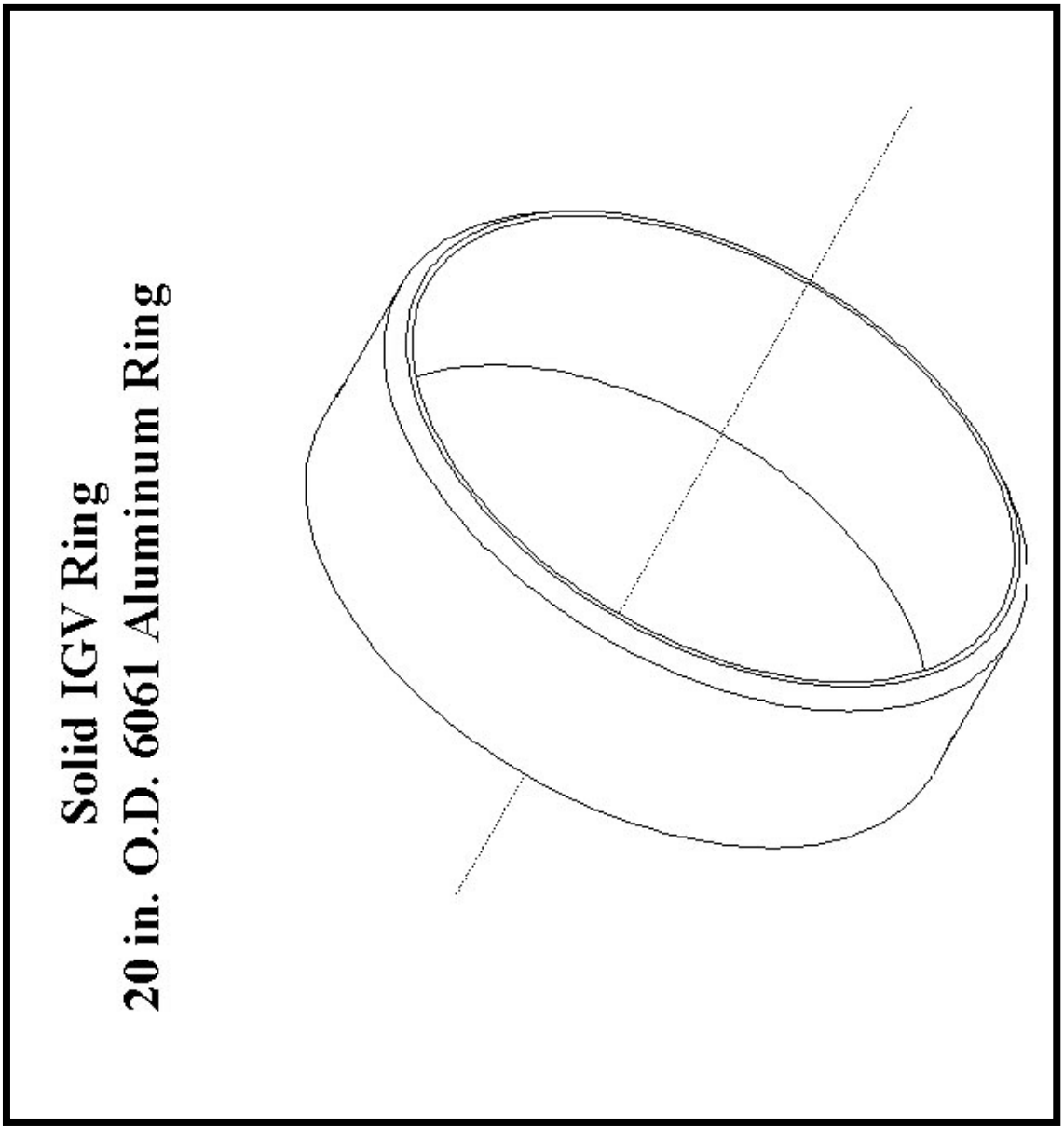

Figure B.13 IGV Ring Orthogonal View

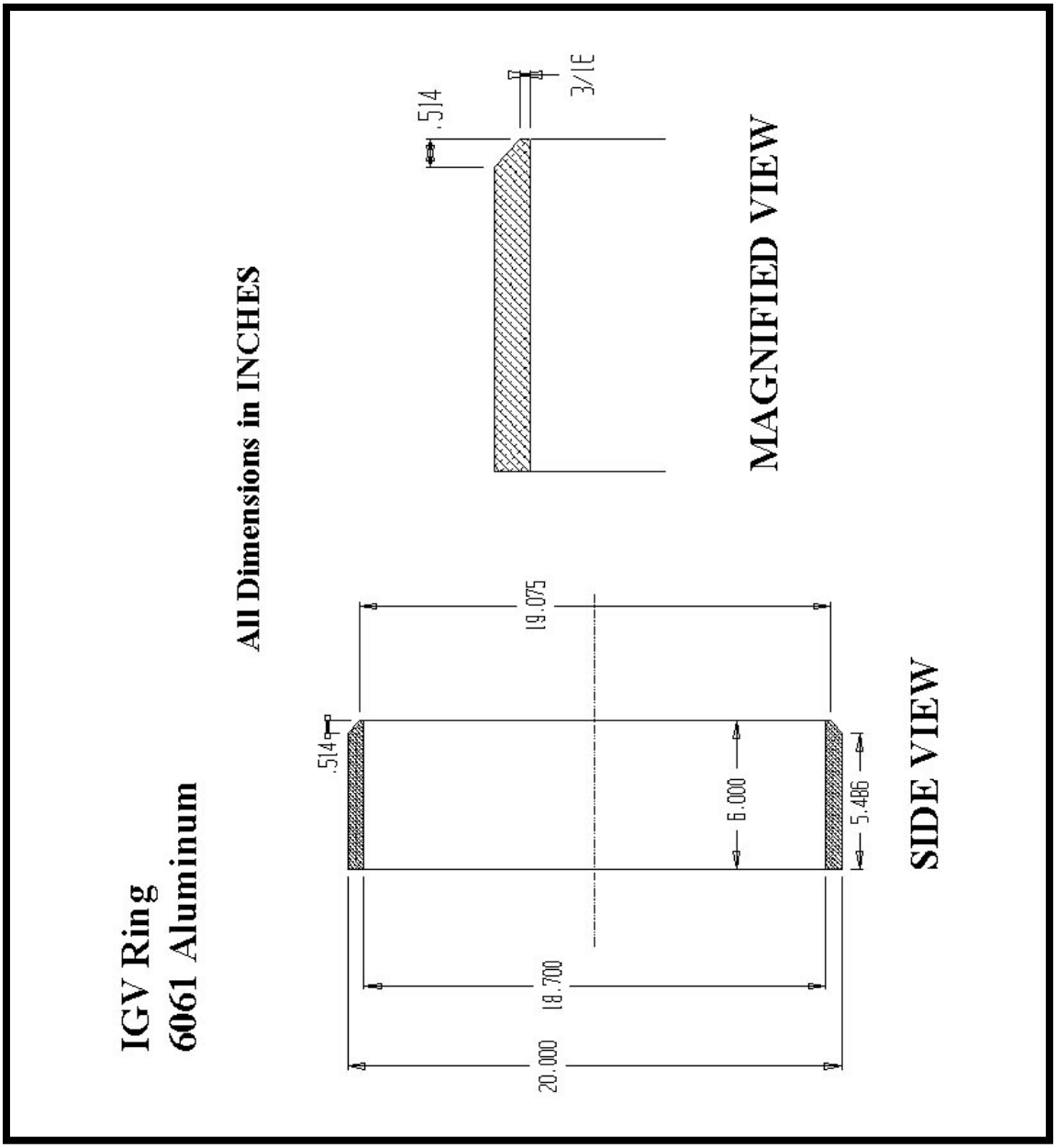

Figure B.14 IGV Ring Dimensions

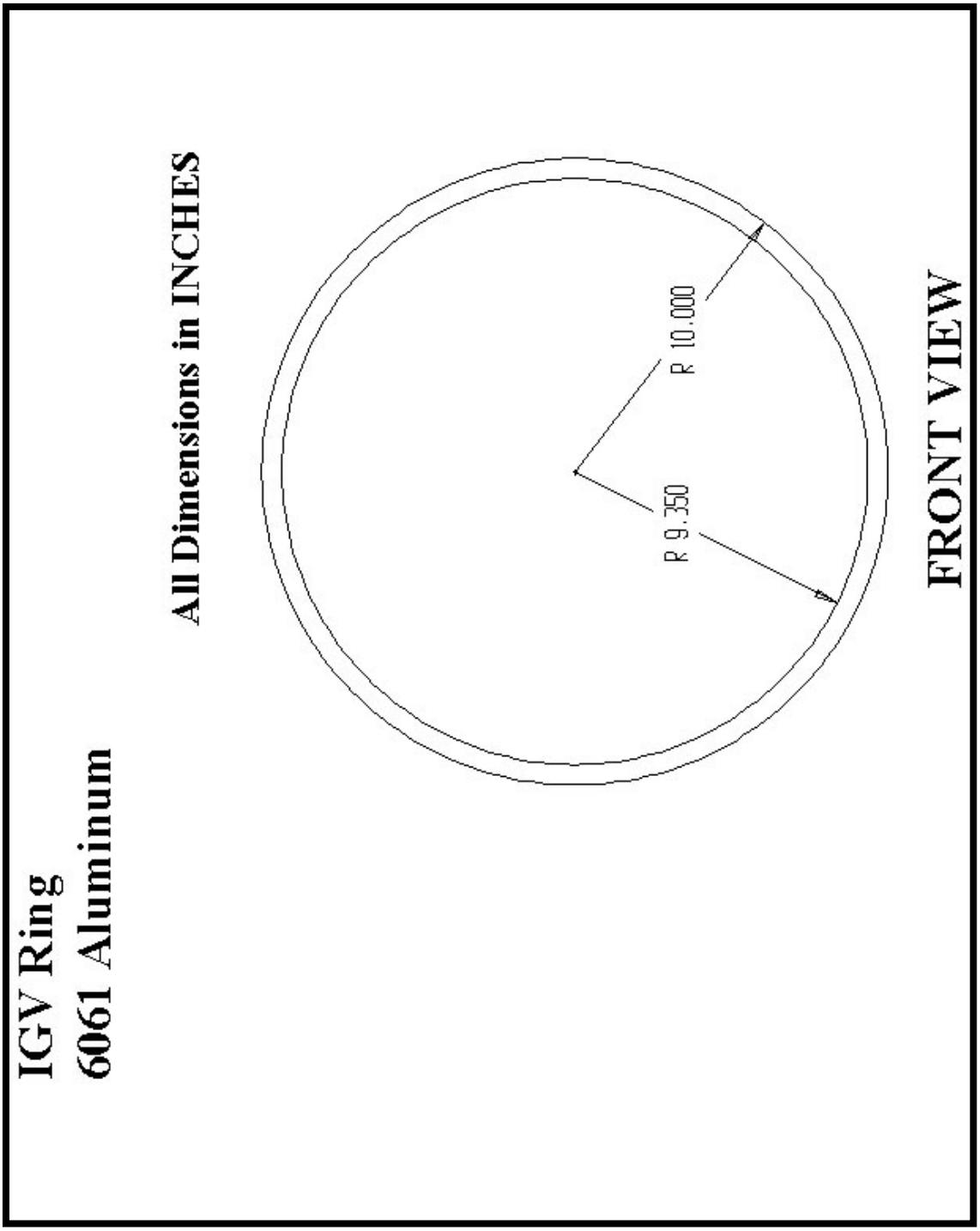

Figure B.15 IGV Ring Front View Dimensions

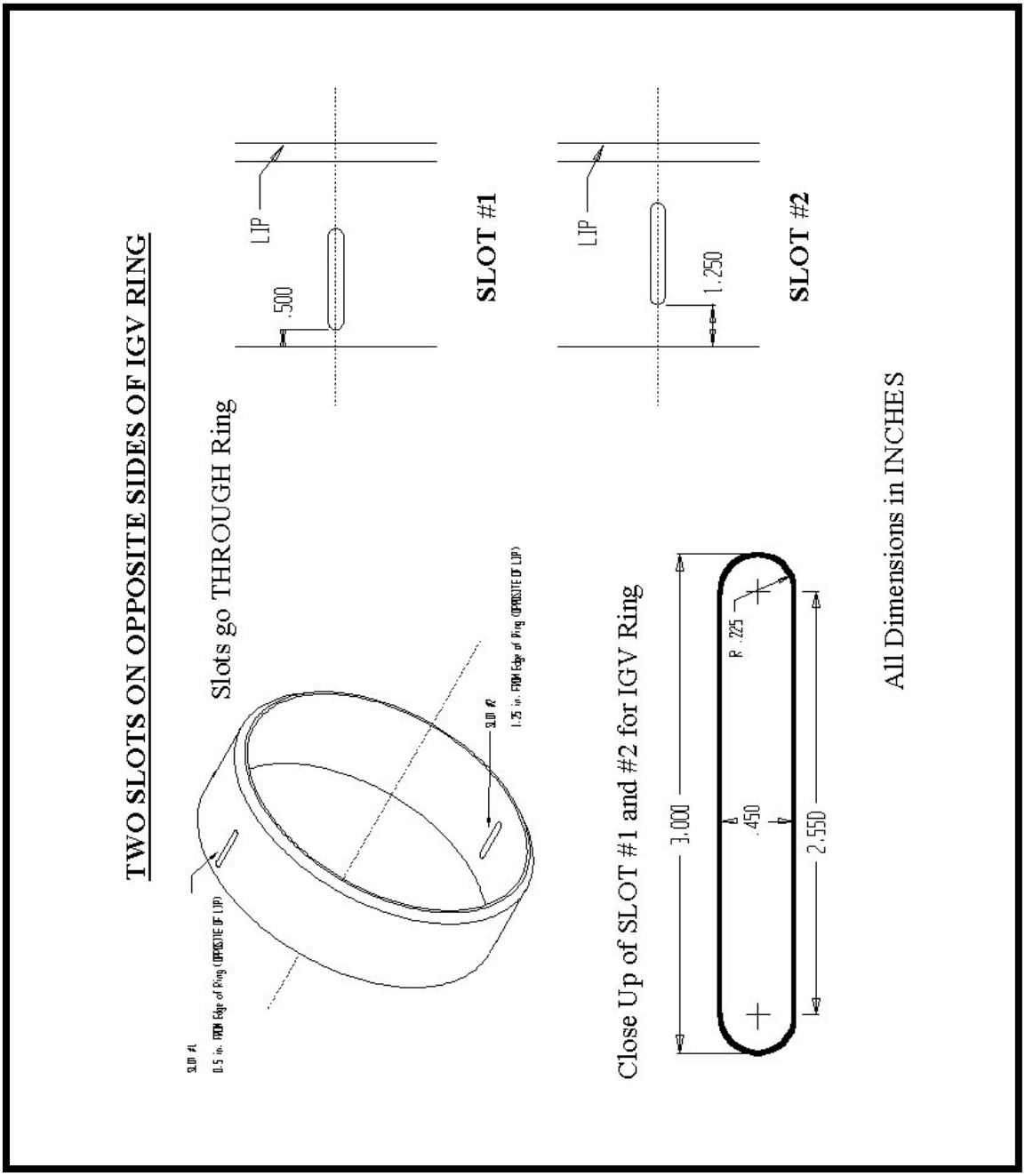

Figure B.16 IGV Ring Slots for IGV Placement

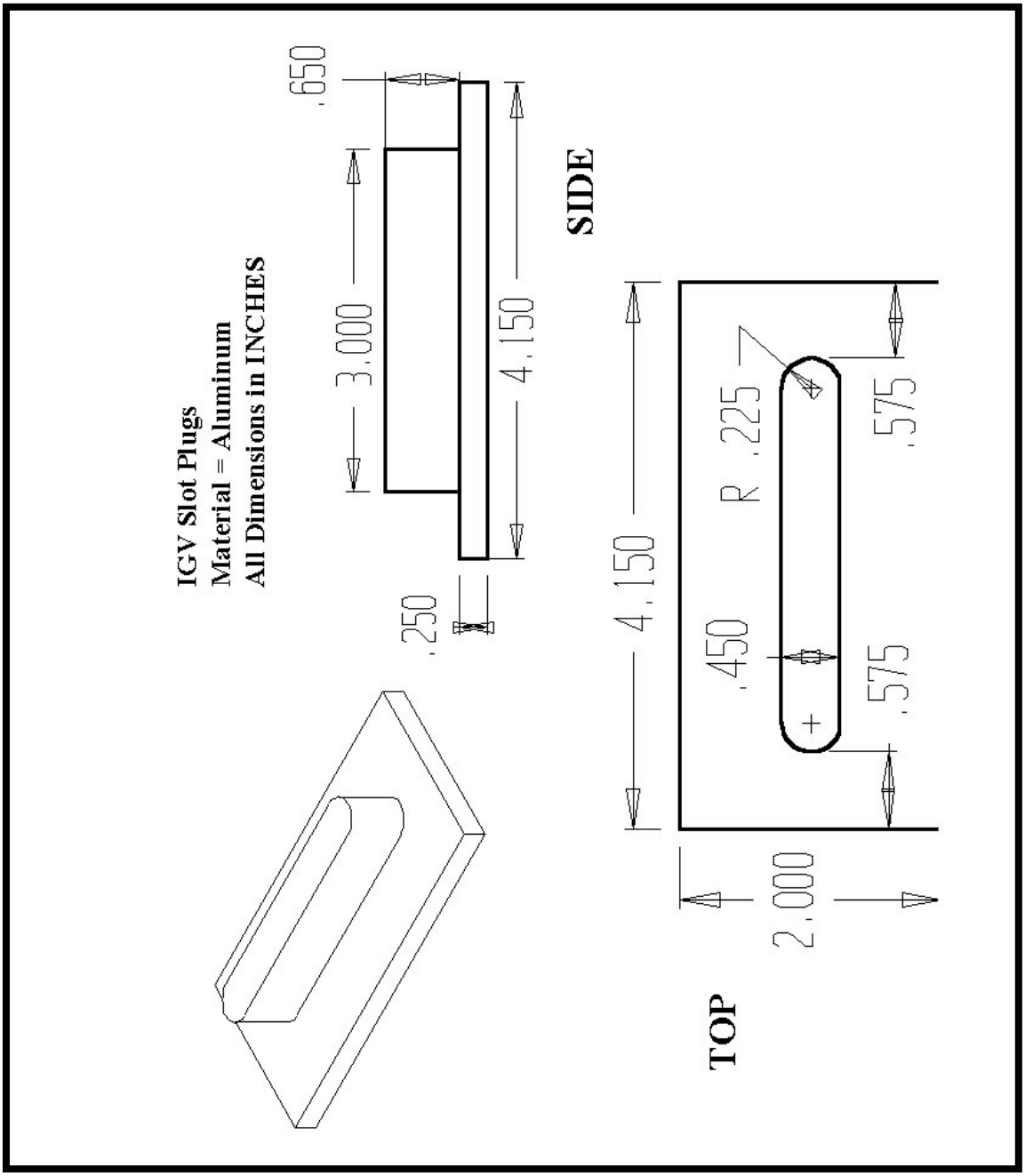

Figure B.17 IGV Slot Plugs

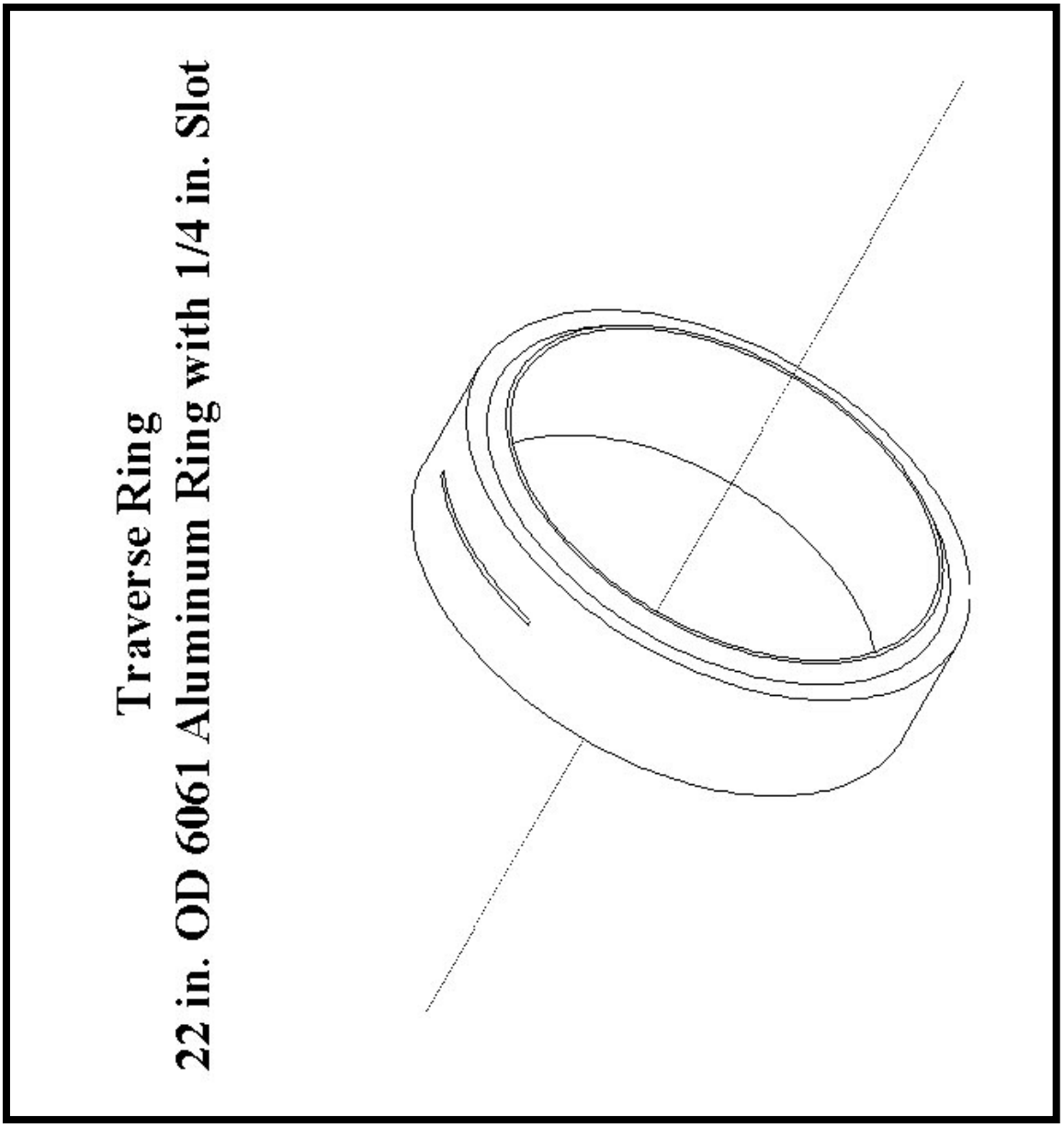

Figure B.18 Traverse Ring Orthogonal View

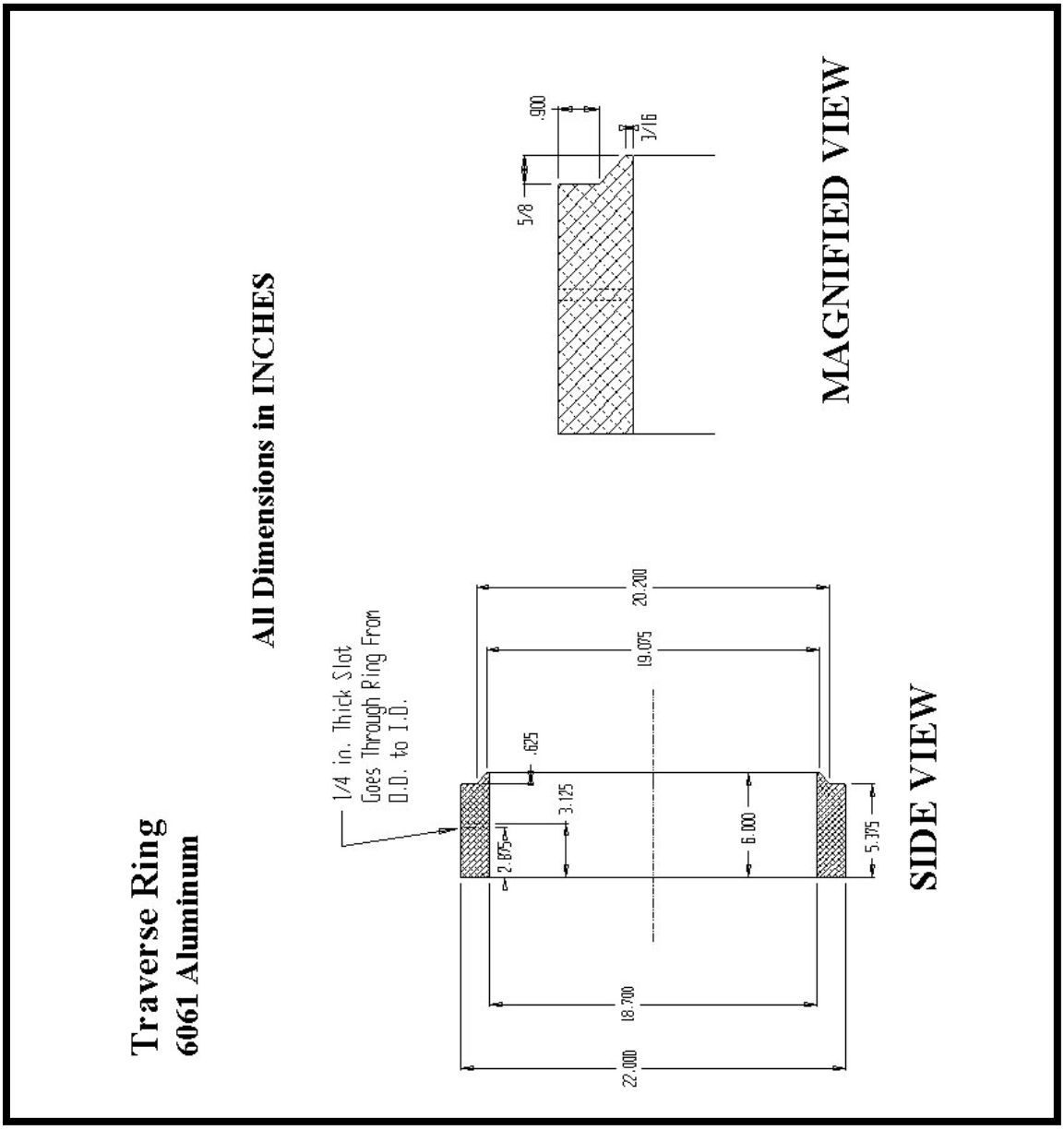

Figure B.19 Traverse Ring Dimensions

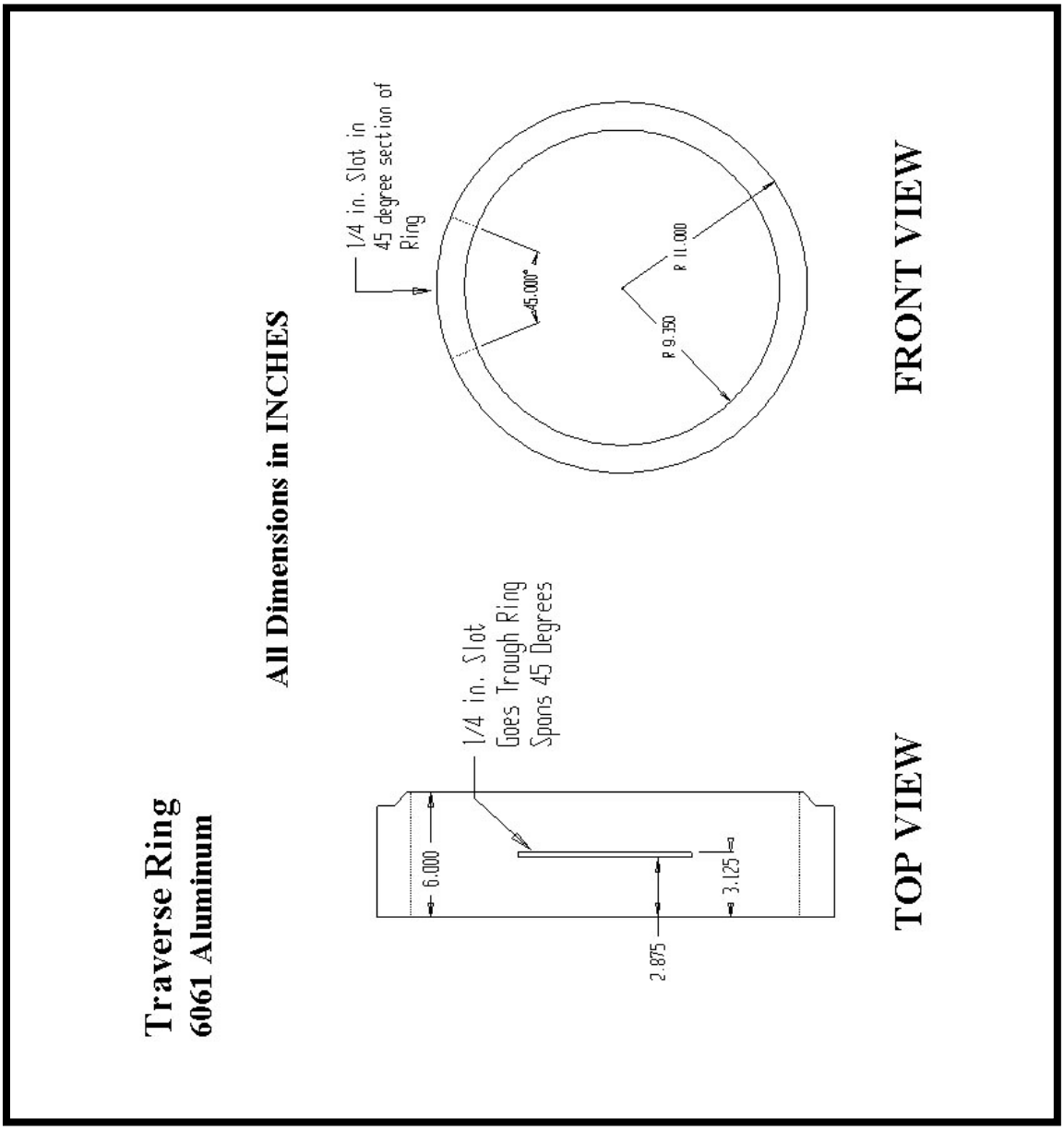

Figure B.20 Traverse Ring Front and Top Dimensions

Vita

Jeffrey D. Kozak was born on April 3, 1971 at McConnell AFB, Kansas. He attended Paul VI high school in Fairfax, VA where he graduated in 1989. The author received his Bachelor's in Mechanical Engineering in 1993 from Gannon University in Erie, PA. While in Erie, he was employed by Johnson Controls, Smith Meter and General Electric over the summers. The author received his Master's of Science in Mechanical Engineering from Virginia Tech under Dr. Wing-Fai Ng in August of 1995. The title of his Master's thesis was "Three-Dimensional Viscous Flow Calculations of a Bifurcated 2D Supersonic Engine Inlet at Takeoff". The author continued working with Dr. Ng for his doctoral work. While at Virginia Tech, the author worked as a lab instructor for five semesters, conducted published research on Supersonic Inlet Instabilities and Fiber-Optic pressure transducers, and served on the College of Engineering's Graduate Student Committee. The author is currently employed at Technology In Blacksburg, Inc., where he began employment in January 2000. He has accepted a tenure-track assistant professorship at the Rochester Institute of Technology, Rochester, NY, which will begin in September 2000. The author defended his Dissertation on August 3, 2000.

_____

Jeffrey D. Kozak